Characterization of Platinum Group Minerals in the UG-2 chromitite flotation concentrates from the western Bushveld Complex, South Africa.

By

Junior Itumeleng Molebale

Submitted in partial fulfillment of the requirements for the degree

Magister Scientiae Applied mineralogy

In the Faculty of Natural and Agricultural Sciences,

University of Pretoria

Pretoria

February 2011

I, Junior Itumeleng Molebale, declare that the thesis/dissertation, which I hereby submit for the degree of Magister Scientiae Applied Mineralogy at the University of Pretoria, is my own work and has not previously been submitted by me for a degree at this or any other tertiary institution.

SIGNATURE: 

DATE: February 2011

The thesis is part of MINTEK automated mineralogy project and therefore Mintek procedures were followed.

Acknowledgements

I would like to thank God for giving me wisdom and strength. To my family and friends who gave me support throughout my studies. I would also like to thank MINTEK for funding this project.

Many thanks to Prof. R.K.W. Merkle, the man who taught me everything I know concerning scientific research and mineralogy.

Thanks to the staff at Mintek mineralogy division (Deshenthree Chetty, Charles Bushell, Lelanie Gryffenberg, Lucky Lesele, Bernard Moeketsi, Archie Corfield, and Chris MaClaren) for their technical support and fruitful discussions. To the staff at Lonmin platinum – K4 Concentrator, thanks for assisting with sampling, and not forgetting staff at Mintek mineral processing division, and analytical service division, thanks for assisting with sample preparation and chemical analysis. Thanks also to Awelani Moila and Wendy Tshawe for proof reading the thesis.

ABSTRACT

The Bushveld Igneous Complex (BIC) of South Africa hosts approximately 80 percent of the world economic resources of platinum group elements (PGE). Platinum group elements in the Upper Group 2 (UG-2) chromitite layer of the Bushveld Igneous Complex of South Africa are recovered by the process of comminution and flotation.

The recovery of Platinum Group Minerals (PGM) from the UG-2 chromitite is mostly dependent on mode of occurrence, degree of liberation, and grain sizes. PGM in the UG-2 chromitite are recovered by means of flotation. Flotation occurs both in the primary rougher circuit (PRC) and secondary rougher circuit (SRC). In the primary rougher circuit, PRC 1 and PRC 2 are considered as fast floating cells, while PRC 3 to PRC 10, considered as moderate to slow floating cells.

The highest recovery of PGM is in PRC 1 and PRC 2. PGM that are recovered in PRC 1 and PRC 2 are mostly coarser, liberated PGM, and PGM associated with coarser liberated Base Metal Sulphides (BMS). PGM recovered from PRC 3 to PRC 10 have smaller grain sizes and are mostly associated with BMS and gangue minerals.

In the primary rougher concentrates more than 90 volume percent of PGM recovered are platinum containing sulphides. PGM alloy, PGM containing arsenic, and PGM containing tellurium make up only less than 10 volume percent of recovered PGM in the primary rougher concentrates.

The platinum containing sulphides recovered in the primary rougher concentrates in the order of decreasing abundance are braggite (PtPdNiS), cooperite (PtS), malanite (Pt_2CuS_4), and laurite (RuS_2).

Table of Contents

Acknowledgements iv

ABSTRACT v

List of abbreviations ix

List of figures xi

List of tables xvi

1. Introduction 1

1.1. Objectives for this study 2

1.2. Investigation techniques 2

2. Geological setting 3

2.1. Bushveld Igneous Complex 3

2.2. UG-2 Chromitite layer 9

2.2.1. Mineralogy in the UG-2 Chromitite layer 9

3. Mineral beneficiation 11

3.1. Comminution 11

3.2. Concentration 13

3.2.1 Froth flotation 13

4. Sampling 15

4.1. Plant conditions 15

4.2. Sampling 17

4.3. Sample preparation 18

4.3.1. Sample preparation procedure 18

4.4. Polished section preparation 20

5. Methods 22

5.1. Chemical analysis 22

5.2. Mineralogical analysis 23
5.2.1. X-ray diffraction spectroscopy (XRD) - phase analysis of UG-2 material. 23
5.3. Mineral Liberation Analyzer (MLA) 24
5.3.1. BSE Image analysis 25
5.3.2. Mineral identification with X-ray analysis 26
5.3.4. PGM identification 29
5.4. Electron probe micro analyzer (EPMA) 30
6. Results 31
6.1. Concentration of PGE 32
6.1.1. Concentration of base metals 36
6.1.2. Chemical analysis of total sulphur 40
6.1.3. Chemical analysis for total chromium (Cr) and total iron (Fe). 42
6.2. XRD Analysis 42
6.3. Mineralogy of the primary rougher circuit. 46
6.3.1. PGM modal distribution 46
6.3.2. PGM species in the UG-2 chromitite layer 46
6.3.3. PGM mode of occurrence and liberation. 48
6.3.4. PGM grain size distribution 54
6.4. Characterization of PGM phases. 56
6.4.1. Quantitative characterization of selected PGM phases. 56
6.4.2. Cooperite, Braggite, and Vysotskite. 57
6.4.3. Malanite, cuprorhodsite, and cuproiridsite. 59
6.4.4. Laurite. 60
7. Discussion 61
7.1. Behavior of silicates and chromite during flotation. 61

7.2. Flotation behavior of PGM. 63

8. Conclusions 79

9. References 81

Appendix A – Percentage solids 89

Appendix B.1 - Fire Assay results 90

Appendix B.2 – Acid solubility results of Nickel, copper, and cobalt. 90

Appendix B.3 – Acid solubility results of total iron and chromium. 91

Appendix C – XRD Results (wt %) 91

Table C.2 92

Appendix D.1 – Modal distribution of PGM (Vol %) 92

Appendix D.2 – Modal distribution of dominating PGM sulphides and platinum alloy (Vol %). 93

Appendix D.3 – Mode of occurrence along the primary rougher circuit. 93

Appendix D.5 – PGM size distribution, along the primary rougher circuit (%). 94

Appendix E – Micro probe results 95

List of abbreviations

6E's:	platinum, palladium, rhodium, ruthenium, iridium, and gold
BIC:	Bushveld Igneous Complex
BMS:	Base Metal Sulphides
BSE:	Back Scattered Electrons
CMC:	Carboxy Methyl Cellulose
ECD:	Equivalent Circle Diameter
EDS:	Energy Dispersive Spectroscopy
EPMA:	Electron Probe Micro Analyser
FA:	Fire Assay
ICP-OES:	Inductively Coupled Plasma Optical Emission Spectroscopy
LCZ:	Lower Critical Zone
LG:	Lower Group
LLD:	Lower Limit of Detection
MF2:	Mill Float - Mill Float
MG:	Middle Group
MLA:	Mineral Liberation Analyser
PGE:	Platinum Group Elements
PGM:	Platinum Group Minerals
PRC:	Primary Rougher Concentrates
PRF:	Primary Rougher Feed
PRT:	Primary Rougher Tail
QemScan:	Quantitative Evaluation of Minerals Using Scanning Electron Microscopy
SACC:	South African conventional concentrator

SEM:	Scanning Electron Microscope
UCZ:	Upper Critical Zone
UG-1:	Upper Group 1 Chromitite
UG-2:	Upper Group 2 Chromitite
WDS:	Wavelength Dispersive Spectroscopy
XRD:	X-ray diffraction
µm:	micrometer

List of figures

Figure 2.1: Simplified geological map of South Africa (Wilson and Anhaeusser, 1998). The BIC is indicated with the circle. 4

Figure 2.2: Geological map of the BIC, showing three major limbs (courtesy of RKW Merkle). 5

Figure 2.3: Geological map showing the southern portion of the western limb of the BIC of South Africa BIC (courtesy of RKW Merkle). The study area is in the Marikana section, in the southern part of the western limb of the stratigraphy. 6

Figure 2.4: Profile showing subdivision of Rustenburg Layered Suite (Viljoen and Schurmann, 1998). 8

Figure3.1: Ore beneficiation process at Lonmin platinum, South Africa. 11

Figure 3.2: Schematic representation of MF 2 plant, indicating the primary, and secondary milling, primary, and secondary flotation. It also indicates the High Grade Cleaner (HGC) and Low Grade Cleaner (LGC). In the MF2 plant a high grade fast floating and a low grade slow floating concentrate are produced (Merkle and McKenzie, 2002). 12

Figure 4.1: Filtration system, MINTEK South Africa. 18

Figure 4.2: Samples after drying, MINTEK, South Africa. 19

Figure 4.3: Screening of sample using 850 µm sieve and a rubber bar. 20

Figure 5.1: X'Pert Pro PANalytical x-ray diffractometer at Department of Geology, University of Pretoria. 23

Figure 5.2: FEI Quanta 600, Mineral Liberation Analyzer at MINTEK,

South Africa. 29

Figure 5.3: 14 sample holder round (JK tech ops training 2008). 30

Figure 6.1: Percentage solids of samples in the primary rougher circuit. 31

Figure 6.2: Analysis of 6E's using ICP-OES. From bottom to top: Pt, Pd, Ru, Rh, Ir, and Au. 32

Figure 6.3: Analysis of 6E's using ICP-OES on the PRF sample. 34

Figure 6.4: Analysis of 6E's using ICP-OES on PRC 1 and PRC 2. 34

Figure 6.5: Analysis of 6E's using ICP-OES on the PRC 3 and PRC 4. 35

Figure 6.6: Analysis of 6E's using ICP-OES on the PRC 5 to PRC 10. 35

Figure 6.7: Analysis of 6E's using ICP-OES on the PRT. 36

Figure 6.8: Base Metal results of PRF. 37

Figure 6.9: Base Metal results of PRC1 and PRC2. 38

Figure 6.10: Base Metal results of PRC3 and PRC4. 34

Figure 6.11: Base Metal results of PRC5 to PRC10. 39

Figure 6.12: Base Metal results of PRT. 39

Figure 6.13: Analysis of Total S of PRF and PRT. 40

Figure 6.14: Analysis of Total S from PRC1 and PRC2. 41

Figure 6.15: Analysis for total S from PRC3 to PRC10. 41

Figure 6.16: Analysis of total Fe and total Cr in primary rougher circuit. 42

Figure 6.17: Phase quantification using X'Pert High score plus software. 43

Figure 6.18: Phase quantification of talc using X'Pert High score plus software. 44

Figure 6.19: Phase quantification using X'Pert High score plus software, for major silicates and chromite. 45

Figure 6.20: Phase quantification using X'Pert High score plus software,

for minor silicates. 45

Figure 6.21: Modal distribution of PGM in the primary rougher circuit based on 3354 grains. 47

Figure 6.22: Modal distribution of dominating platinum containing sulphides, ruthenium sulfide, and platinum-iron alloy along the primary rougher circuit. 48

Figure 6.23: Backscatter electron image of liberated PtPdNiS grain from the UG-2 chromitite. 49

Figure 6.24: Backscatter electron image of PtFe and pentlandite grains from the UG-2 chromitite. 50

Figure 6.25: Backscatter electron image of pyrite and PtPdS grains from the UG-2 chromitite. 50

Figure 6.26: Backscatter electron image of chalcopyrite, PtPdNiS, and PtRhCuS from the UG-2 chromitite. 51

Figure 6.27: Mode of occurrence of PGE minerals and associated minerals along the circuit based on 3354 grains. 51

Figure 6.28: PGM combined liberation index along the primary rougher circuit based on 3354 grains. 53

Figure 6.29: Schematic representation illustrating combined liberation index (CLI), of three different PGM associations (from Penberthy 2000). 54

Figure 6.30: PGM size distribution along the primary rougher circuit. 55

Figure 6.31: Compositional variation of PtS, PdS, and NiS from the UG2 concentrate. 58

Figure 6.32: Compositional variation of Pt_2CuS_4, Ir_2CuS_4, and Rh_2CuS_4

from the UG-2 concentrate. 59

Figure 6.33: Compositional variation of RuS_2, IrS_2, and OsS_2 from the UG2 concentrate. 60

Figure 7.1: Analysis of total Fe and total Cr in primary rougher circuit. 63

Figure 7.2: Summary diagram of Pt:Pd ratio along the primary rougher circuit. 65

Figure 7.3: Summary diagram of acid solubility results of primary rougher circuit. 68

Figure 7.4: Summary diagram of total S from primary rougher concentrate. 68

Figure 7.5: Relationship between acid soluble nickel and sulphur from PRC 1 to PRC 10. 69

Figure 7.6: Relationship between acid soluble cobalt and sulphur from PRC 1 to PRC 10. 70

Figure 7.7: Relationship between nickel and cobalt from PRC 1 to PRC 10. 70

Figure 7.8: Relationship between acid soluble copper and sulphur from PRC 1 to PRC 10. 71

Figure 7.9: Relationship between copper and nickel from PRC 1 to PRC 10. 72

Figure 7.10: Relationship between palladium and sulphur from PRC 1 to PRC 10. 73

Figure 7.11: Relationship between copper and palladium from PRC 1 to PRC 10. 74

Figure 7.12: Relationship between nickel and palladium from PRC 1 to PRC 10. 75

Figure 7.13 a: Relationship between platinum and palladium from PRC 1 to PRC 10. 75

Figure 7.13 b: Relationship between platinum and palladium from PRC 2 to PRC 10. 76

Figure 7.14 a: Relationship between rhodium and palladium from PRC 1 to PRC 10. 77

Figure 7.14 b: Relationship between rhodium and palladium from PRC 2 to PRC 10. 77

Figure 7.15 a: Relationship between platinum and rhodium from PRC 1 to PRC 10. 78

Figure 7.15 b: Relationship between platinum and rhodium from PRC 2 to PRC 10. 78

List of tables

Table 3.1: Reagents used in froth flotation (Summary operations of one of the primary circuit of South African conventional concentrator). 14

Table 4.1: Concentrate dispatched – high grade (HG) (Summary operations of one of the primary circuit of South African conventional concentrator). 16

Table 4.2: Head grade and tail grade (Summary operations of one of the primary circuit of South African conventional concentrator). 17

Table 4.3: Concentrate produced and mass pull (Summary operations of one of the primary circuit of South African conventional concentrator). 17

Table 6.1: Grade of 6E's (grams per ton). 32

Table 6.2: Total number of PGM from sections analyzed. 46

Table 6.3: Liberation characteristics of PGM, BMS and gangue minerals. 49

Table 6.4: PGM floatability index. 55

1. Introduction

The approximately 2060 Ma Bushveld Igneous Complex (BIC) of South Africa hosts approximately 80 percent of the resource of economic platinum group minerals (PGM) in the world. It also hosts nickel, copper, cobalt, and vanadium (Viljoen and Schurmann, 1998). PGM are mined in the Upper Group 2 chromitite (UG-2) and Merensky Reef in the western and eastern limb, and in the Platreef of the northern limb of the BIC.

The ore that is mined from the BIC is treated in South Africa using stepwise mineral processing techniques. The first step in PGM production is to transport ore from the mine to the processing plant. At the processing plant, ore is crushed using jaw crushers, and then taken to the concentrator, where it is milled and floated. The process whereby ore is crushed, milled and floated is called comminution and flotation. Most of the platinum concentrators in South Africa are mill float- mill float plants (MF2): the MF2 plant consists of primary milling, primary rougher cells, secondary milling and secondary rougher cells.

Primary milling is a process whereby ore is milled so that 50 percent of the particle sizes of the feed to the primary flotation circuit are smaller than 75 µm. In primary milling, PGM and Base Metal Sulphides (BMS) are liberated from silicates and oxide minerals. After the ore has been milled, it is floated in the primary rougher cells. In these cells, PGM that are liberated or PGM associated with BMS (attached or locked) will float and will be recovered.

All material that is not properly milled in the primary milling is re-milled in the secondary milling, so that 80 percent of the particle size of the feed to secondary flotation circuit is smaller than 75 µm. After the ore has been re-milled, it is then re-floated in the secondary rougher cells. PGM locked or attached to silicates or oxides are not easily recovered.

The material that is recovered through the process of flotation is called a concentrate and it is transported to the smelters with chromite content of less than 5 weight percent. The smelting and converting stage is followed by the base metal refinery stage, where nickel, copper, and cobalt are produced. The final stage is the platinum metal refinery stage where platinum group elements and gold are being produced (Valenta, 2007).

1.1. Objectives for this study

- To evaluate the process control of the processing plant. This is achieved by monitoring process efficiency through chemical analysis. Chemical analysis of the concentrate is carried out using fire assay followed by inductively coupled plasma optical emission spectrometry (ICP-OES), for the analysis of 6E's (i.e. platinum, palladium, rhodium, iridium, ruthenium and gold).
- To determine whether there is deviation from different flotation cells in terms of PGM. This is achieved by checking mineralogy and textural intergrowths and also by cross checking mineralogy and assays of PGM.
- To determine the mode of occurrence of PGM in different flotation cells.
- To determine the relationship between PGM species and the associated BMS or silicate species using Mineral Liberation Analyzer (MLA).
- To determine the recovery characteristics of PGM using MLA.
- To characterize PGM in terms of composition and size at less than ten micrometer (<10µm), using Electron Micro Probe Analyzer (EMPA).

1.2. Investigation techniques

Mineralogical analysis of the concentrate is carried out using:

- X-ray diffraction spectrometry (XRD),
- Mineral liberation analyzer (MLA) coupled with scanning electron microscopy, and
- Electron microprobe analyzer (EMPA)

2. Geological setting

2.1. Bushveld Igneous Complex

The Bushveld Igneous Complex (BIC) is located in the Kaapvaal Craton in South Africa. Other layered complexes in the Kaapvaal Craton are (a) the Molopo farms complex situated in Southern Botswana adjacent to South Africa (area extent of approximately 13000 km^2) (Reichhardt, 1994) and (b) the Trompsburg complex situated in the Southern portion of the Orange Free State (area extent of approximately 2500 km^2) (Maier et al., 2003).

The BIC (figure 2.1) intruded the rocks of the Transvaal supergroup approximately 2050 million years ago (Hamilton, 1977). It is a best known layered mafic intrusion in the world (Vermaak, 1985, Merkle and Mckenzie, 2002) and it is the host of most of world's economic PGE (Von Gruenewaldt, 1977). It has a total estimated extent of about 66 000 km^2 (Willemse, 1969; Vermaak, 1985, Buick et al., 2001).

The BIC is divided into three major compartments (Figure 2.2), namely:

a) The western Bushveld (in North West province) which extends approximately 200 km

b) The eastern Bushveld (in Mpumalanga province) which also extends for approximately 200 km,

c) The northern Bushveld (in Limpopo province) which is covered by Waterberg.

Mining of PGE occurs in all three compartments, but the study area for the project is in the southern portion of the western limb of the BIC in the Marikana area (Figure 2.3).

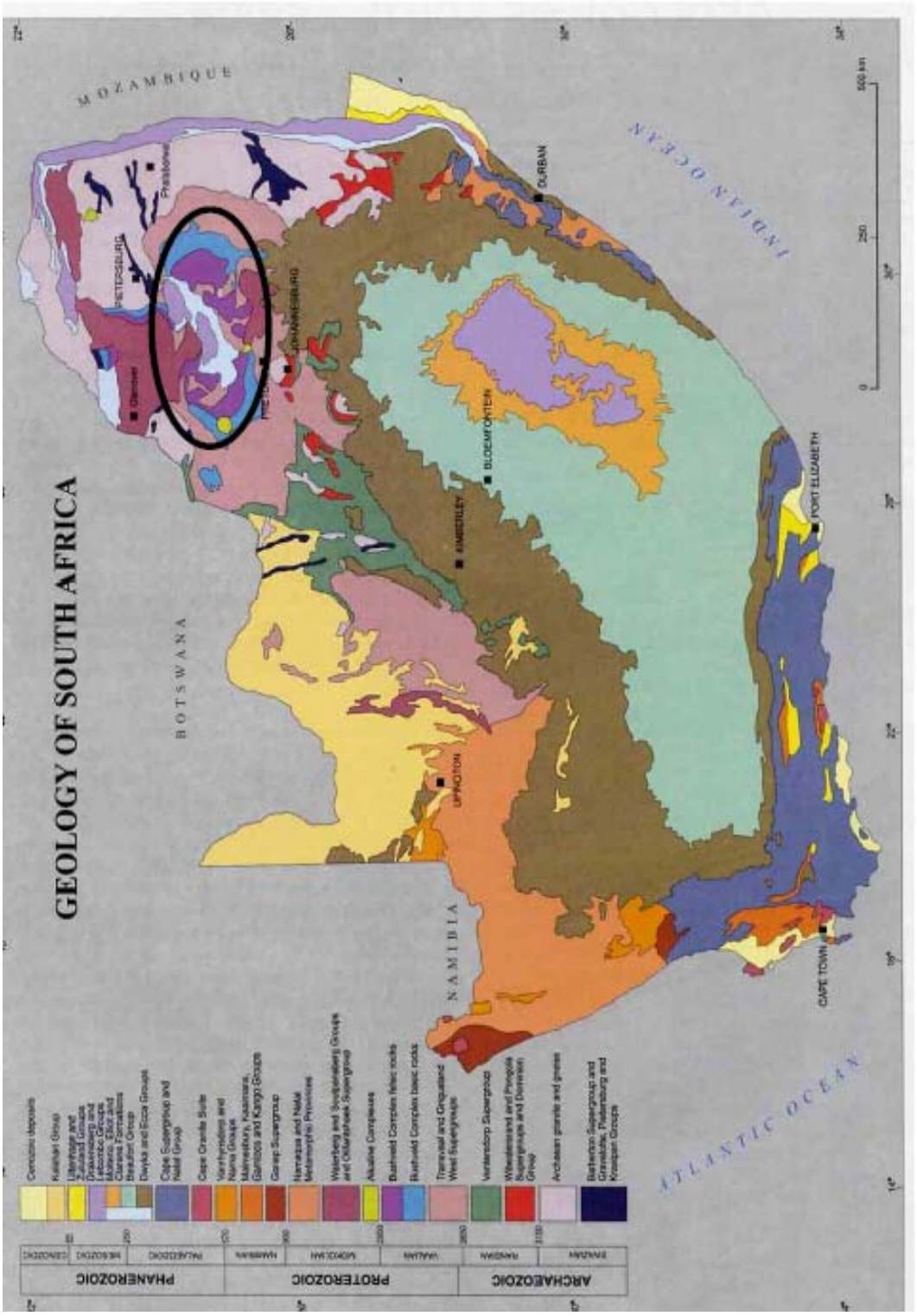

Figure 2. 1: Simplified geological map of South Africa (Wilson and Anhaeusser, 1998). The BIC is indicated with the circle.

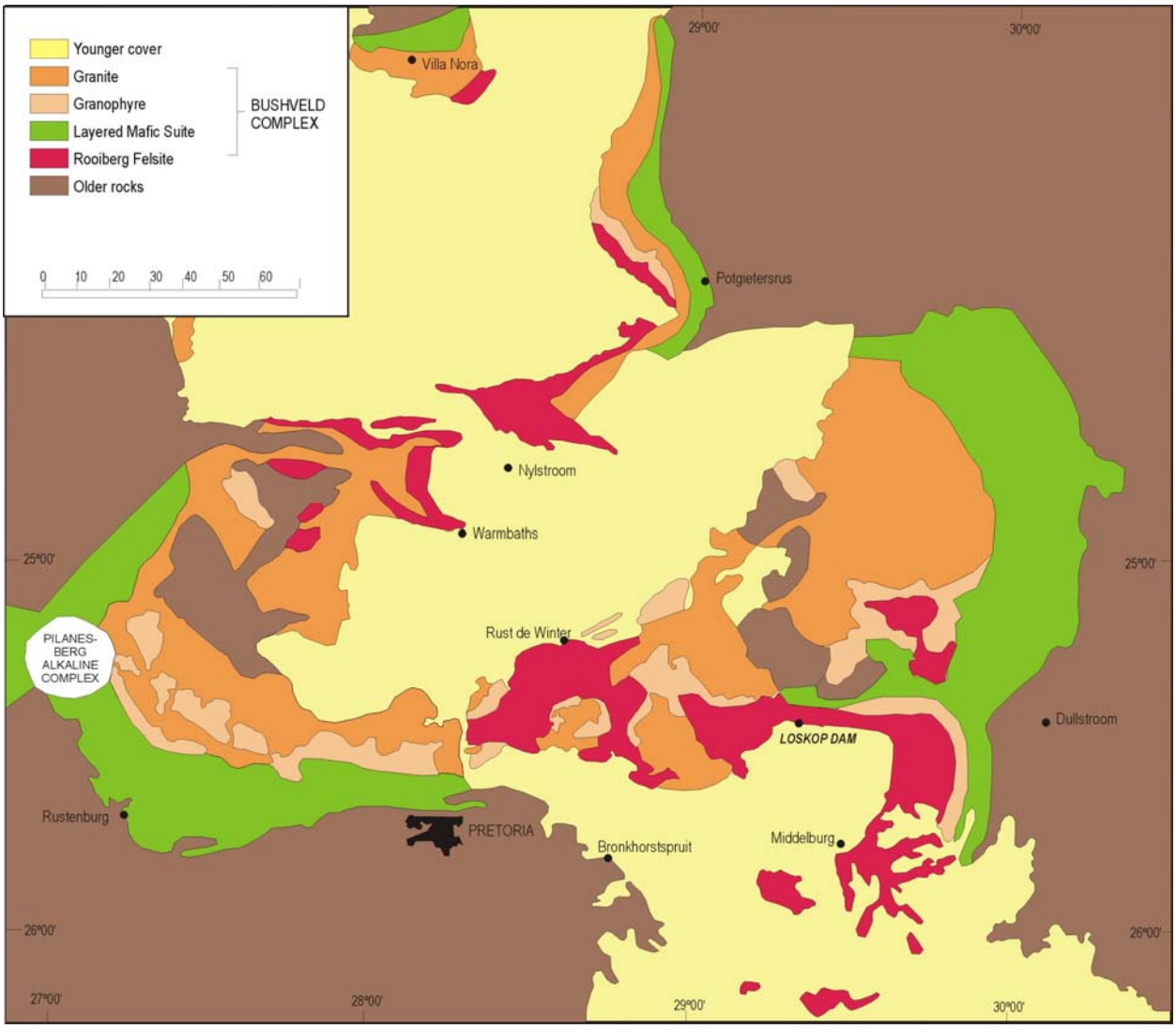

Figure 2. 2: Geological map of the BIC, showing three major limbs (courtesy of R.K.W Merkle).

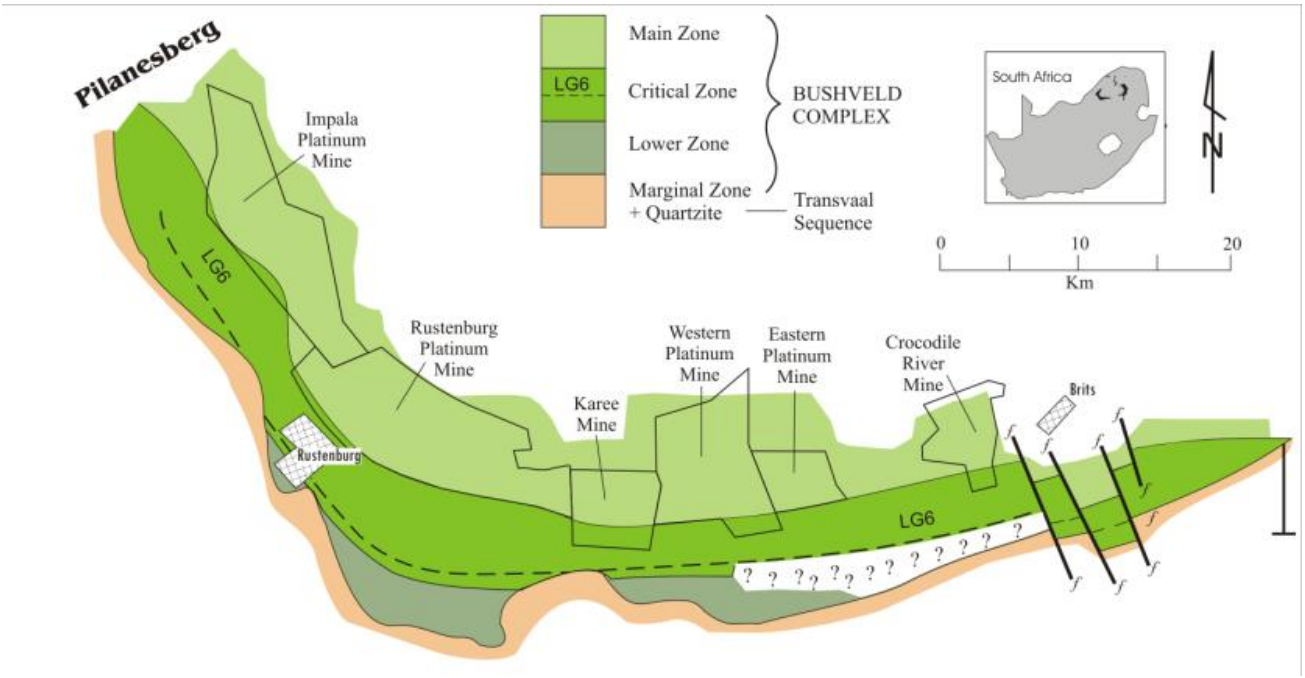

Figure 2. 3: Geological map showing the southern portion of the western limb of the BIC of South Africa (courtesy of RKW Merkle). The study area is in the Marikana section, in the southern part of the western limb of the BIC.

The Rustenburg layered suite (SACS 1980) is divided into five zones, known as the Marginal, Lower, Critical, Main, and Upper zones, from base to the top (Wager and Brown, 1968) (Figure 2.4).

The **Marginal Zone (MZ)** is marked by the presence of norite with minor pyroxenite (Schwellnus et al., 1962, Willemse, 1959, Engelbrecht, 1990, Kruger, 2005). Emplacement of this zone might be due to crystallization of contaminated magmas (Cawthorn et al., 2002). The approximately 1700m thick **Lower Zone (LZ)** is marked by the presence of dunite, harzburgite, and pyroxenite (Cameron, 1978). The LZ is also characterized by the absence of chromitite layers (Von Gruenewaldt et al., 1985). It is succeeded by the **Lower Critical Zone (LCZ),** which is marked by the presence of dunite, harzburgite, and pyroxenite. The rocks of the LZ and LCZ are ultramafic in nature (Scoon et al., 1994, Kruger, 2005). In the approximately 800 meter thick LCZ, nine chromitites layers are present, LG-1 to LG-7 and MG-1 to MG-2 (Von

Gruenewaldt et al., 1985). Plagioclase as a cumulus phase occurs for the first time above the MG-2 (Vermaak, 1975).

The **Upper Critical Zone (UCZ)** is marked by the presence of chromitite, pyroxenite, norite, and anorthosite. The rocks of the UCZ are ultramafic and noritic-anorthositic in nature (Scoon et al., 1994). Well defined thin layers of cumulus chromitite are present within this zone (Eales et al., 1990, Teigler et al., 1992, Maier and Eales 1994). In the UCZ, four chromitites layers are present, MG-3 to MG-4 and UG-1 to UG-2 (Davey, 1992, Scoon et al., 1994). The middle group chromitite overlap the boundary between the LCZ and UCZ (Davey, 1992, Scoon et al., 1994). Most of the economically significant PGM and chromitites are hosted within the UCZ (Vermaak, 1975, Von Gruenewaldt et al., 1985, Schouwstra et al., 2000), which is considered as the world largest platinum bearing ore body (Lee, 1996 and Kruger, 2005).

The UCZ is overlain by the **Main Zone (MZ),** which consists of pyroxenite, norite, anorthosite, and gabbro (Kruger 1990, 1994; Mitchell 1990, Mitchell et al., 1998; Nex et al., 1998). The MZ is subdivided into lower and upper MZ (Kruger, 1990). The MZ is overlain by the **Upper Zone** (**UZ**), which is the host of magnetite layers in the BIC (Molyneux, 1974).

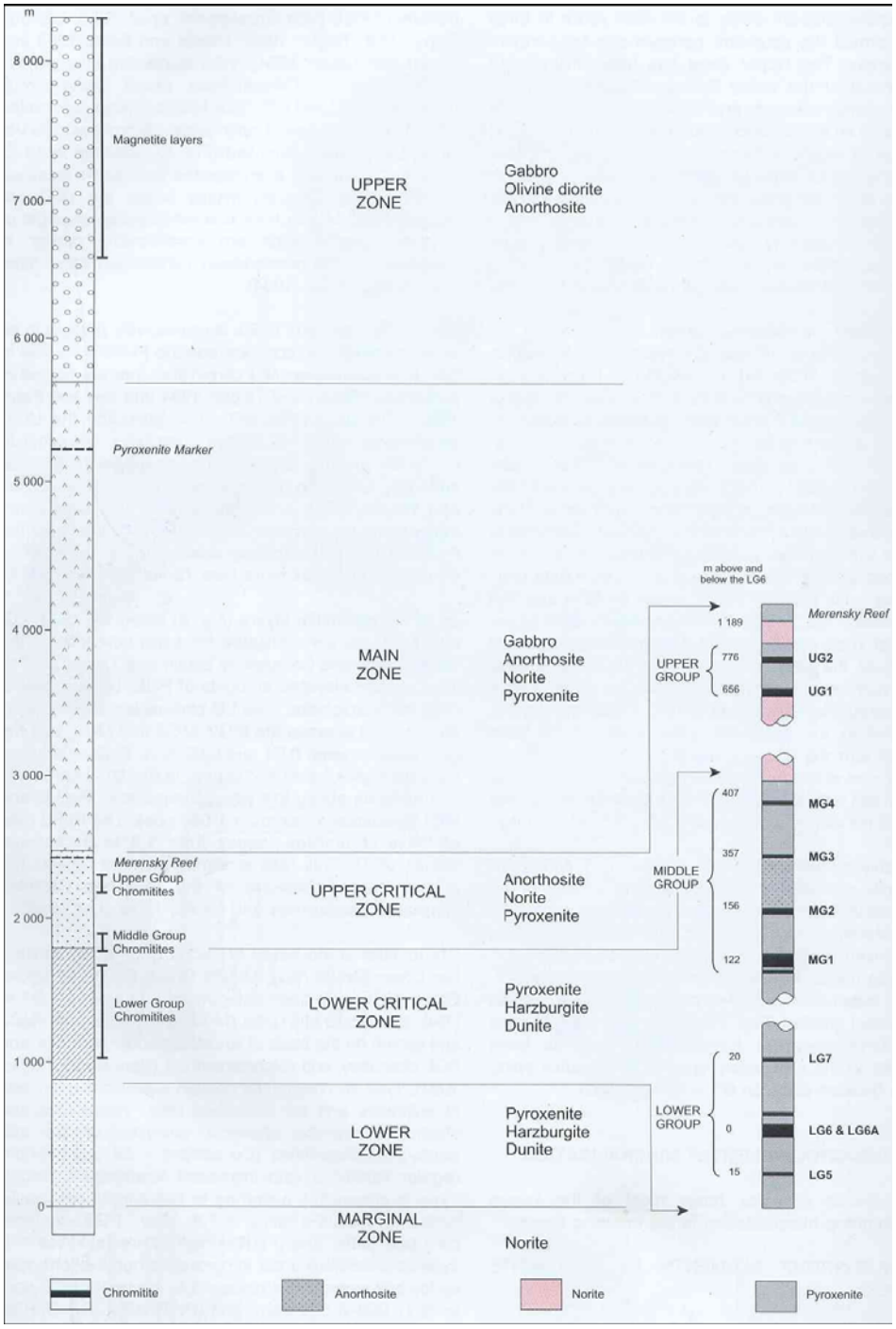

Figure 2. 4: Profile showing Subdivision of Rustenburg Layered Suite (Viljoen and Schurmann, 1998).

2.2. UG-2 Chromitite layer

The UG-2 chromitite layer is situated in the succession between UG-1 and Merensky Reef (MR). It is underlain by pegmatoidal feldspathic pyroxenite and overlain by feldspathic harzburgite (Eales and Reynolds, 1986, McLaren and de Villiers, 1982). The stratigraphic distance between the MR and the UG-2 varies along strike, but is typically smallest in the western limb (as little as 15 m) and up to 400 m in the eastern limb (Lee, 1996, Schouwstra et al., 2000).

The thickness of the UG-2 chromitite layer is approximately 0.15 to 2.55 m and has a dip angle that ranges between 5° and 70°, dipping towards the centre of the BIC (McLaren and de Villiers, 1982, Lee, 1996). The UG-2 chromitite layer can be traced for a distances of approximately 280 km (McLaren and de Villiers, 1982).

The UG-2 chromitite layer is mostly disturbed by faulting, both in the eastern and western limb. It is also affected by potholes that are circular in shape and ranges between 50 and 100 m (Viljoen and Hieber, 1986, Viljoen, 1994, Carr et al., 1994, Carr et al., 1999). It is considered to be the largest economic PGE resource on earth (Vermaak, 1975), and it is the only chromitite layer that is being currently mined for the PGM in the BIC (Maier, 2005).

2.2.1. Mineralogy in the UG-2 Chromitite layer

The UG-2 chromitite layer differs in proportion and distribution of PGE both in the western and eastern limb. The Pt/Pd ratio and the Rh are much higher in the western limb as compared to the eastern limb of the BIC (Lee, 1996). The PGM are predominantly interstitial to the chromitite grains (Lee, 1996).

Oxide minerals in the UG-2 chromitite layer are 60 – 90 percent in abundance, while major silicate minerals such as orthopyroxene are present (5 – 25 percent), and plagioclase (5 – 15 percent) (McLaren and De Villiers, 1982, Kinloch, 1982, Vermaak, 1985, Schouwstra et al., 2000, Ekmekci et al., 2003, Nel et al., 2005). The UG-2 chromitite layer also contains minor

amounts of clinopyroxene, biotite, phlogopite, talc, chlorite, quartz, serpentine, ilmenite, magnetite, rutile, and calcite (McLaren and De Villiers, 1982, Kinloch, 1982, Vermaak, 1985, Penberthy et al., 2000, Schouwstra et al., 2000, Cole and Ferron, 2002).

The UG-2 chromitite layer also contains Base Metal Sulphides (BMS), that are secondary in nature and they formed due to post magmatic processes (McLaren and De Villiers, 1982, Kinloch, 1982). The BMS that are present in the UG-2 chromitite layer in the order of abundance include; pentlandite ($(Fe, Ni)_9S_8$), chalcopyrite ($CuFeS_2$) with lesser pyrrhotite ($Fe_{1-x}S$), pyrite (FeS_2), and millerite (NiS) (McLaren and De Villiers, 1982, Kinloch, 1982, Peyerl, 1982,Vermaak, 1985, Liddell et al., 1986, Pentberthy et al., 2000, Schouwstra et al., 2000, Cole and Ferron, 2002).

BMS frequently occur in association with PGE bearing minerals (McLaren and De Villiers, 1982, Kinloch, 1982, Valenta, 2007). The Pt-Pd sulphides and telluride's are mostly associated with base metal sulphides (McLaren and de Villiers, 1982 and Penberthy et al., 2000). Laurite is commonly associated with chromite; this type of PGM is non-recoverable (Kinloch, 1982, Lee, 1996, Schouwstra et al., 2000).

The most dominating PGM in the UG-2 Chromitite layer are usually grouped in the following manner:

- PGE sulphide (laurite, cooperite, braggite, vysotskite, and malanite). Comprise 70percent of the PGE in the UG-2 (Liddell et al., 1986, Cole and Ferron, 2002, Nel et al., 2005)
- PGE iron alloy
- PGE bismuth telluride
- PGE arsenide sulphide

The UG-2 also contains minor phases of PGE with Hg, Pb, Ge, Sb, As, Bi, Te, and Sn (Kinloch, 1982, McLaren and De Villiers, 1982, Penberthy and Merkle, 1999, Schouwstra et al., 2000, Cole and Ferron, 2002, Nel et al., 2005).

3. Mineral beneficiation

The process of mineral beneficiation consists of comminution and concentration (figure 3.1). Comminution is divided into crushing and milling stages, while concentration is a stage where by PGM are recovered using flotation (Ekmekci et al., 2003, Merkle and McKenzie, 2002, Becker et al., 2008).

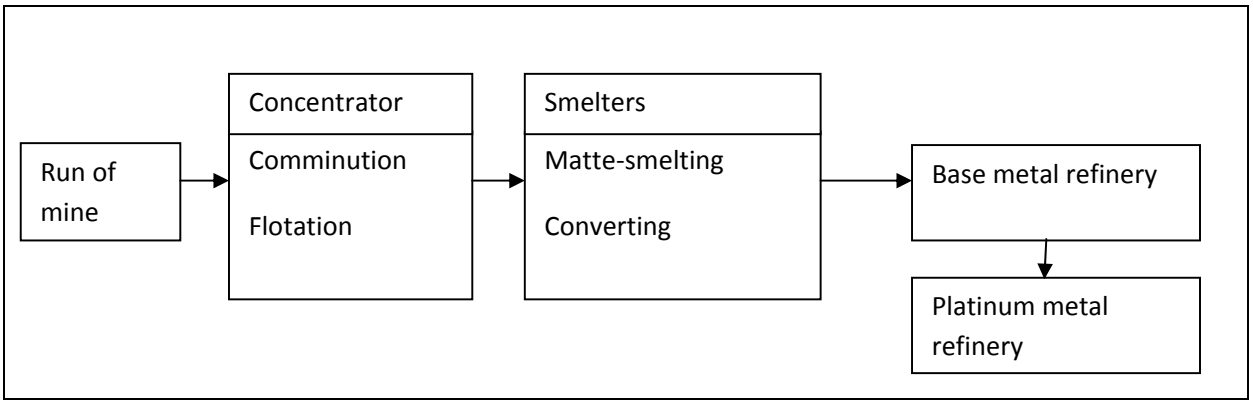

Figure 3.1: Ore beneficiation process, South Africa.

3.1. Comminution

Comminution is a process whereby valuable ore minerals are liberated from silicates and oxide minerals, by means of crushing and milling (figure 3.2). Different metallurgical plants use different crushers, but conventional or jaw crushers are usually used (Merkle and McKenzie, 2002).

For the purpose of milling, standard rod or ball mills are used. The type of milling that is usually conducted is divided into two stages. The first stage uses closed circuit for primary milling, which uses screens for size classification. It reduces the particle size to approximately 50 percent by mass to less than 75 µm (Merkle and McKenzie, 2002, Valenta, 2007). During primary milling the detachment of small PGM grains is avoided (Merkle and McKenzie, 2002).

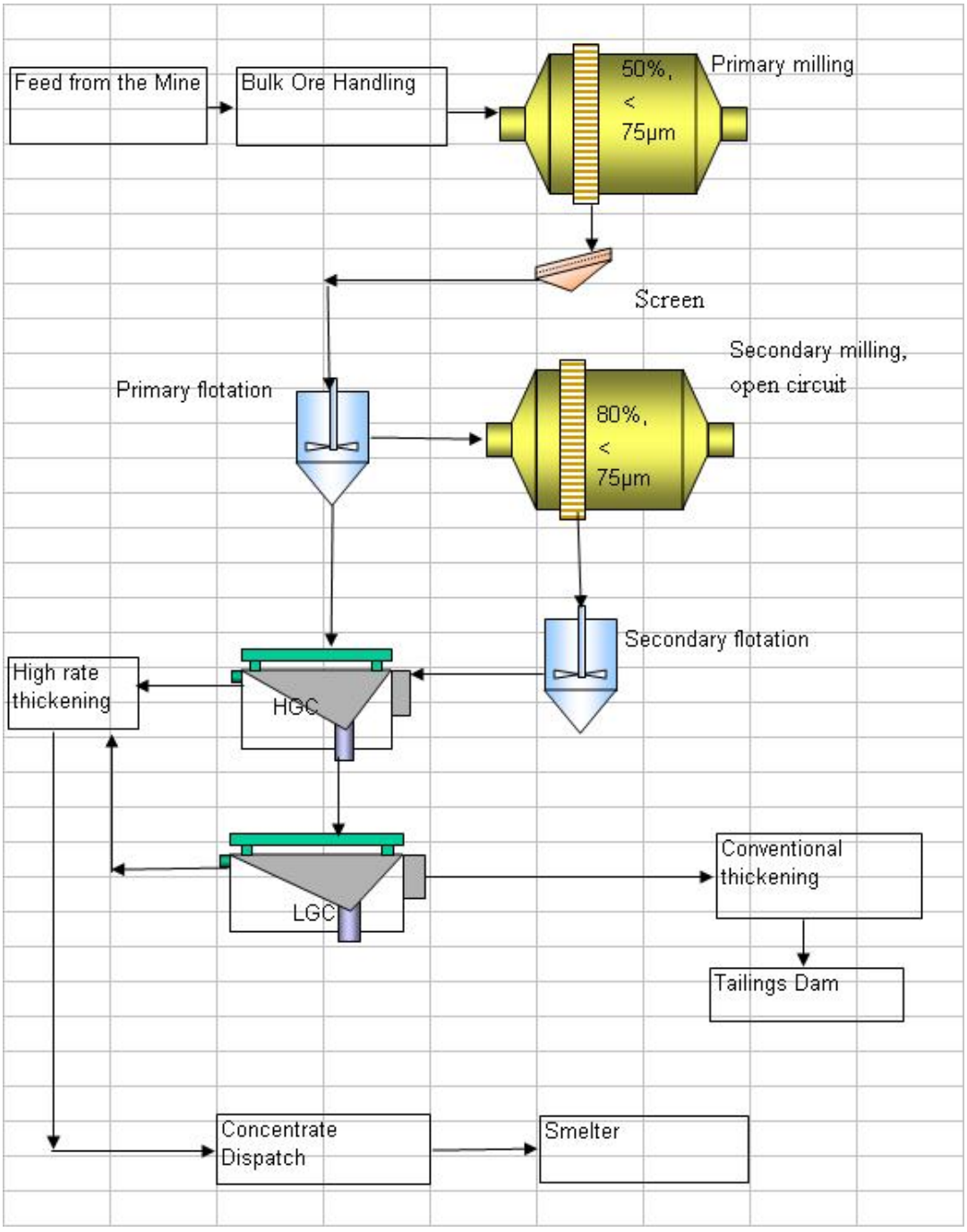

Figure 3. 2: Schematic representation of MF2 plant, indicating the primary, and secondary milling, primary, and secondary flotation. It also indicates the high grade cleaner (HGC) and low grade cleaner (LGC). In the MF2 plant a high grade fast floating and a low grade slow floating concentrate are produced (Merkle and McKenzie, 2002).

The second stage of milling uses an open circuit for secondary milling, which uses cyclones for size classification. It reduces the particle size to approximately 80 percent by mass to less than 75 µm. During this stage, the small PGM grains locked in the gangue minerals are released (Merkle and McKenzie, 2002).

Strict measures are put in place so as not to over mill, since this will create fine grained material. Fine grained material doesn't usually float. This will lead to valuable materials not being recovered during the process of flotation (Merkle and McKenzie, 2002).

3.2. Concentration

3.2.1 Froth flotation

In the process of froth flotation, hydrophobic minerals such as sulphides and PGM are attached to air bubbles, rising through the pulp under specific chemical conditions (Penberthy, 2000, Merkle and McKenzie, 2002, Valenta, 2007). The bubbles will be transported to the surface of the pulp and form a stabilized froth. The froth will be skimmed off while the gangue minerals remain submerged in the pulp (Penberthy, 2000, Valenta, 2007).

PGM and BMS in the platiniferous UG-2 are recovered by the process of froth flotation, in order to produce bulk concentrate (Becker et al., 2008, Ekmekci et al., 2003, Schouwstra et al., 2000). Their recovery is determined by their surface characteristics (Penberthy et al., 2000, Merkle and McKenzie, 2002). The fine grained material doesn't usually float; instead it reports to the concentrate by means of entrainment. The recovery of PGM and BMS is affected by the presence of talc, chromite, and pyroxene (Martinovic et al., 2004).

Chromite and pyroxene which are hydrophilic in nature have a tendency of reporting to the concentrate by means of entrainment (Ekmekci et al., 2003, Wesseldijk et al., 1999, Merkle and McKenzie, 2002, Martinovic et al., 2004, Nel et al., 2005, Valenta, 2007). The chromite content in the final concentrate must not exceed 5 percent, because it reduces the efficiency of the

smelting process, since some of the spinel minerals become stable at 2000°C (Ekmekci et al., 2003, Wesseldijk et al., 1999, Merkle and McKenzie, 2002, Martinovic et al., 2004, Valenta, 2007). It must not be allowed to deposit into the furnace, since it will cause build up in the furnace hearth and reduces the furnace volume (Jones, 1999). Chromite will also form an impermeable barrier between matte and slag, thereby causing a tapping problem (Merkle and McKenzie, 2002).

Naturally floating talc has a tendency of enhancing the froth stability, and increases the entrainment of other silicate minerals (Merkle and McKenzie, 2002, Martinovic et al., 2004). The presence of silicate minerals in the final concentrates affects the grade of the concentrate negatively, hence it is undesirable (Merkle and McKenzie, 2002).

Different chemicals are utilized in the flotation cells to help recover the PGM. The most utilized reagents in the UG2 flotation cells includes copper sulfate ($CuSO_4$) as an activator, to enhance the adsorption of the thiol collectors to the sulphide mineral surface, thereby causing sulphide minerals to float and separate them from silicate and oxide minerals (table 3.1, Wesseldijk et al., 1999).

Table 3.1: Reagents used in froth flotation (Summary operations of one of the primary circuit of South African conventional concentrator.

Reagents grams per ton	**Reagents grams per ton**	**Reagents grams per ton**	**Reagents grams per ton**	**Strength**		
Activator	**Collector**	**Depressor**	**Frother**	**Activator**	**Collector**	**Depressor**
150.00	170.00	80.71	16.57	5percent	10percent	2percent

To ensure that the naturally floatable silicate and oxide minerals do not float, depressant such as carboxy methyl cellulose (CMC) are added to the system (Harris, 1982, Wesseldijk et al., 1999, Buswell et al., 2002, Ekmekci et al., 2003, Vos et al., 2007). Complete depression of unwanted mineral phase could lead to loss of valuable mineral phases; therefore care should be taken when depressing unwanted phases (Merkle and McKenzie, 2002).

Collectors such as xanthane and dithiophosphates are used to adsorb sulphide minerals. DOW200 (derived from polyglycol ethers) is used as a frother (Harris, 1982, Wesseldijk et al., 1999, Buswell et al., 2002, Ekmekci et al., 2003, Vos et al., 2007). DOW200 is the most stable frother that is soluble in water and produce stable dense froth structures (Ekmekci et al., 2003). This reagents suite is mostly used to maximize the recovery of PGM and BMS (Wesseldijk et al., 1999, Vos et al., 2007).

4. Sampling

The sampling campaign took place at the primary circuit of a South African conventional concentrator (SACC). This conventional concentrator circuit is a mill-float-mill-float (MF 2) plant, treating the ore from the western limb of the Bushveld Igneous Complex. In the MF2 plant, ore from bulk ore handling is coarsely milled (closed circuit milling), screened, and floated in the primary roughers in the first stage. In the second stage, ore is again milled, and floated in the secondary roughers (Schouwstra et al., 2000, Merkle and McKenzie, 2002, Nel et al., 2005).

4.1. Plant conditions

During the sampling campaign at the primary circuit of SACC, four thousand five hundred and seven (4507) tons of ore were milled, with 188 tons milled per hour. The run time availability for primary and secondary mill was 24 hours at 100 percent.

The primary mill had an average power consumption of 1676 kW and the secondary mill had an average power consumption of 1750 kW. The average flow rate for the primary rougher feed was

301.72 m^3/h. The specific gravity was 1.48. The average flow rate for the primary rougher tail was 260.27 m^3/h.

The primary rougher feed had a grading of 49.5 percent smaller than 75.00 µm, while that of the secondary rougher feed was 73.8 percent smaller than 75.00 µm. The tonnage of the high grade UG-2 concentrate is approximately 51.37, and the grade is approximately 223.595 grams per ton (table 4.1 indicates). The nickel plus copper content is approximately 1.36 percent, with a chrome content of approximately 2.67 percent.

Table 4.1: Concentrate dispatched – high grade (HG) (Summary operations of one of the primary circuit of South African conventional concentrator).

CONCENTRATE DISPATCHED - HG				
Tons	**PGE** **grams per ton**	**PGE** **kg**	**(Ni+Cu)** **Weight percent**	**Cr_2O_3** **Weight percent**
51.373	223.595	11.487	1.36	2.67

The PGE in the head grade is approximately 3.08 grams per ton, with nickel and copper contents of approximately 0.023 percent and 0.012 percent (Table 4.2). The PGE in the tail grade is approximately 0.74 grams per ton, with nickel and copper contents of approximately 0.012 percent and 0.006 percent (Table 4.2).

Table 4.2: Head grade and tail grade (Summary operations of one of the primary circuit of South African conventional concentrator).

HEAD GRADE			**TAIL GRADE**		
PGE grams per ton	**Ni percent**	**Cu percent**	**PGE grams per ton**	**Ni percent**	**Cu percent**
3.08	0.023	0.012	0.74	0.012	0.006

The tons that were produced during the time of sampling had the recovery of approximately 80.84 percent. This was achieved with a mass pull of about 1.18 percent (table 4.3).

Table 4.3: Concentrate produced and mass pull (Summary operations of one of the primary circuits of a South African conventional concentrator).

Concentrate produced	**RECOVERY**	**MASS PULL**
Tons	**percent**	**percent**
53.00	80.84	1.18

4.2. Sampling

The samples were collected from the primary rougher circuits, of a South African conventional concentrator. At the time of sampling, the ore that was being treated was from a single mining area. Thirty six (36) samples were taken from the primary rougher feed (PRF), primary rougher concentrate (PRC 1 – PRC 10), and primary rougher tail (PRT). Triplicate samples were taken from each cell, using 20-litre buckets. The sampling campaign lasted for of five hours, under stable plant conditions.

4.3. Sample preparation

The samples that were obtained from the primary rougher circuit of South African conventional concentrator were prepared at Mintek, mineral processing division, to obtain a laboratory sample.

4.3.1. Sample preparation procedure

Samples that were obtained from the primary rougher circuit of South African conventional concentrator were weighed, to obtain the mass of the bucket plus wet samples. Samples were then filtered using a 20-litre filter pot and a 3.2 mm filter paper (Figure 4.1).

Figure 4.1: Filtration system, MINTEK South Africa.

After the process of filtration, the samples were air dried for two days. Samples were placed away from each other in order to minimize contamination. The mass of the dry samples was then recorded.

Figure 4.2: Samples after drying, MINTEK, South Africa.

Dried samples were then screened using 850 µm sieve and a rubber bar (Figure 4.3). Individual samples were blended (blending is a process whereby a sample is thoroughly mixed until it becomes homogeneous) and a representative sample was taken from each sample. One kilogram (1 kg) was taken from each bulk sample. Then three, one kilogram (1 kg) samples were mixed and blended together to create a composite sample (a representative of the three buckets). One kilogram (1 kg) was then sampled from the composite sample to represent the three buckets. A spinning riffle was used for sample size reduction.

Figure 4.3: Screening of sample using 850 µm sieve and a rubber bar.

The one kilogram (1 kg) sample was reduced further to 300 g sample and 700 g sample. The 300 g sample was milled using a tungsten carbide steel milling pot for sixty seconds. After the process of milling, the sample was sent to Analytical Service Division for the analysis of 6E's, (i.e. platinum (Pt), palladium (Pd), rhodium (Rh), ruthenium (Ru), iridium (Ir), and gold (Au)), acid solubility (chromium (Cr), iron (Fe), nickel (Ni), copper (Cu), cobalt (Co)), and total sulphur (S) (see analytical methods, chapter 5 for details). Twenty grams (20 g) was also obtained for XRD analysis. The remainder of the uncrushed sample was used for polished section preparation.

4.4. Polished section preparation

A rotary splitter was used to obtain a representative sample for polished section preparation and to minimise errors. One gram (1g) sample was weighed into a 10 ml pill vial bottle. The sample was then mixed with one gram (1g) graphite (passing 38µm). The sample was again mixed with

4ml resin mixed with hardener. The sample was then mixed thoroughly and placed in vacuum overnight to cure. After curing, the resin impregnated sample vial, the vial was cut into two equal halves using the Struers labotom-3 cutter with a corundum cut-off wheel of 32 mm in size. The reason for cutting the sample into two equal halves is to compensate for possible segregation of heavy particles that settle to the bottom (gravity separation).

Samples were placed into a mould, with resin mixed with hardener, after they were placed into a vacuum to cure, then ground using 200, 600, and 1200 µm grinding disc. After the process of grinding, they were then polished using a Saphir 550 polishing machine with 6, 3, and 1 µm polishing cloths and diamond suspension. Lastly the samples were carbon coated and ready to be used for image analysis.

During polished section preparation, rip outs of sample must be avoided, since this might lead to loss of information during image analysis, also contamination must be avoided, since this can introduce errors during image analysis measurement. Source of contamination could be a cut off-wheel that is used to cut the samples. The polishing cloth and the grinding material could also lead to cross contamination when not cleaned properly during the process of grinding and polishing.

5. Methods

5.1. Chemical analysis

Chemical analyses were undertaken at Mintek Analytical Service Division (ISO 9001 and 17025 accredited), using fire assay techniques with nickel sulphide as a collector, followed by crushing, leaching, and dissolution of the nickel sulphide button in aqua-regia (Gros et al., 2002). ICP-OES with a detection limit of 0.1 parts per million was used for the analysis of 6E's.

Nickel (Ni), copper (Cu), cobalt (Co), and iron (Fe) were analysed by ICP-OES. The analyses were carried out by preparing a fusion sample of 0.2 g, with sodium peroxide flux, leached in water and HCL. The solution is made up to volume in a volumetric flask (200 ml) with internal standard and analysed with a Varian Vista Pro.

For carbon (C), and sulphur (S) determination, either the LECO CS200 or the Eltra CS2000 was used. The principle of analysis for C and S by combustion is basically the same. A portion of the sample is weighed into a ceramic crucible, along with an accelerator (iron chip, or tungsten, depending on the element required and the concentration level). The crucible is placed into the instrument, where it moves into the furnace chamber. The sample is heated by induction, and melts. The sulphur present is released as SO_2 and carbon as CO_2, and travels in a stream of high-purity oxygen to the infrared detector.

Before analyzing the samples, certified reference material of similar matrix are analysed, and the signal intensity is used to calibrate the instrument. (Blanks – reagent only with no sample – and other reference materials (sarm 77 and sarm 71) are also analysed to confirm the results).

5.2. Mineralogical analysis

5.2.1. X-ray diffraction spectroscopy (XRD) - phase analysis of UG-2 material.

The XRD analyses were carried out at the University of Pretoria in the X-ray analytical facility, Department of Geology. The samples were prepared for XRD analysis using a back loading preparation method (Loubser and Verryn, 2008). They were analysed with a PANalytical X'Pert Pro powder diffractometer. The XRD was coupled with X'Celerator detector, and variable divergence, and receiving slits with Fe filtered Co-Kα radiation (Figure 5.1) (Loubser and Verryn, 2008). The phases were identified using X'Pert High score plus software ®. The relative phase amounts (weight percent) were estimated using the Rietveld method (Young, 1993, Liu and Kuo, 1996) using the Autoquant Program (Kleeberg and Bergmann, 1998 and 2002). Errors are on the 3 sigma level (Table 1, Appendix b).

Figure 5. 1: X'Pert Pro PANalytical x-ray diffractometer at Department of Geology, University of Pretoria.

5.3. Mineral Liberation Analyzer (MLA)

In process mineralogy, mineral liberation analyzer (MLA) (Gu, 2003) and quantitative evaluation of minerals using scanning electron microscopy (QEMSCAN) (Gottlieb, 2000) are basically known as automated SEM (Sutherland et al., 1988, Gottlieb et al., 2000, Sutherland, 2007, Lastra, 2007). They are accurate, fast, and user friendly techniques. This was made possible by the recent developments in the fields of electronic and computing technology. The developments were made to ensure that the automated SEM can handle more samples in a short period of time and produce more data (Sutherland et al., 1988, Weller et al., 1996, Gottlieb et al., 2000, Gu, 2003).

Automated SEM coupled with EDS detectors are used for quantitative and qualitative analysis of minerals (Jones, 1987, Sutherland and Gottlieb, 1991, Gottlieb et al., 2000). Data that is acquired from the automated SEM is mostly used in processing plant design and optimization (Gottlieb et al., 2000, Gu, 2003).

The automated SEM consists of a software and hardware module, which is coupled with a scanning electron microscope (SEM) (Sutherland et al., 1988, Gottlieb et al., 2000). The SEM collects raw data, constructs digital images, and process data (Sutherland et al., 1988, Weller et al., 1996, Gottlieb et al., 2000). It uses the backscattered electron (BSE) image intensity and energy dispersive X-ray spectra (EDX), to give information about the minerals under investigation (Sutherland et al., 1988, Sutherland and Gottlieb, 1991, Gottlieb et al., 2000, Goodall et al., 2005). Minerals are identified by their chemical composition using low EDX spectra preferential to BSE brightness (Gottlieb et al., 2000, Goodall et al., 2005).

Minerals with similar X-ray spectra and backscatter electron image, are usually differentiated from each other by their element ratios. Those with similar X-ray spectra, but different backscatter electron intensity are usually differentiated with their backscatter electron intensity

(Sutherland et al., 1988, Sutherland and Gottlieb, 1991, Gottlieb et al., 2000, Goodall et al., 2005).

5.3.1. BSE Image analysis

For the purpose of this investigation, MLA was utilized for the PGM search.

Imaging and image analysis are important in mineral liberation analysis, since they are the fundamentals of mineral identification in automated SEM technology. In MLA, it is highly recommended to use low noise images, in order to do proper mineral identification, and quantification (Gu, 2003, Fandrich et al., 2007).

The two most important functions used in image analyses, for the purpose of mineral liberation analysis include; de-agglomeration and image segmentation. Agglomeration occurs during the stage of drying and sample preparation for polished sections, when the sample in the form of fine particles is mixed with graphite in an epoxy resin (Sutherland and Gottlieb, 1991, Gottlieb et al., 2000, Gu, 2003). During this stage, some of initially liberated particles may touch each other, leading to biased liberation results, if not treated properly (Sutherland and Gottlieb, 1991, Gottlieb et al., 2000, Gu, 2003). During image analyses, when agglomeration has been detected, the automated de-agglomeration function will attempt to separate it. The de-agglomeration function can be performed both offline and online (Gu, 2003, Fandrich et al., 2007).

Image segmentation plays an important role in determining the boundaries of a particle and identifying each mineral grain in the particle (Gu, 2003). It outlines the regions of homogeneous BSE in a particle image (Gu, 2003). A mineral of a unique average atomic number is directly related to a specific average BSE intensity (Sutherland and Gottlieb, 1991, Gu, 2003). Minerals that have similar average atomic number can be further differentiated using X-ray analysis (Sutherland and Gottlieb, 1991, Gu, 2003). MLA uses de-agglomeration and Image segmentation functions, to perform proper mineral identification, and quantification within the particles (Gu, 2003, Fandrich et al., 2007).

5.3.2. Mineral identification with X-ray analysis

In MLA, three x-ray analysis techniques are used to identify mineral species:

1.) Point x-ray – is mostly used for modal analysis (Sutherland and Gottlieb, 1991, Gu, 2003).

2.) Area x-ray – is mostly used to produce mineralogical data, including liberation information (Weller et al., 1996)

3.) X-ray mapping – X-ray analysis method is widely used when a sample contains two mineral phases with the same average atomic number and these phases are attached to each other (Gu, 2003). During x-ray analysis, a regular grid will be imposed on a particle image and x-ray data will be collected at each grid point to determine the mineral identity (Gu, 2003).

MLA can be operated in seven measurement modes. These are:

1.) Standard BSE liberation analysis (BSE)

In the liberation analysis method, images are collected on-line and then processed off-line to produce liberation data. BSE grey level distribution determines mineral identification. This method relies only on image analysis (Fandrich et al., 2007). Minerals with sufficient grey level contrast are suitable for this method e.g. lead-zinc ores and copper sulphide ores (Gu, 2003).

2.) Extended BSE liberation analysis (XBSE)

In this method, BSE images are collected and segmented, the X-rays are used to efficiently and effectively analyze mineral grains of complex ore samples (Gu, 2003, Fandrich et al., 2007).

3.) Grain-based X-ray mapping (GXMAP)

Phases that can not be segmented by the BSE grey levels are usually mapped by the GXMAP. This is achieved by employing the faster X-ray analysis for phases that are readily segmented (Fandrich et al., 2007). It is widely used for identifying sulphide

minerals such as sphalerite and chalcopyrite ores, as well as complex nickel ores containing pentlandite as fine flames in pyrrhotite (Fandrich et al., 2007)

4.) Sparse phase liberation analysis (SPL)

XBSE analysis is performed on particles of interest. BSE images containing particles of interest are searched using BSE grey level scale (Gu, 2003). The processing is performed off line. This method is designed to handle tailings and low grade feed ores such as platinum ores (Gu, 2003, Fandrich et al., 2007).

5.) X-ray modal analysis (XMOD)

In this method mineral identification is determined by one X-ray analysis at each counting point (Fandrich et al., 2007). Particle matter can be discriminated from the back ground by the use of BSE imaging and one x-ray spectrum from each grid point across the particle can be collected (Fandrich et al., 2007). This technique is useful for providing the modal mineralogy information (Fandrich et al, 2007).

6.) Rare phase search (RPS)

BSE images for the phases of interest are searched using an X-ray trigger (a trigger is a method that is used to target grains of interest, within particles to be mapped by using a grey scale), and the corresponding characteristic X-ray spectrum is collected. The image found will be saved by the system together with its stage location and its X-ray spectrum (Fandrich et al., 2007). Rare phase search technique is suitable for locating very fine grained components in large particle population e.g. gold in tailings (Fandrich et al., 2007).

7.) Latti analysis (SXBSE)

This method compensates for the elemental quantification to the XBSE analysis. An X-ray trigger standard is employed in the similar way as in the GXMAP mode (Fandrich et al., 2007).

For the purpose of PGM research on the MLA, Sparse Phase Liberation analysis (SPL) was used to do the PGM identification. In this method, images are collected and segmented. The X-rays are used to efficiently and effectively analyze particles of interest. BSE images containing particles of interest are searched using a BSE grey level scale (Gu, 2003, Fandrich et al., 2007). "The measurement mode combines the advantage of a rapid search, for the phase of interest at low resolution (1024*800), and that of accurate imaging at high resolution (up to 4096 * 3200)" (Fandrich et al., 2007). The processing is performed off line. This method is designed to handle tailings and low grade feed ores such as PGM (Gu, 2003, Fandrich et al., 2007).

5.3.3. Analysis by Mineral Liberation Analyzer (MLA)

The FEI Quanta 600 (Figure 5.2) at MINTEK mineralogy division was used to perform the PGM search. The SEM of the FEI Quanta 600 is coupled with two EDAX detectors. The instrument was operated with a voltage of 25 kV, and the beam current of 40 µA. The counting time was approximately 40 – 50 milli seconds (mS). The magnification was set to 300 times and the spot size of 7.6 µm. The grey level was between 140 and 250, and that of the gold standard was between 250 and 252.

Figure 5. 2: FEI Quanta 600, Mineral Liberation Analyzer at MINTEK, South Africa.

5.3.4. PGM identification

PGM in the UG-2 chromitite layer are generally small, mostly less than 5 µm. This makes it difficult to analyze and characterize the PGM (McLaren and de Villiers, 1982, Pentberthy et al., 2000).

In the feed and tailings samples of the UG-2, there is a low concentration of PGM. In order to obtain statistically reliable data, large numbers of polished sections must be prepared and analyzed. For the concentrate samples, smaller numbers of polished sections were prepared for high grade concentrates, to obtain statistically reliable data. Large numbers of polished sections were prepared for low grade concentrates.

During the time of investigation, the samples that were used for polished section preparation were un-sized and diluted with graphite. The prepared polished sections were placed in a round holder that carriers fourteen polished sections (Figure 5.3).

Figure 5.3: 14 sample holder round (JK tech ops training 2008).

Fully automated search of PGM was done without attempting to classify the grains. PGM have higher average atomic weight, therefore their BSE image appear much brighter. The potential PGM are identified based on the concept of high BSE intensity.

5.4. Electron probe micro analyzer (EPMA)

The EPMA analyses were contracted out at Laboratoire de Microanalyse - Universite Laval, Canada. The analyses were performed by the CAMECA SX50 electron microprobe. It was operated at a voltage of 15 kV and current of 20 nano amps (nA), with a beam diameter of 2 – 5 µm. Run time data was acquired for 15 seconds peak count. Type of detectors used includes wavelength dispersive spectroscopy (WDS) proportional counters using PET, LIF crystals.

The main objective of the analysis of PGE with electron microprobe was to identify and characterize the PGM in the primary rougher cells at less than ten microns, and to confirm

whether the MLA identified the PGM grains correctly. PGM in the primary rougher cells have very small grain sizes due to crushing and milling, making it difficult to analyze with electron microprobe. The elements that were analyzed for with wavelength dispersive x-ray analysis includes; Fe, Co, Ni, Cu, Os, Ir, Te, Sb, Sn, Pd, Rh, Pt, Hg, S, Pb, Bi, Ru, As.

6. Results

The samples that were obtained from SACC are suspensions with 10 to 40 percent solids. Primary rougher feed (PRF) and primary rougher tail (PRT) have higher percentages of solids, as compared to primary rougher concentrates (PRC). The percentages of solids of PRF and PRT are above 40 percent. In the primary rougher circuit the percentages of solids decreases from PRC 1 to PRC 4, then remains fairly constant from PRC 5 to PRC 10 (Figure 6.1).

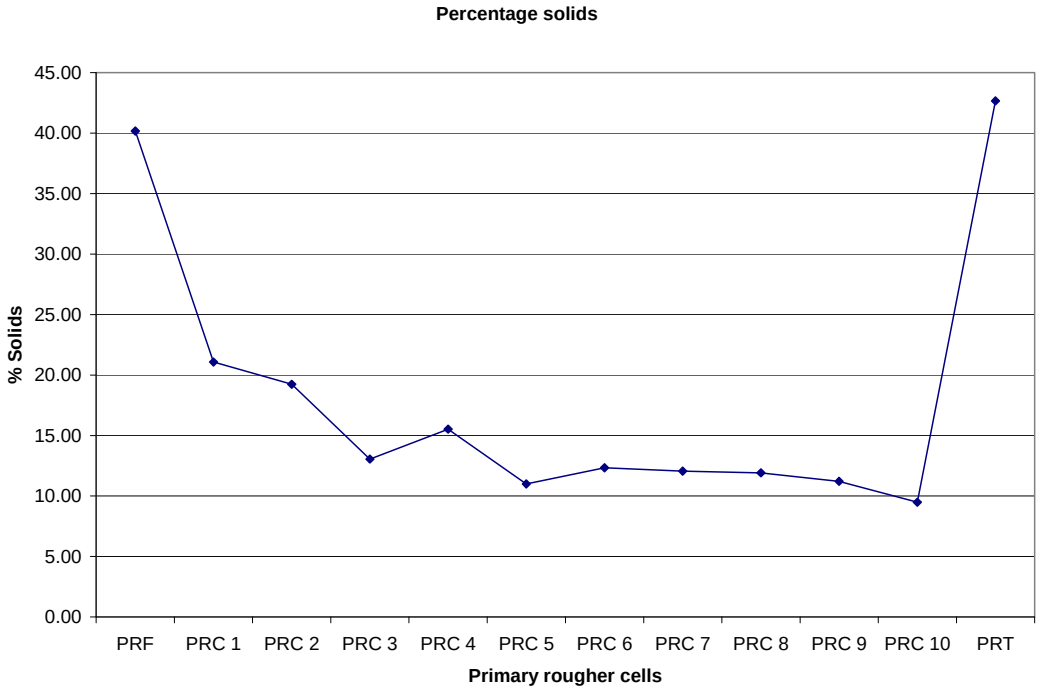

Figure 6.1: Percentage solids of samples in the primary rougher circuit.

6.1. Concentration of PGE

Analyses of PGE were carried out using ICP-OES, at Mintek Analytical Service Division. The results were reported in parts per million (or grams per ton) (Figure 6.2)

Table 6.1: grade of 6E's (grams per ton)

	grade of ore (grams per ton)
PRF	5.51
PRC 1	199.48
PRC 2	101.3
PRC 3	44.51
PRC 4	38.15
PRC 5	26.02
PRC 6	24.7
PRC 7	18.37
PRC 8	23.09
PRC 9	20.45
PRC 10	13.96
PRT	1.81

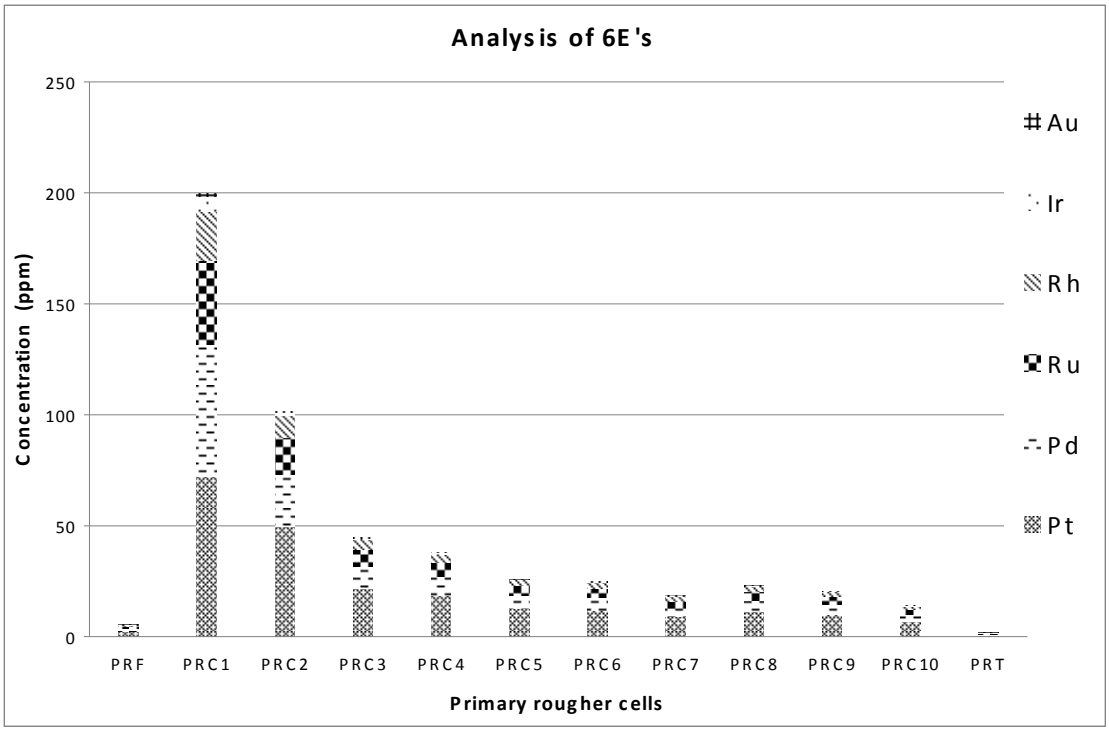

Figure 6. 2: Analysis of 6E's using ICP OES. From bottom to top: Pt, Pd, Ru, Rh, Ir, and Au.

The grade of the UG-2 chromitite layer is approximately 5.5 grams per ton in the feed sample (Ekmekci et al., 2003, Valenta, 2007, Voordouw et al., 2010). The ratio of Pt and Pd in PRF is 2:1 (Table 6.1 and Figure 6.3). The dominant PGE in order of decreasing abundance is Pt, Pd, Ru, and Rh, with Ir, and Au occurring as minor elements. The values of Pt/ (Pt+Pd) and Cu/ (Cu+Ni) are 0.6 and 0.2 respectively.

The grade of PGE in primary rougher circuit decreases, going down along the circuit (Table 6.1 and Figure 6.2). PRC 1 has the highest grade of PGE, approximately 200 grams per ton, followed by PRC 2, with the grade of approximately 100 grams per ton (Table 6.1 and Figure6.2 and 6.4). PRC 3 and PRC 4 have moderate grades of PGE. The grade ranges from 38 to 44 grams per ton. The grade is almost half of PRC 2. The ratio of Pt and Pd in PRC 3 and PRC 4 is 2:1 (Table 6.1 and Figure 6.5).

Low grade of PGE occurs from PRC 5 to PRC 10. The grade ranges from 26 grams per ton to 14 grams per ton. The ratio of Pt and Pd in these cells is also 2:1 (Table 6.1 and Figure 6.6).

PRT has a low grade of approximately 1.81 grams per ton (Table 6.1 and Figure 6.7).

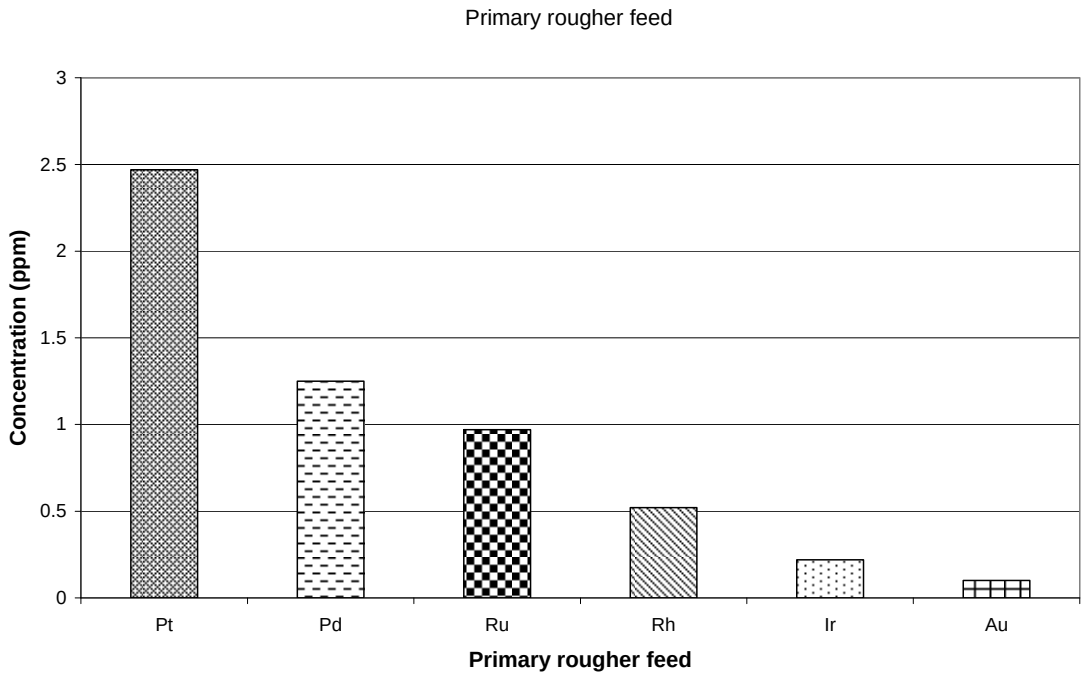

Figure 6. 3: Analysis of 6E's using ICP-OES on the PRF sample.

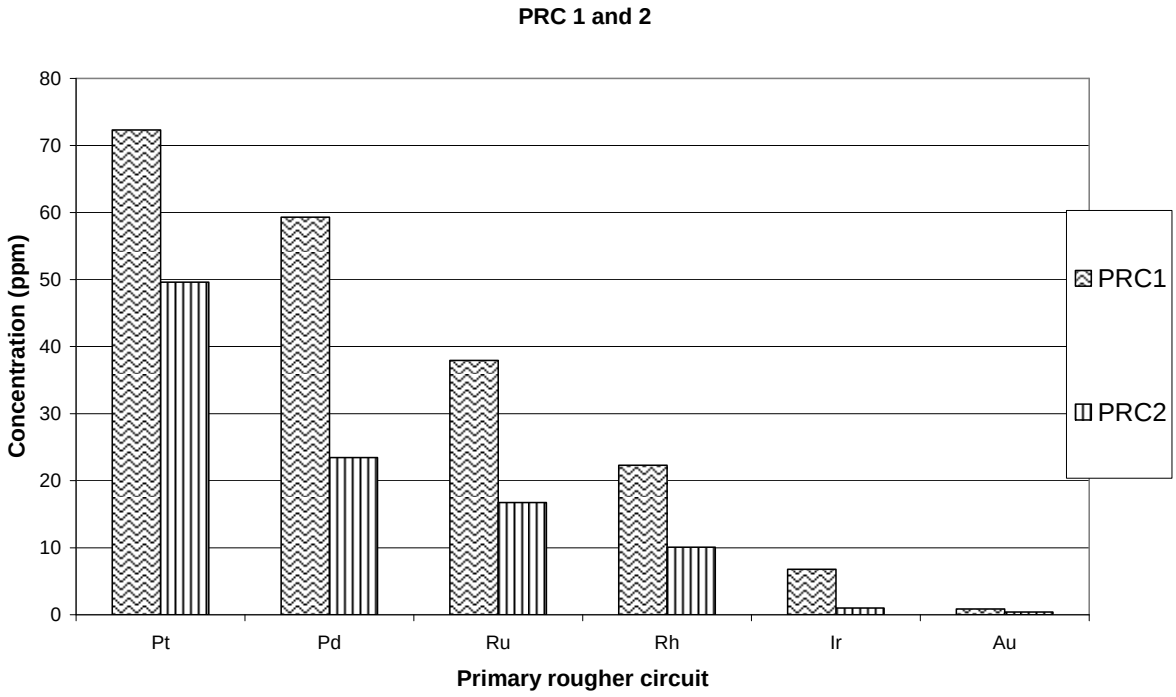

Figure 6. 4: Analysis of 6E's using ICP-OES on PRC 1 and PRC 2.

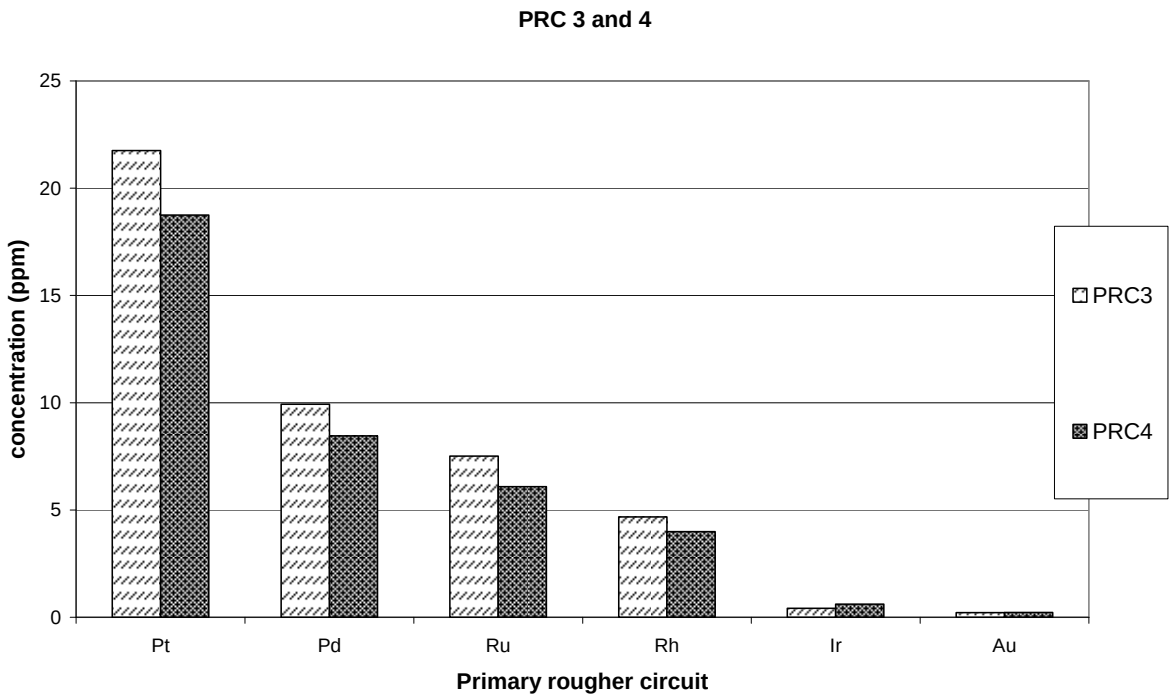

Figure 6. 5: Analysis of 6E's using ICP-OES on the PRC 3 and PRC 4.

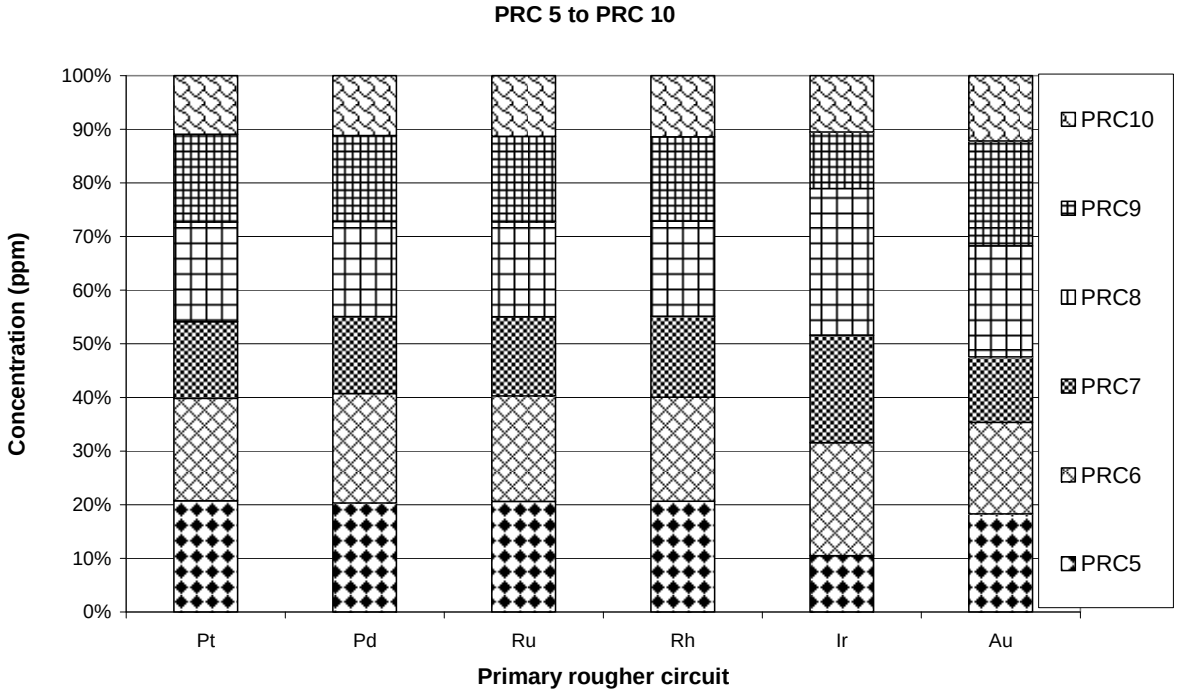

Figure 6. 6: Analysis of 6E's using ICP-OES on the PRC 5 to PRC 10.

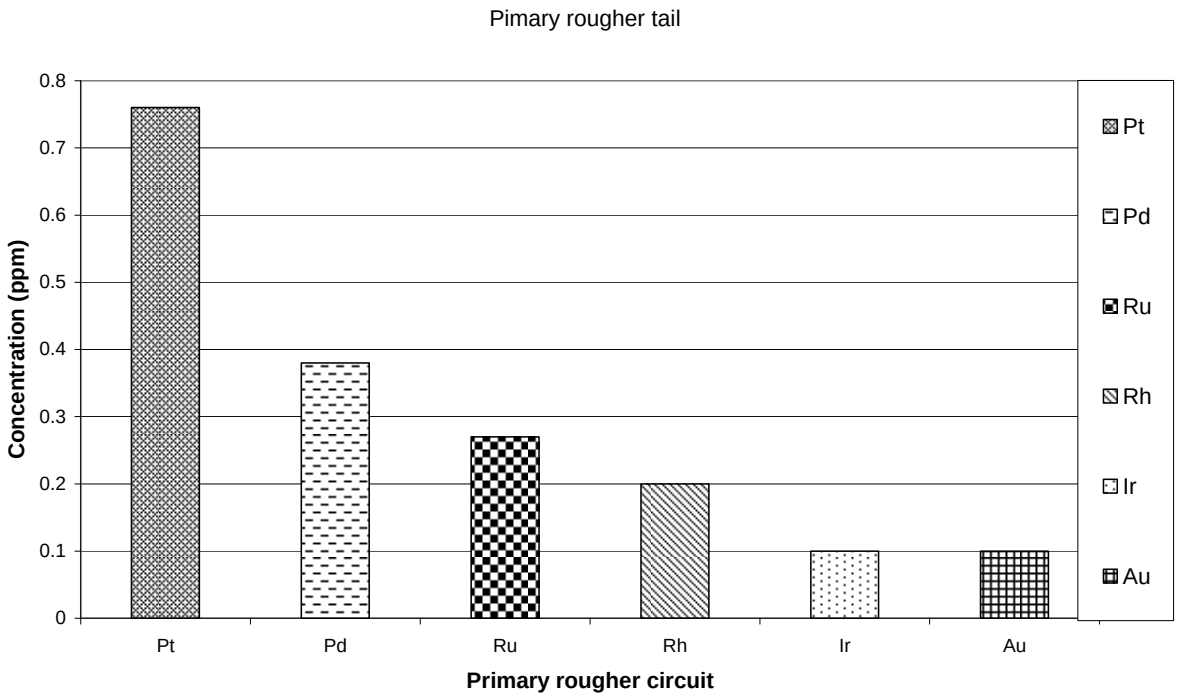

Figure 6. 7: Analysis of 6E's using ICP-OES on the PRT.

6.1.1. Concentration of base metals

Analyses for nickel (Ni), copper (Cu), and cobalt (Co) were carried out using ICP-OES, with a determination limit of 500 parts per million. From the three above elements, Ni is the most abundant, followed by Cu and Co. The concentration of Ni, Cu, and Co decreases along the circuit (Figure 6.8 to Figure 6.12).

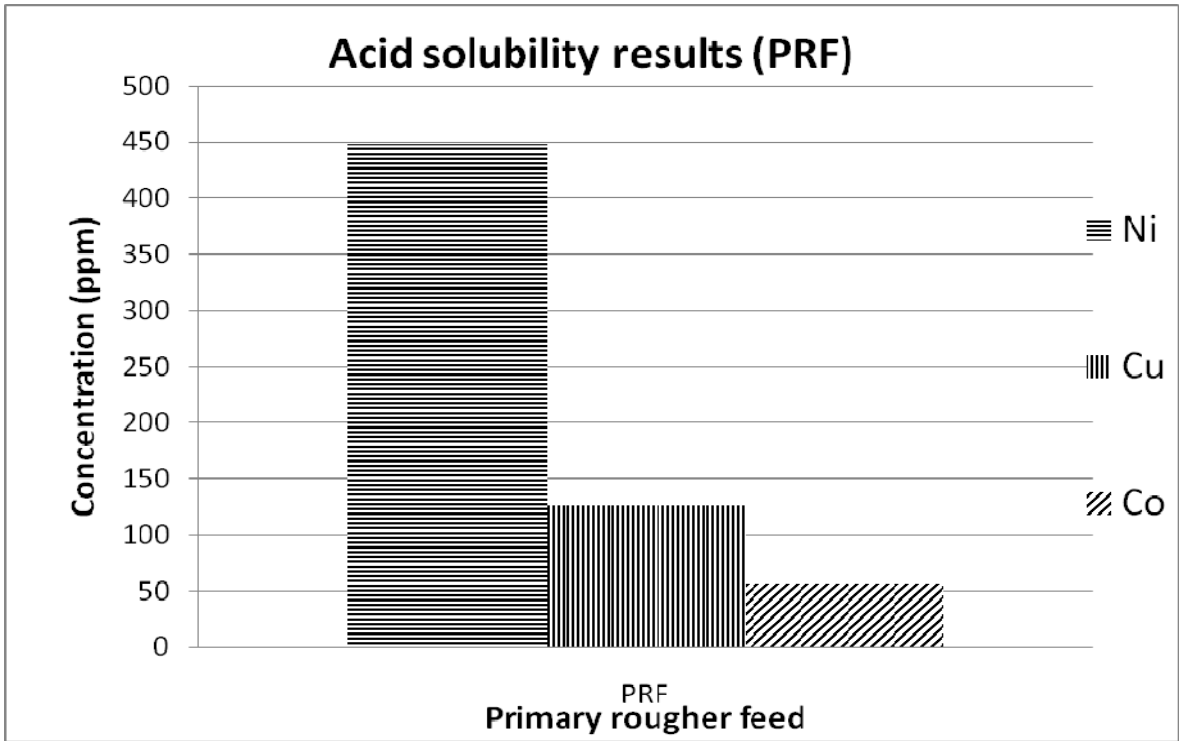

Figure 6. 8: Base metals results of PRF.

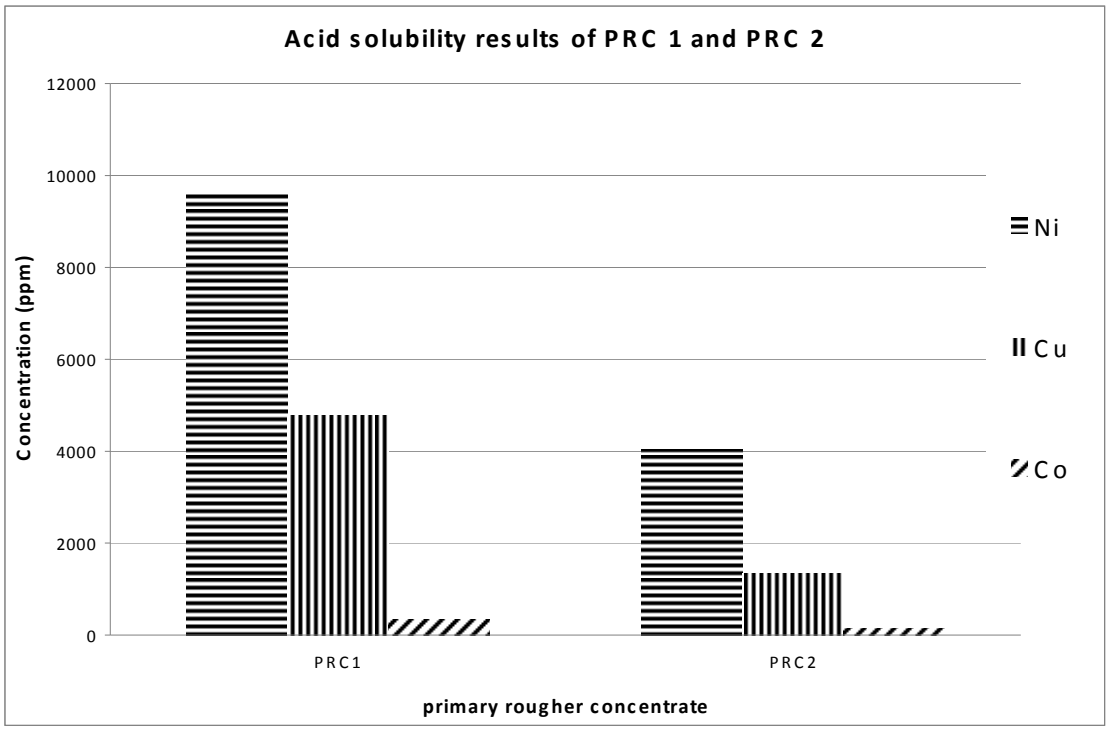

Figure 6. 9: Base metals results of PRC1 and PRC2.

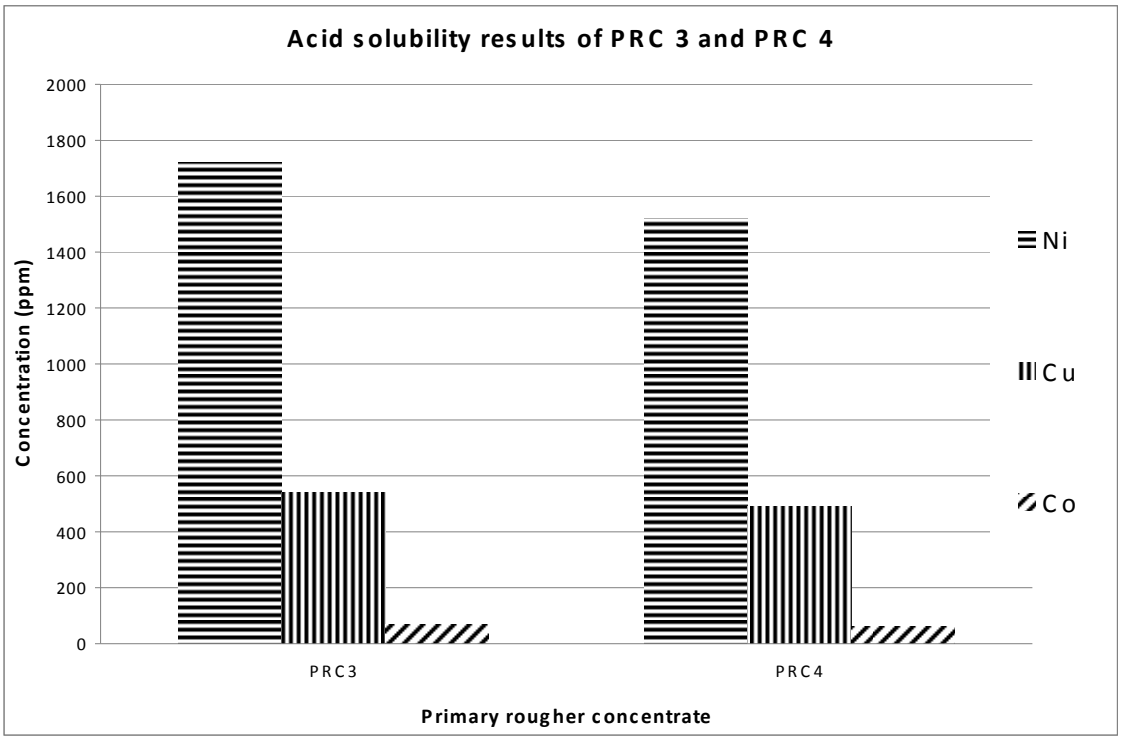

Figure 6. 10: Acid solubility results of PRC3 and PRC4.

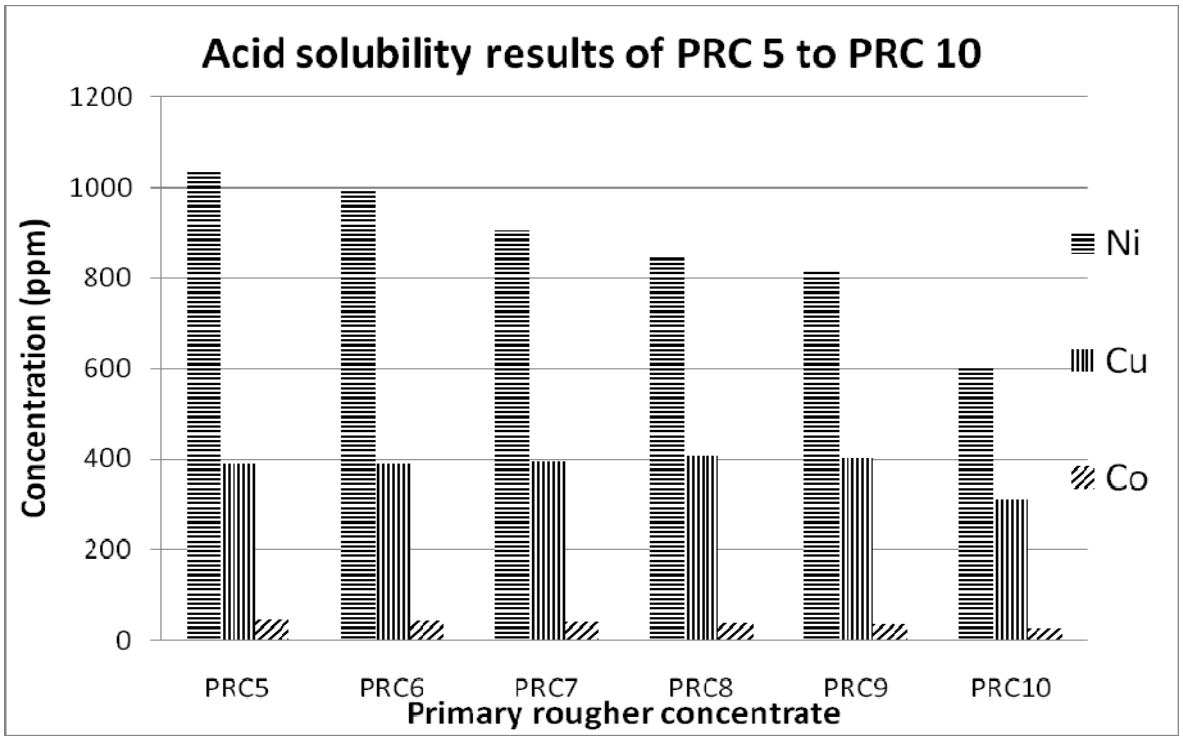

Figure 6. 11: Base metals results of PRC5 to PRC10.

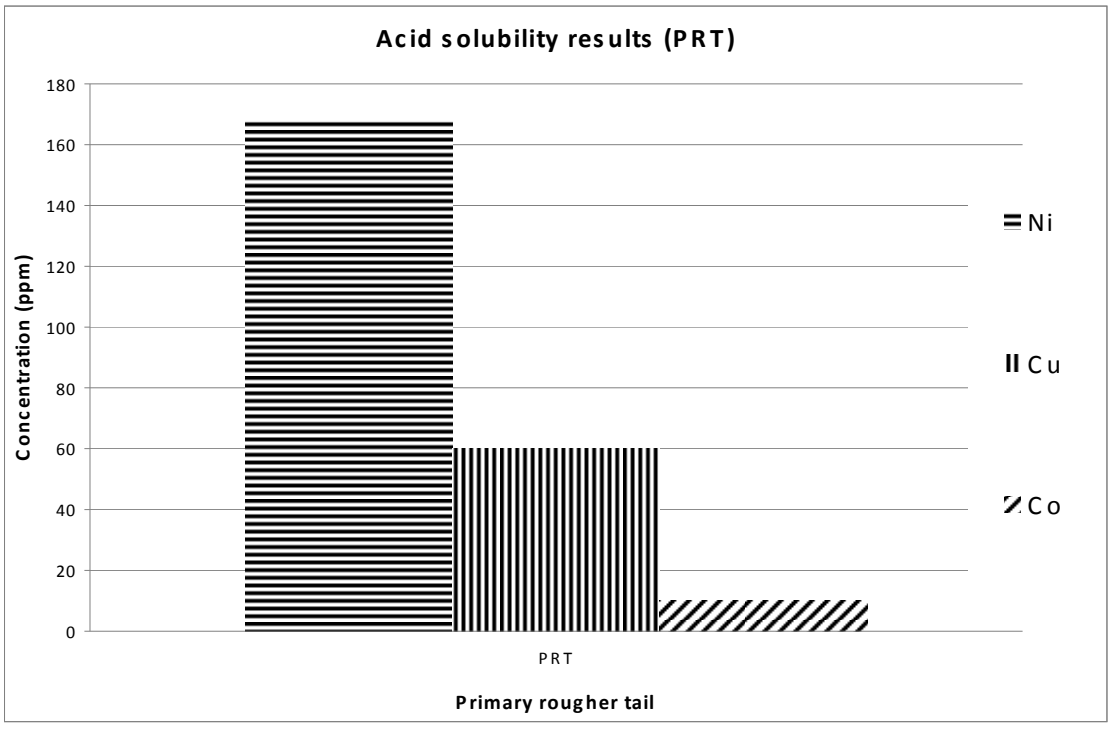

Figure 6. 12: Base metals results of PRT.

6.1.2. Chemical analysis of total sulphur.

The total sulphide were analyzed using Leco combustion, with a determination limit of 100 parts per million. The sulphide is most abundant in PRC 1. Its abundance decreases along the flotation cells.

The sulphur content of PRF is approximately 0.05 weight percent and of PRT is approximately 0.02 weight percent. The sulphur content for the primary rougher concentrates ranges from 0.15 weight percent to 1.8 weight percent. Sulphur is more abundant in PRC 1 and PRC 2, while PRF and PRT are characterized by low sulphur concentration (Figure 6.13 to Figure 6.15).

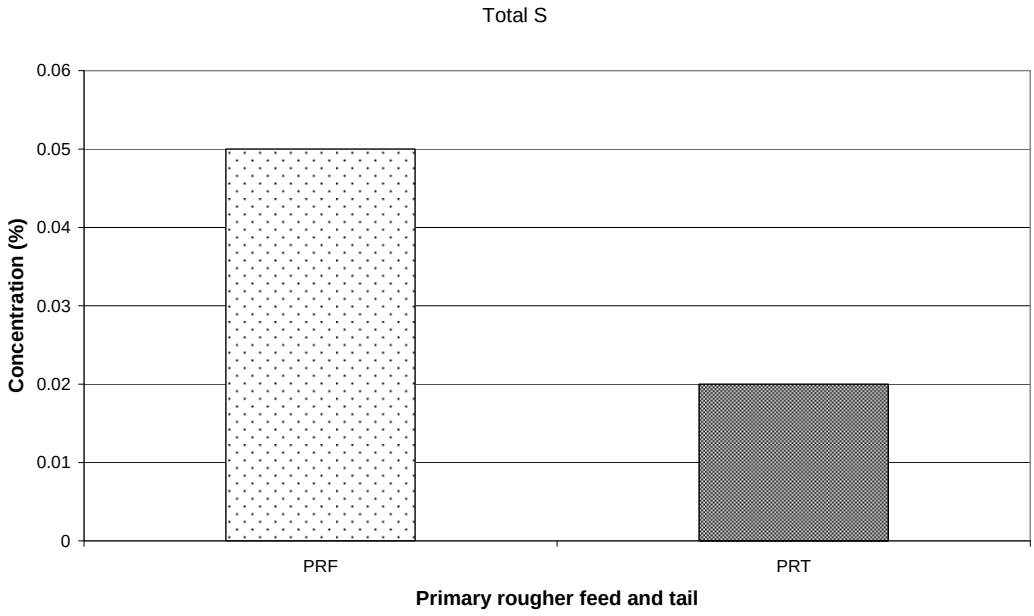

Figure 6.13: Analysis of Total S of PRF and PRT.

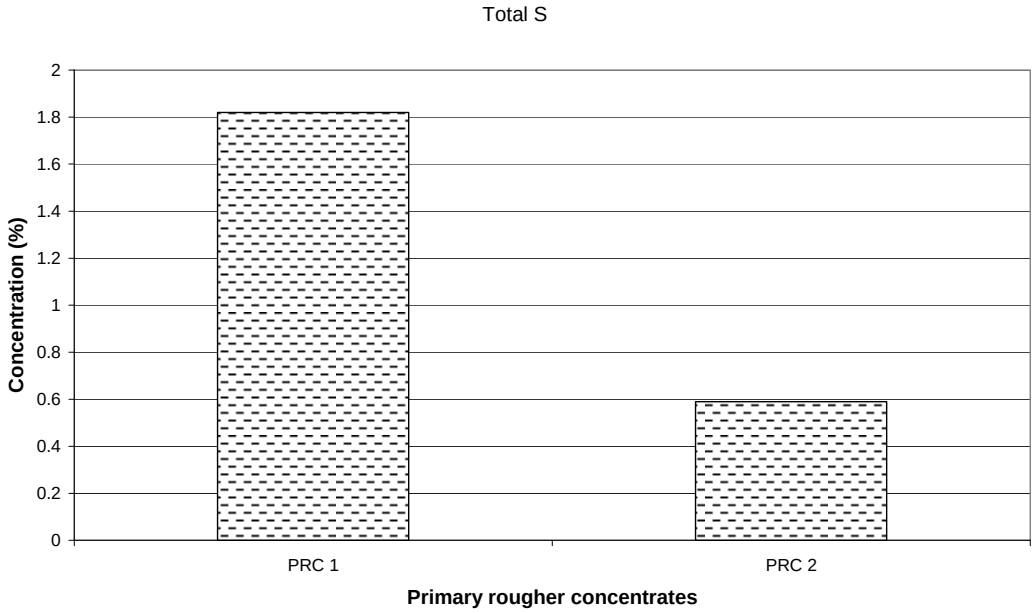

Figure 6.14: Analysis of Total S from PRC1 and PRC2.

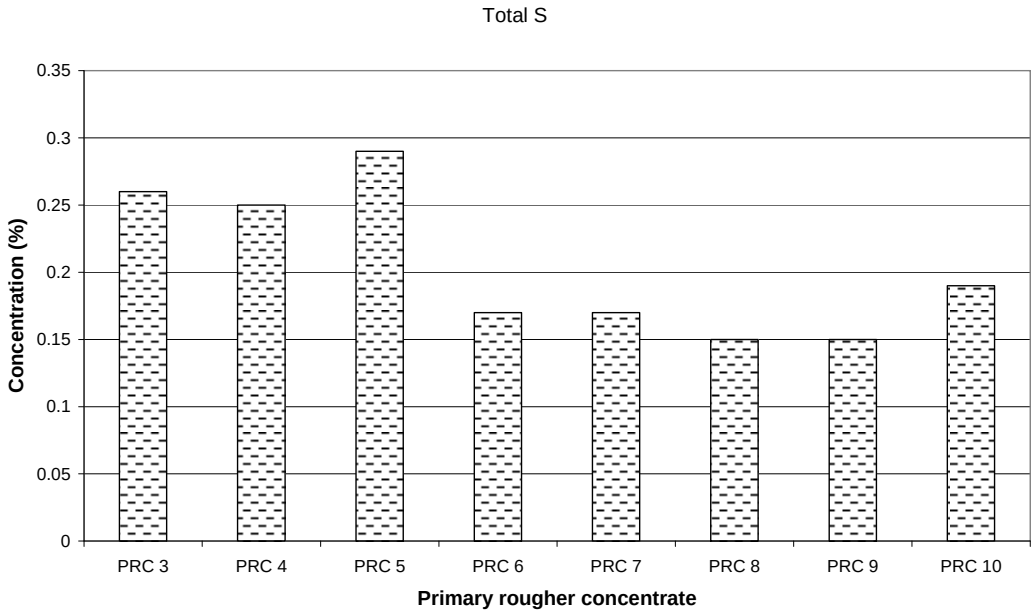

Figure 6.15: Analysis for total S from PRC3 to PRC10.

6.1.3. Chemical analysis for total chromium (Cr) and total iron (Fe).

The total iron was analyzed using ICP-OES. The results were reported in weight percent. The iron content increases along the flotation circuit, with the concentration between 2 weight percent and 7 weight percent, in the primary rougher concentrates. Both PRF and PRT have iron content of approximately 15 weight percent (Figure 6.16).

The chromium content is also analyzed using ICP-OES. The results were reported in weight percent. PRF and PRT have the high chromium content. Chromium content is lowest in PRC 1, and increases along the flotation cells from PRC 2 to PRC 10 (Figure 6.16).

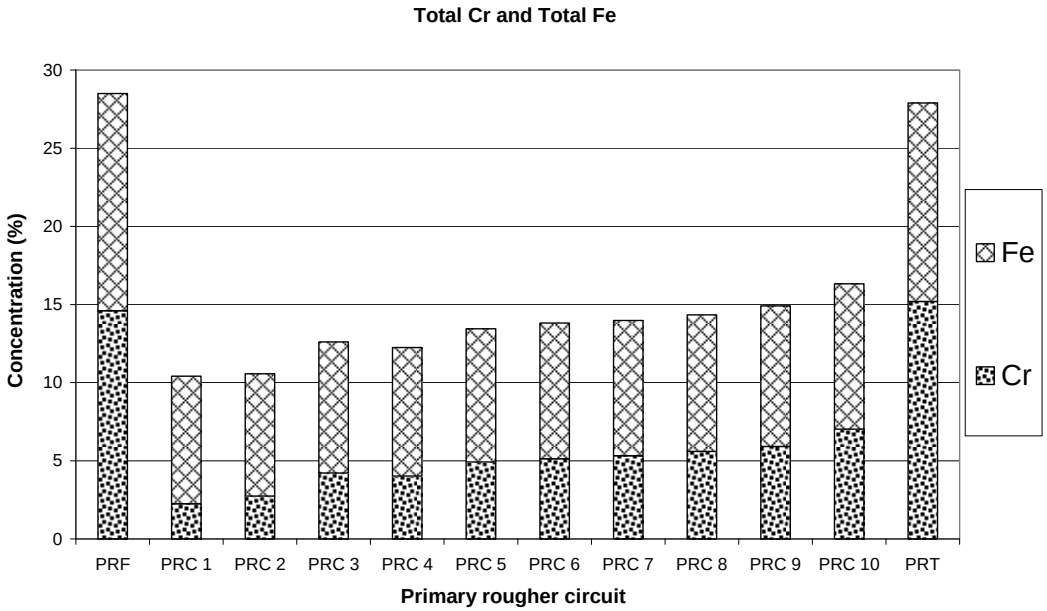

Figure 6.16: Analysis of total Fe and total Cr in primary rougher circuit.

6.2. XRD Analysis

The silicate phases that were found in the UG-2 samples using XRD include: enstatite, plagioclase, talc, chlorite, hornblende, and phlogopite. Chromite was also found in the UG-2 samples using XRD (Figure 6.17, 6.18, 6.19, and 6.20).

The concentration of talc in PRF is less than 10 weight percent, but it increases along the circuit, until PRC 5. From PRC 8 the concentration decreases until PRT. PRT also has the concentration below 10 weight percent (Figure 6.18). This will be discussed later.

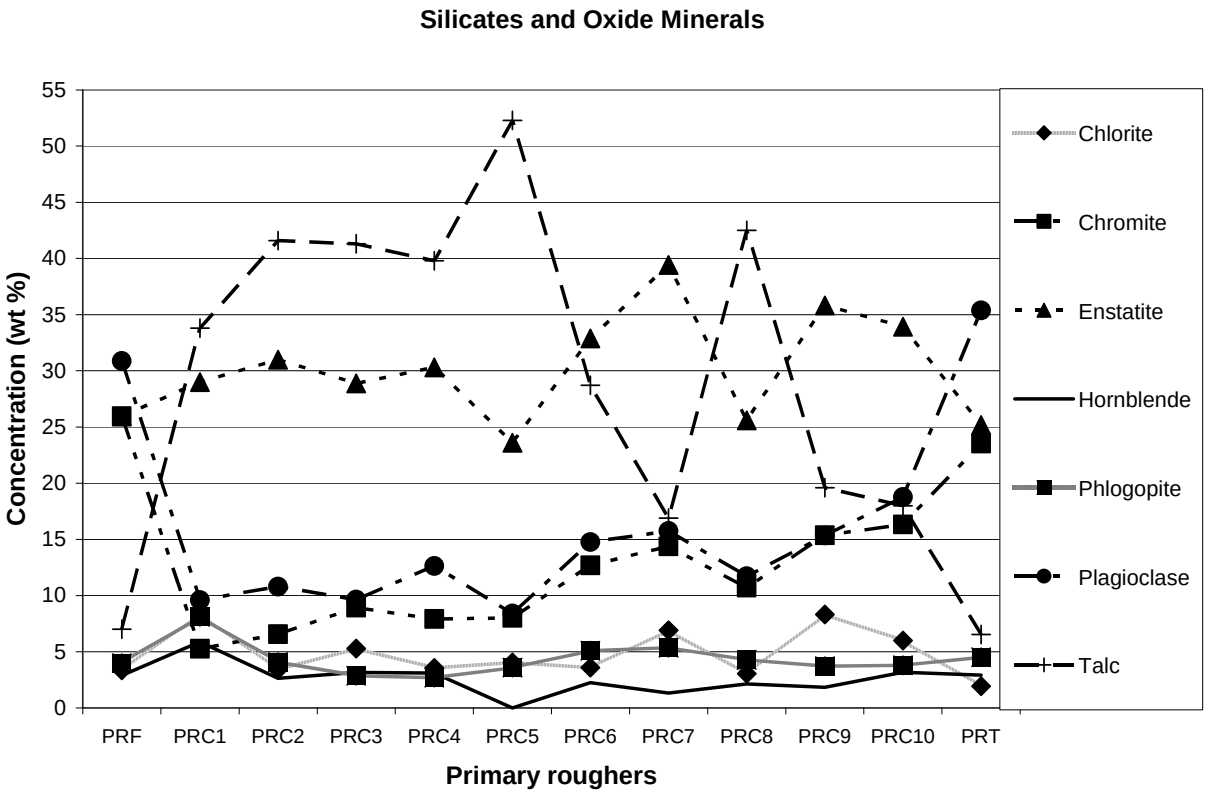

Figure 6. 17: Phase quantification using X'Pert High score plus software.

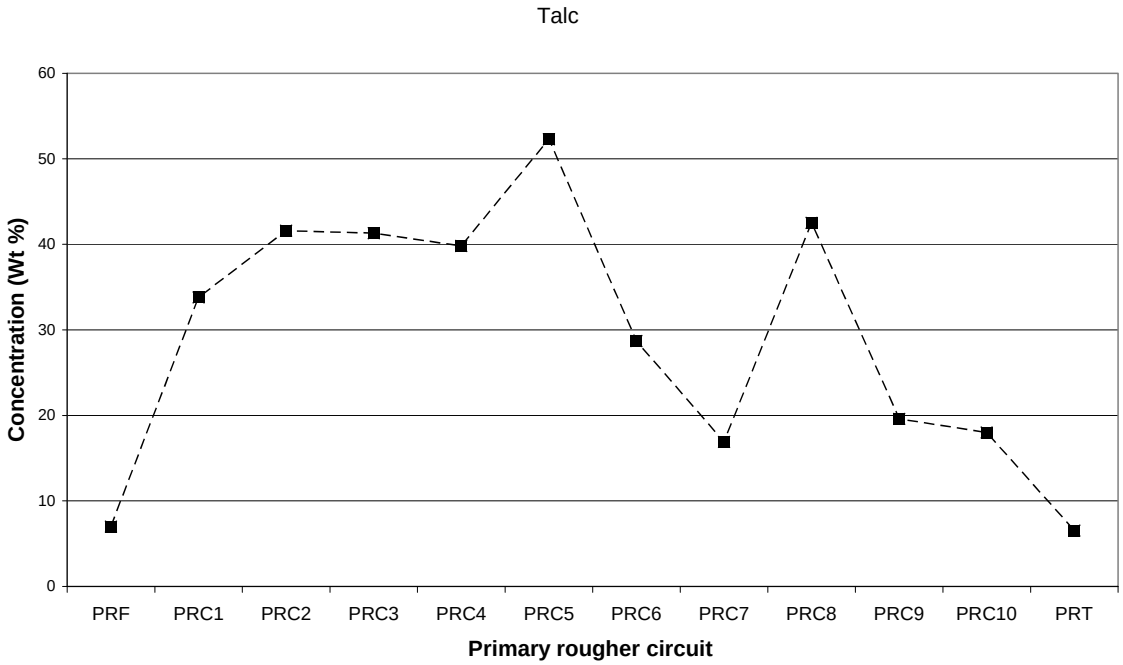

Figure 6. 18: Phase quantification of talc using X'Pert High score plus software.

In the primary rougher feed, the concentrations of enstatite, plagioclase, and chromite range from 25 weight percent to 35 weight percent. In PRC 1, the concentrations of plagioclase and chromite decrease to approximately 5 weightpercent and 10 weight percent respectively. From PRC 2 the concentration of both plagioclase and chromite increase along the circuit. Enstatite has a concentration that ranges from 25 weight percent to 40 weight percent. The concentration remains fairly constant between PRF and PRC 4, and then changes from PRC 5 to PRT. PRT has the highest concentration of plagioclase, enstatite, and chromite (Figure 6.19).

The concentrations of hornblende, chlorite, and phlogopite range from 3 weight percent to 4 weight percent. The concentrations of these minerals fluctuate throughout the circuit. The concentration is high in PRC1, PRC 7, and PRC 10 and low in PRC2, PRC 4, PRC 5, PRC 6, PRC 8, PRC 9, and PRT (Figure 6.20).

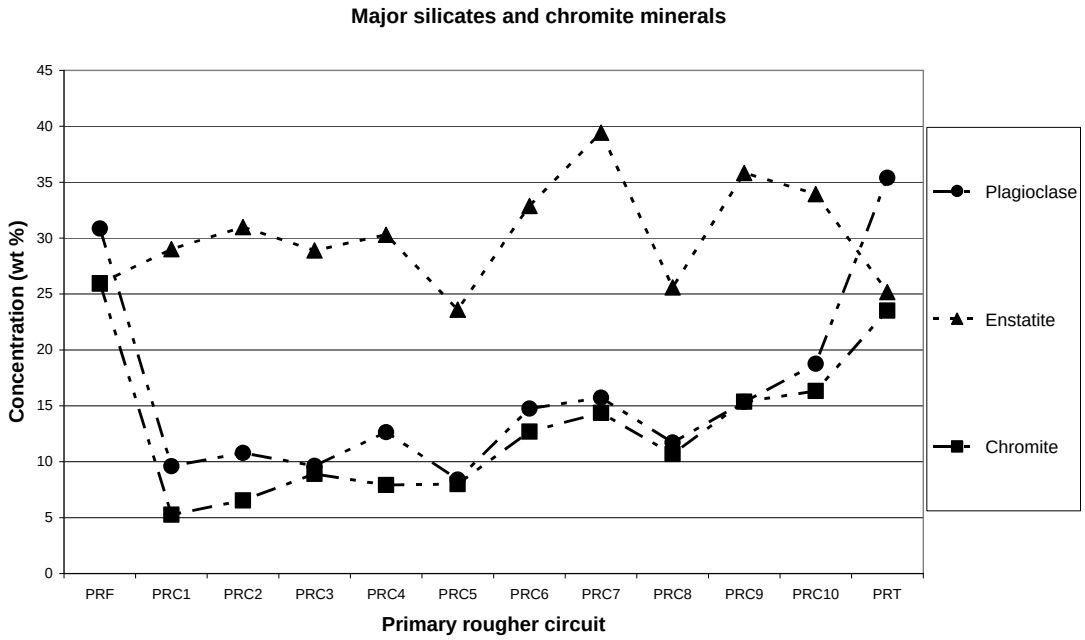

Figure 6. 19: Phase quantification using X'Pert High score plus software, for major silicates and chromite.

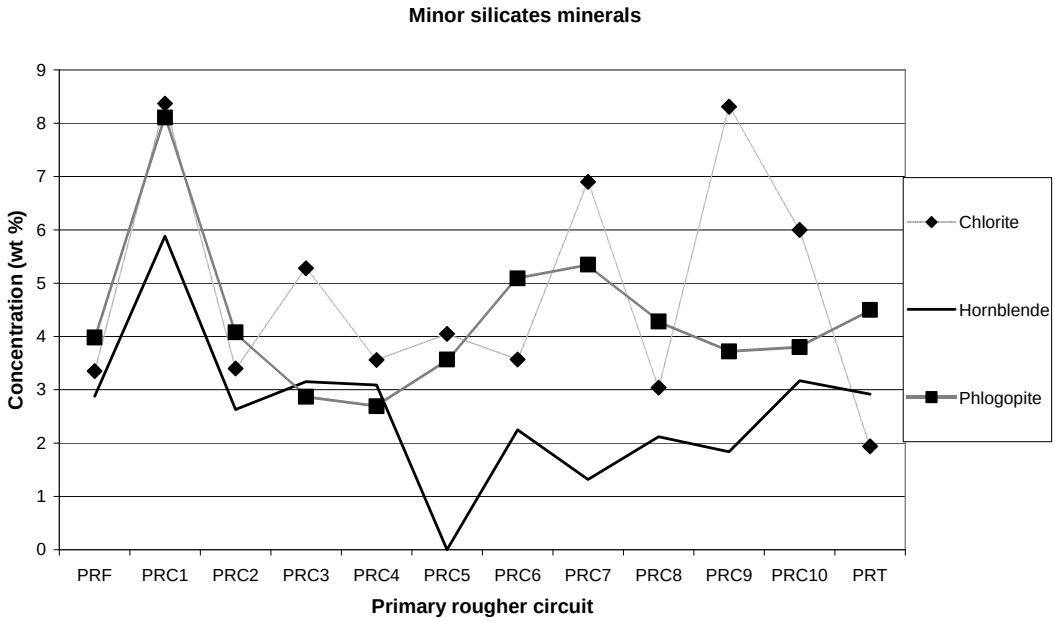

Figure 6. 20: Phase quantification using X'Pert High score plus software, for minor silicates.

6.3. Mineralogy of the primary rougher circuit.

6.3.1. PGM modal distribution

To obtain statistically representative data of the PGM, a search of 190 polished section of UG-2 chromitite was performed for nine months. This yielded data of 3354 PGM grains. The feed sample contains data of 140 grains from 32 polished sections, the concentrate samples has data of 3074 grains from 118 polished sections, and the tail sample with data of 140 grains from 40 polished sections (Table 6.2). The PGM phases were identified and classified according to the major elements present, using semi quantitative EDS analysis.

Table 6.2: Total number of PGM from sections analyzed

Sample	Number of grains	Number of sections
PRF	140	32
PRC 1	770	6
PRC 2	450	7
PRC 3	225	8
PRC 4	284	6
PRC 5	312	12
PRC 6	260	12
PRC 7	205	11
PRC 8	256	24
PRC 9	132	14
PRC 10	150	18
PRT	140	40
Total	3354	190

6.3.2. PGM species in the UG-2 chromitite layer

The PGM that were identified using MLA coupled with scanning electron microscope were not given names, because the identification is based on a semi quantitative technique. The species were named according to their major peaks in the X-ray spectra.

The most dominating PGM species in the UG-2 concentrate include: platinum containing sulphides, followed by laurite, PGM alloys (Pt-Fe alloy, Pd-Hg, and Pd-Pb), PGM containing

arsenic (mainly Pt-As, Pd-As, Pt-Rh-Ru-S-As, Pt-S-As, Rh-S-As, and Pt-Ru-As), and PGM containing tellurium (mainly Pt-Pd-Te, Pd-Pt-Te-Bi, Pt-Te, and Pt-Te-Bi) (Figure 6.21 and 6.22).

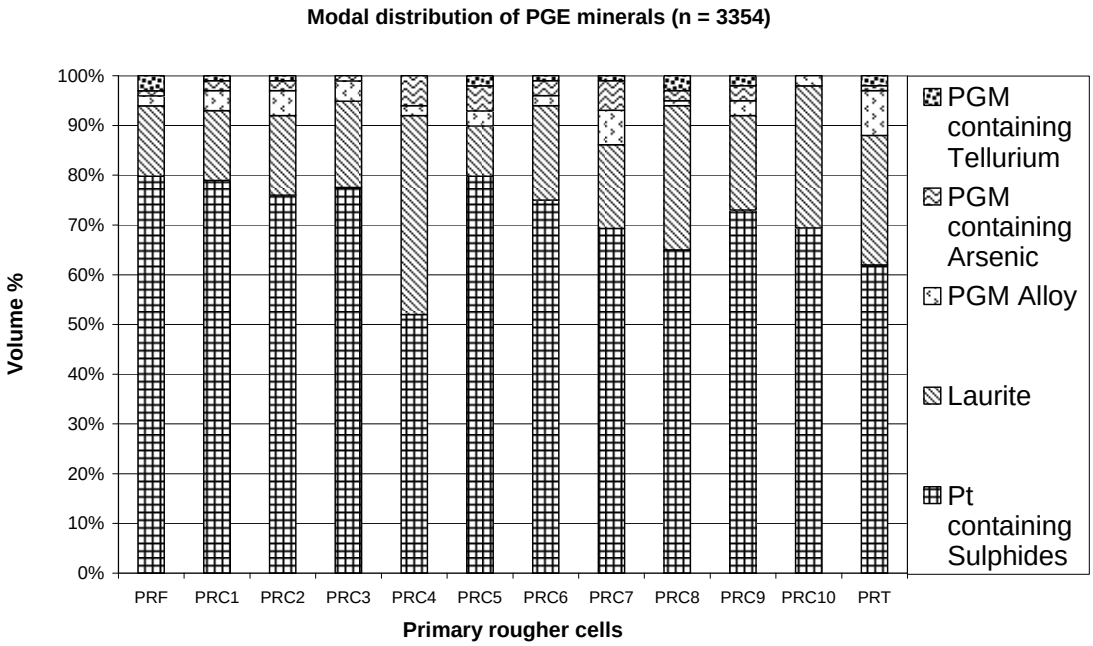

Figure 6.21: Modal distribution of PGM in the primary rougher circuit based on 3354 grains.

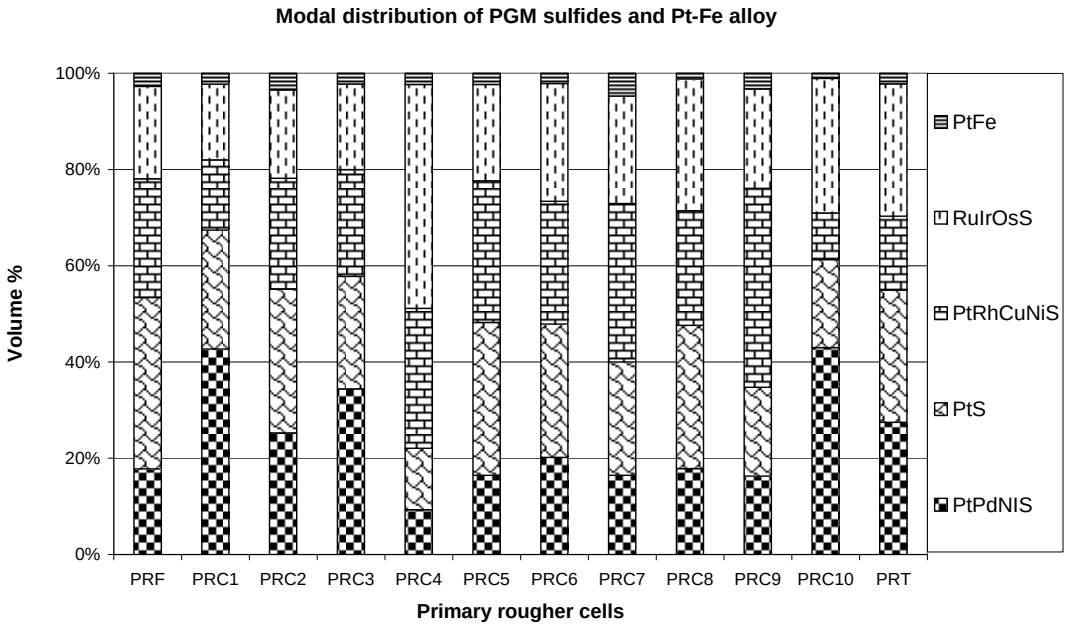

Figure 6.22: Modal distribution of dominating platinum containing sulphides, ruthenium sulfide, and platinum-iron alloy along the primary rougher circuit.

6.3.3. PGM mode of occurrence and liberation.

In PRF, more than 50 volume percent (volume percent = area percent) of the PGM are liberated, i.e., they are not attached to any other mineral grains such as BMS, silicates, or chromite (Figure 6.27, Table 6.3). Liberated PGM (Figure 6.23), and PGM associated with liberated BMS (Figure 6.24, 6.25, and 6.26), make up approximately 65 volume percent of the valuable minerals in PRF. This is followed by PGM associated with BMS, attached to silicate, or oxide gangue particles (approximately 22 volume percent), followed by PGM attached to silicate or chromite particles.

PGM locked within silicate or chromite particles occurs mostly in PRF, PRC 8, and PRT, while PGM associated with BMS locked in silicate or chromite particles occur mostly in the PRF and PRT (figure 6.27, Table 6.3).

Table 6.3: Liberation characteristics of PGM, BMS and gangue minerals (standard Mintek reporting style).

LP	Liberated PGM (PGM were freed from the rock matrix)
PLB	PGM associated with liberated BMS (this PGM are either locked or attached to the grain boundaries of the BMS)
PBCG	PGM associated with BMS locked in silicate or oxide gangue particles (This refers to PGM and BMS locked in silicates or chromite)
PG	PGM attached to silicate or oxide gangue particles
PBG	PGM associated with BMS attached to silicate or oxide gangue particles
PCG	PGM locked within silicate or oxide gangue particles

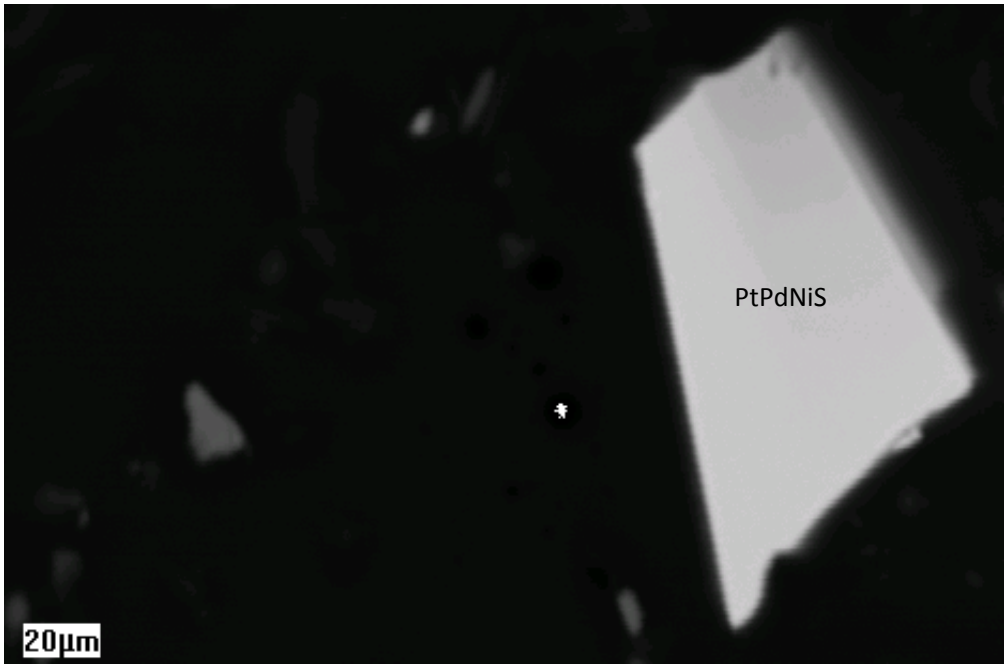

Figure 6.23 : Backscatter electron image of liberated PtPdNiS grain from the UG-2 chromitite.

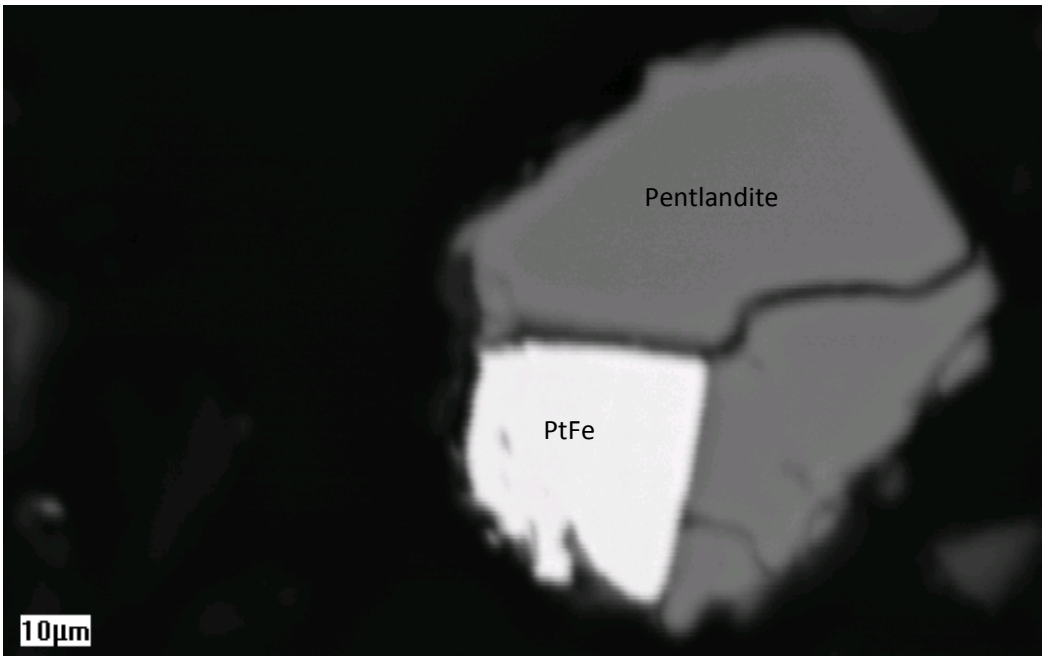

Figure 6.24: Backscatter electron image of PtFe and pentlandite grains from the UG-2 chromitite.

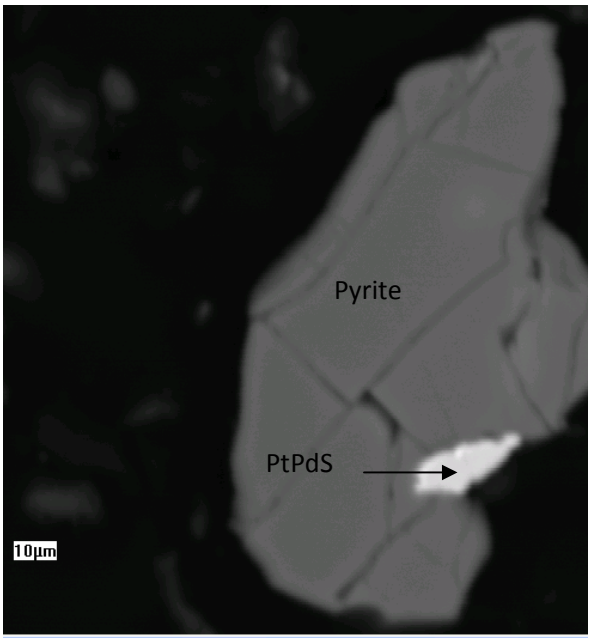

Figure 6.25: Backscatter electron image of pyrite and PtPdS grains from the UG-2 chromitite.

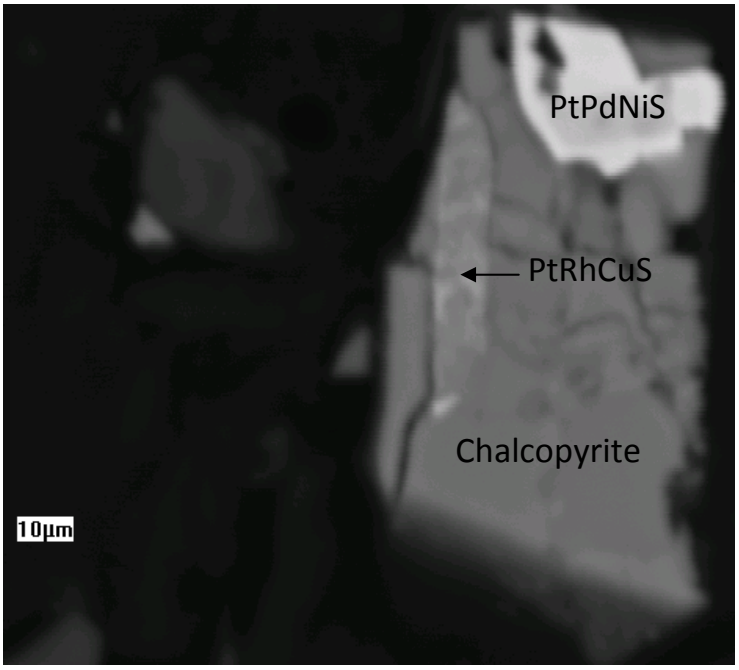

Figure 6.26: Backscatter electron image of chalcopyrite, PtPdNiS, and PtRhCuS from the UG-2 chromitite.

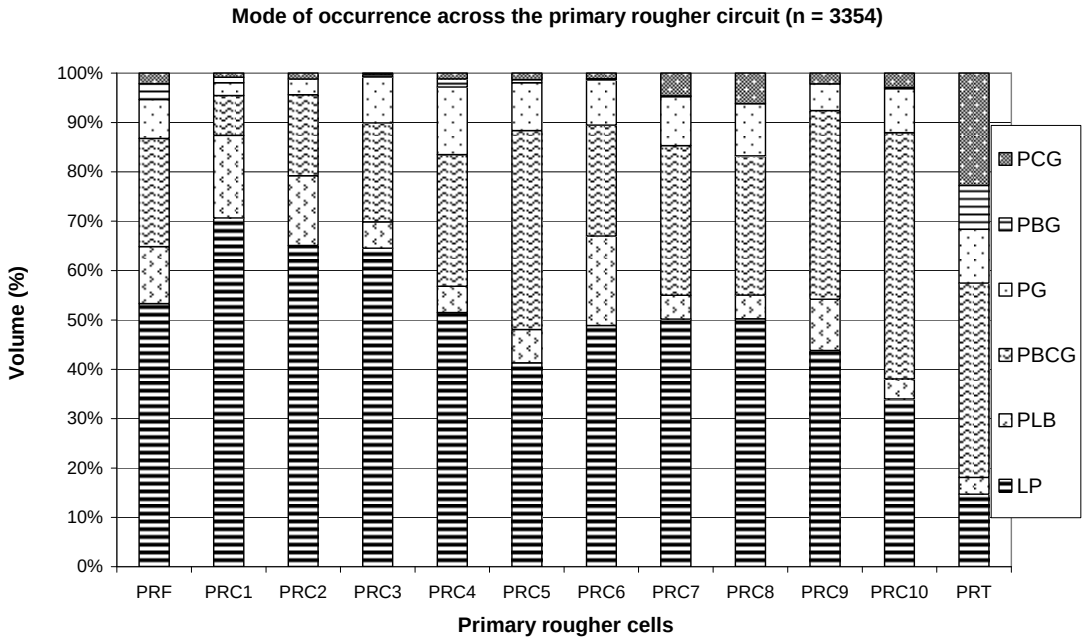

Figure 6.27: Mode of occurrence of PGE minerals and associated minerals along the circuit based on 3354 grains (for abbreviations see table 6.3).

In PRC 1 concentrate, more than 70 volume percent of of the PGM are liberated from the rock matrix. Liberated PGM (LP) and PGM associated with liberated BMS (PLB) make up almost 90 volume percent of valuable minerals in PRC 1. Most of the high grade PGM and BMS are recovered from PRC 1 to PRC 3. The degree of liberation decreases along the circuit and the recovery of PLB also decreases along the circuit.

PGM associated with liberated BMS (PLB) occur mostly in PRC 1, PRC 2, and PRC 6. PGM associated with BMS attached to silicate or oxide gangue particles (PBG) increases in abundance along the circuit, from approximately 10 volume percent in PRC 1 to approximately 50 volume percent in PRC10 (Figure 6.27).

Less than 2 volume percent of PGM in PRC 1 are locked within silicates or oxide gangue particles (PCG). PCG increases in abundance along the circuit. Less than 5 volume percent of PGM associated with BMS locked in silicate or oxide gangue particles (PBCG) and PGM attached to silicate or oxide gangue particles (PG) occurs in PRC 1, but increases in abundance along the circuit (Figure 6.27).

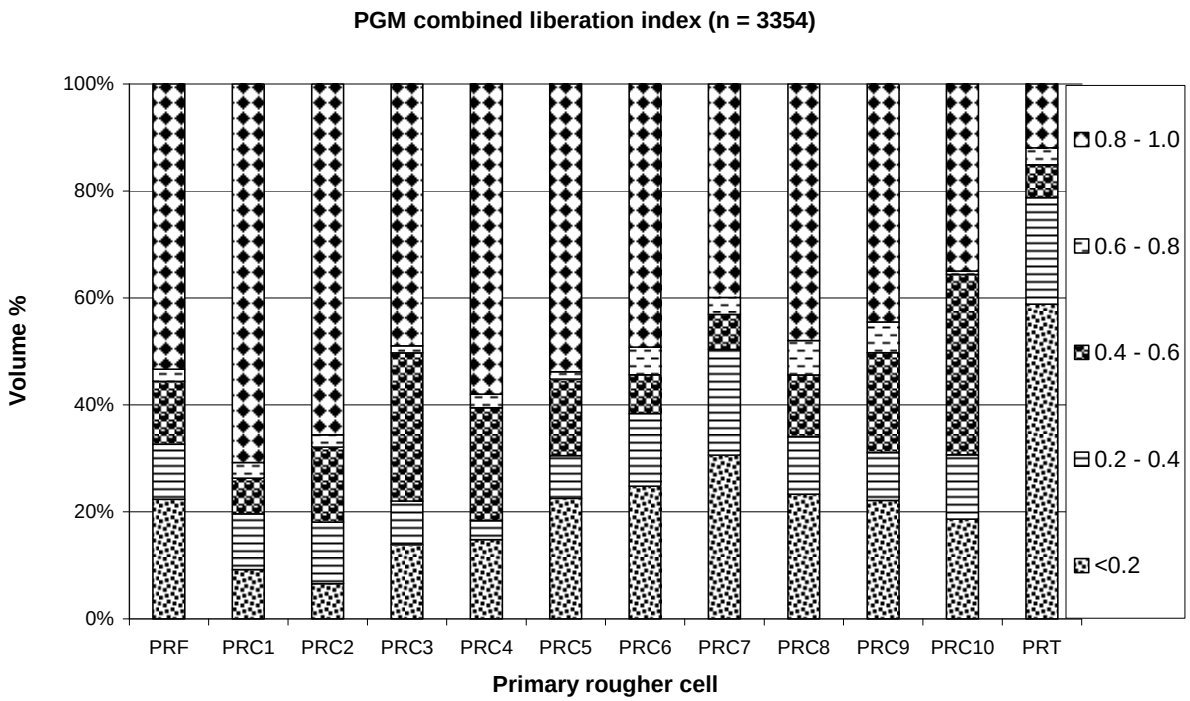

Figure 6.28: PGM combined liberation index along the primary rougher circuit based on 3354 grains.

In PRT, 38 volume percent of the PGM are PGM associated with BMS attached to silicate or oxide gangue particles (PBG), followed by 25 volume percent of the PGM locked within silicate or oxide gangue particles (PCG). Less than 15 volume percent of the PGM are Liberated PGM (LP).

The PGM combined liberation index (CLI) is considered as a measure of *area of floatable mineral in a particle divided by the total area of particle* where the floatable mineral is either liberated or coarser PGM and/or BMS (Penberthy, 2000). CLI range from 0 to 1 (Figure 6.30). PGM with high CLI of greater than 0.8, are considered liberated from the rock matrix, and are recovered from the fast floating concentrates. The PGM associated with liberated BMS also have high CLI and are also recovered from the fast floating concentrates (Figure 6.28, PRC 1 and PRC 2).

PGM with low CLI of less than 0.2, are recovered from the slow floating concentrates and they also report to the primary rougher tailings. This PGM are mostly associated with silicates and chromite (Figure 6.29). PGM reporting to the PRT will be re-milled and re-floated in the secondary milling and secondary rougher circuit.

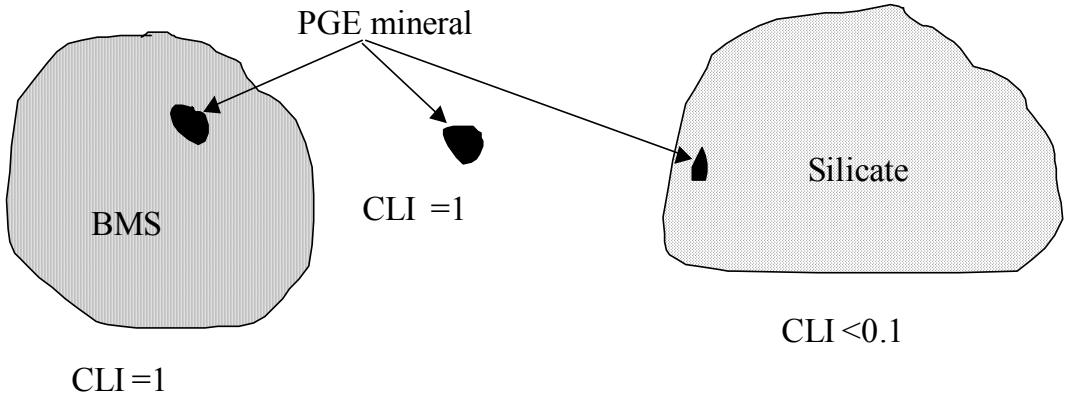

CLI = (area of floatable mineral in a particle) ÷ (total area of a particle)

Figure 6.29: Schematic representation illustrating combined liberation index (CLI), of three different PGM associations (from Penberthy 2000).

6.3.4. PGM grain size distribution

The grain sizes of PGM (as measured on polished sections by MLA) were expressed in equivalent circle diameter, ECD, i.e., the diameter of a circle of area equivalent to that of the measured grain (ECD = 2*square root (area/π)) (Penberthy, 2000, Chetty et al., 2009). The lower limit of detection (LLD) on the MLA FEI quanta 600 is 1µm, therefore all the PGM grains with ECD of less than 1 µm will not be detected using MLA. In PRF, most of the detected PGM grains are over 3 µm in size. Less than 15 volume percent of PGM grains are less than 3 µm in size and are considered slow floaters (Penberthy et al., 2000). In the PRC 1 concentrate, most of the PGM that are recoverd have large grain sizes, 40 volume percent of the PGM grains have grain sizes of more than 9 µm, while 25 volume percent have grain sizes of 6 µm – 9 µm, 30 volume percent have grain sizes of 3 µm – 6 µm, and only 5 volume percent have grain sizes of approximately 1 µm (lower limit of detection - LLD) – 3 µm (Figure 6.30, table 6.4). In the

PRT, 70 volume percent of PGM grains are between 3 µm – 6 µm, 20 volume percent is 1 µm – 3 µm, and only 10 volume percent is more than 9 µm.

Table 6.4: PGM floatability index (Mintek reporting procedure).

Fast floating	Liberated PGM > 3 µm ECD
	Liberated BMS > 10 µm ECD
Slow floating 1	Liberated PGM < 3 µm ECD
	Liberated BMS < 3 µm ECD
	PGM > 3 µm ECD attached to gangue
	BMS > 10 µm ECD attached to gangue
Slow floating 2	PGM < 3 µm ECD attached to gangue
	BMS < 10 µm ECD attached to gangue
Non floating	PGM and/or BMS locked in gangue

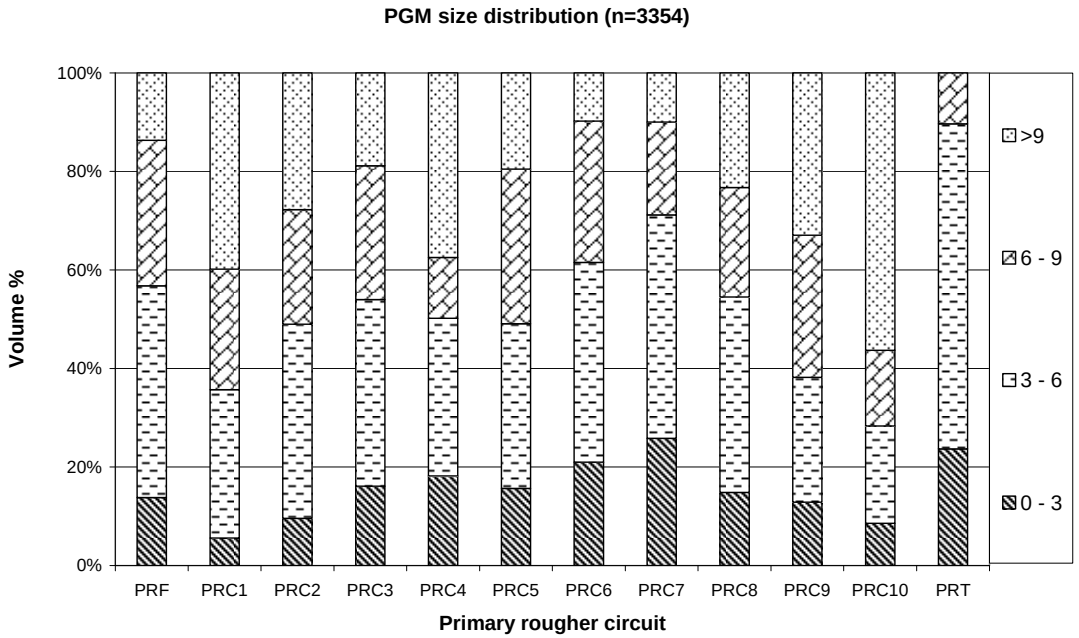

Figure 6.30: PGM size distribution (measured in equivalent circle diameter) along the primary rougher circuit.

6.4. Characterization of PGM phases.

There are approximately 109 identified PGM (Cabri, 2002, Xiao and Laplante, 2004). The identified PGM includes: PGE sulphides, alloys, arsenides, tellurides, bismuth tellurides, antimonides, and native species (Cabri, 2002, Xiao and Laplante, 2004).

PGM in the UG-2 chromitite layer have small grain sizes of less than 10 µm (McLaren and de Villiers, 1982, Penberthy et al., 2000, Becker et al., 2008), and are mostly associated with chromite, and BMS such as pentlandite, pyrrhotite, chalcopyrite, millerite, and pyrite (McLaren and De Villiers, 1982, Kinloch, 1982, Peyerl, 1982, Liddell et al., 1986, Xiao and Laplante, 1994, Penberthy and Merkle, 1999, Penberthy et a., 2000, Nel et al., 2005, Valenta, 2007).

Analyses of PGM using electron microprobe were performed on samples from PRC 1 to PRC 4. PGM from the UG-2 concentrate are usually small and this makes difficult the detection of compositional heterogeneity (Kinloch, 1982, Penberthy and Merkle, 1999, Penberthy et al., 2000, Merkle and Verryn, 2003). Most of PGM that were identified include; braggite, cooperite, malanite as the most occurring PGM, followed by, laurite, platinum-iron alloy, platarsite, and sperrylite.

6.4.1. Quantitative characterization of selected PGM phases.

Quantitative characterization of selected PGM phases was carried out with wavelength dispersive spectroscopy (WDS) (for details see chapter 4). Common phases that were identified include:

- Pd-Pt-Ni sulfide (probably braggite)
- Pt-sulfide (cooperite)
- Pt-Rh-Cu-Ni- sulfide (probably malanite, cuprorhodsite, or cuproiridsite.)
- Ru-Os-Ir- sulfide (laurite)
- PGE- Bi-telluride (probably moncheite or merenskyite)

- PGE-As- sulfide (platarsite, majakite, sperrylite, irarsite, hollingworthite)
- Pt-Fe alloy

6.4.2. Cooperite, Braggite, and Vysotskite.

Cooperite (ideal composition PtS), Braggite (ideal composition (Pt,Pd)S), and Vysotskite (ideal composition PdS), are the major PGM with the element combination of Pt-Pd-S in the BIC (Cabri et al., 1978, McLaren and de Villiers, 1982, Kinloch 1982, Verryn and Merkle, 1994, Penberthy and Merkle, 1999, Merkle and Verryn, 2003). Nickel (Ni) occurs in significant amounts in cooperite, braggite, and vysotskite (Figure 6.31) (Cabri et al., 1978, Merkle and Verryn, 2003, Verryn and Merkle, 1994).

Braggite is more abundant than cooperite in the BIC (Cabri et al., 1978). Braggite forms a solid solution with vysotskite (Cabri, 2002, Verryn and Merkle, 1994).

Vysotskite is less common than braggite in the BIC. It is not considered an important economic ore mineral since it has never been found in large quantities (Cabri, 2002; 1978, Verryn and Merkle, 1994, Merkle and Verryn, 2003). It is also found associated with BMS such as pentlandite and millerite in the UG-2 (Cabri, 2002).

The distinction between braggite and vysotskite is arbitrarily made based on the 10 mol percent PtS, i.e. braggite contains more than 10 mol percent PtS; vysotskite contains less than 10 mol percent PtS (Cabri et al., 1978). Nickel is one of common, but not essential element in braggite, cooperite, and vysotskite (Merkle et al., 2002).

The data that was used to do the compositional variation of Pt-Pd-Ni-S was obtained by analyzing the coarser liberated PGM grains with EPMA. PGM data with the good totals (totals of

98 at percent to 102 at percent), were selected and plotted on the triangular diagram (Figure 6.31).

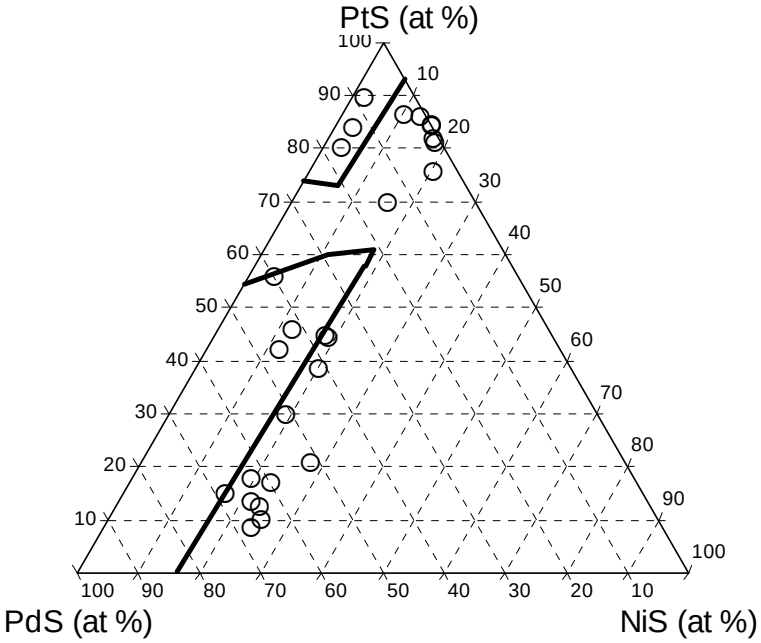

Figure 6.31: Compositional variation of PtS, PdS, and NiS from the UG2 concentrate. Solid lines represent the stability fields of Braggite, cooperite, and vysotskite at 700 °C (Verryn and Merkle1994).

Some of the braggite and cooperite plots outside the experimental 700 °C stability field (Merkle and Verryn 2003). Data of PtPdNiS that plots outside the 700 °C stability field might be due to PtPdNiS that formed at low temperature. Palladium and nickel can be easily leached out during interactions with fluids. Palladium is more mobile than platinum, this might be one of the reasons as to why some data points plots outside the temperature stability field of PtS (Merkle and Verryn 2003). There are few data points that plot between the cooperite and braggite field. The data points that plot between braggite and cooperite might be mixed analyses of both cooperite and braggite in intergrowths, or cooperite and millerite (Merkle and Verryn 2003).

6.4.3. Malanite, cuprorhodsite, and cuproiridsite.

Malanite with the ideal formula ($CuPt_2S_4$), cuprorhodsite with the ideal formula ($CuRh_2S_4$), and cuproiridsite with the ideal formula ($CuIr_2S_4$), have extensive solid solution in the system $CuRh_2S_4$-$CuIr_2S_4$-$CuPt_2S_4$ (Figure 6.32) (Garuti and Gazzotti, 1995, Cabri, 2002).

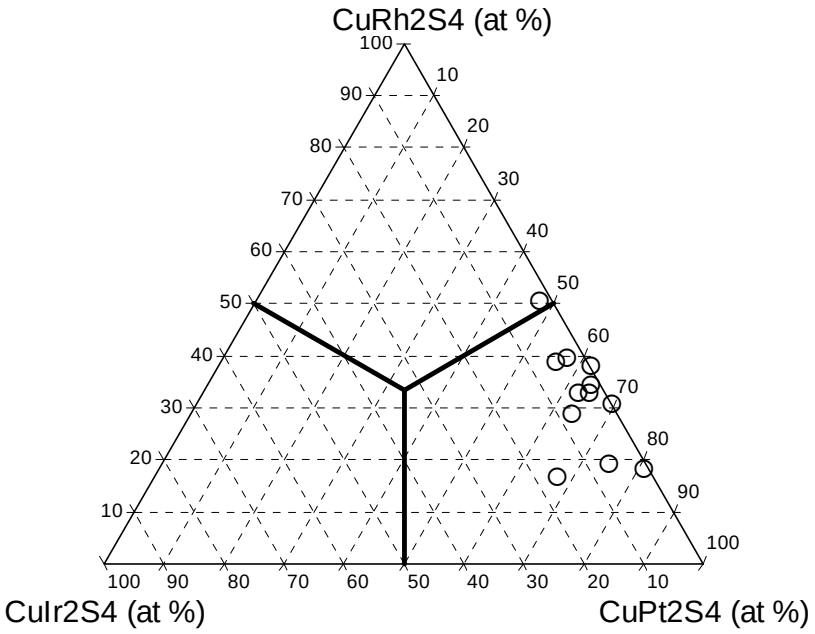

Figure 6.32: Compositional variation of $CuPt_2S_4$, $CuIr_2S_4$, and $CuRh_2S_4$ from the UG2 concentrate. Solid lines represent the stability fields of malanite, cuprorhodsite, and cuproiridsite.

Malanite, a member of the linnaeite group (Cabri, 2002), is considered to be the third most abundant PGM in the UG-2 of the Bushveld Igneous Complex (Penberthy and Merkle 1999, Cabri, 2002).

The data that was used to evaluate the compositional variation of $CuPt_2S_4$, $CuIr_2S_4$, and $CuRh_2S_4$, was obtained by analyzing the coarser liberated PGM grains with EPMA. PGM data with good totals (totals of 98 at percent to 102 at percent), were selected and plotted on the

triangular diagram (Figure 6.32). The lines in the triangular diagram represent the 50-50-50 lines, where minerals can de differentiated. Most of the PtRhCuNiS grains that were characterized using electron microprobe fall within the field of $CuPt_2S_4$ which is malanite, and $CuRh_2S_4$ which is cuprorhodsite.

6.4.4. Laurite.

Laurite with the ideal formula RuS_2, it is mostly found in the chromite rich ores, such as UG-2 chromitite layer in the Bushveld Igneous Complex of South Africa (Kinloch, 1982, Cabri, 2002). Laurite is usually poorly developed if there is insufficient chromite available (Kinloch, 1982, Peyerl, 1982). Laurite is normally richer with osmium than iridium (McLaren and De Villiers, 1982). The RuS grains that were characterized from PRC 1 to PRC 4 fall within the field of RuS_2 which is laurite (Figure 6.33).

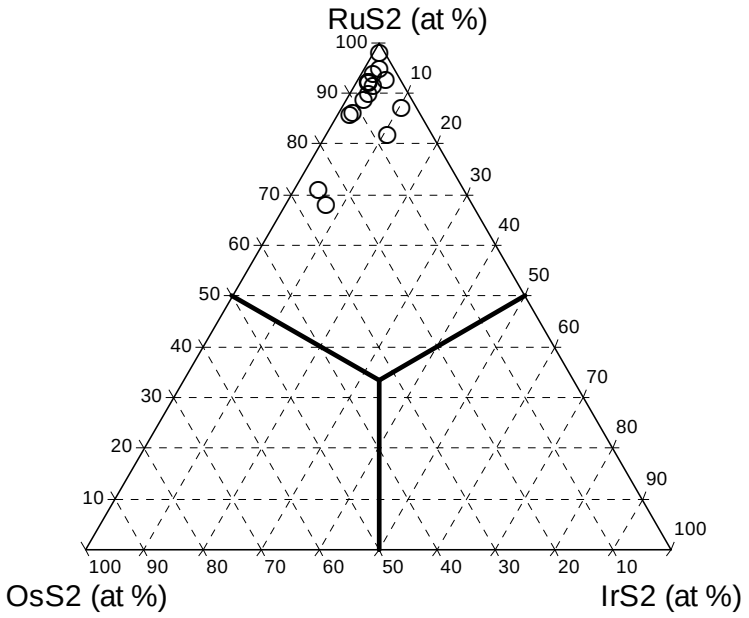

Figure 6.33: Compositional variation of RuS_2, IrS_2, and OsS_2 from the UG2 concentrate. Solid lines represent the stability fields of RuS_2, IrS_2, and OsS_2.

7. Discussion

7.1. Behavior of silicates and chromite during flotation.

PGM and BMS are liberated from silicates and chromite by the process of comminution and size reduction. In order to make the process of flotation more efficient, the ore must be properly milled to ensure loss of valuable minerals doesn't occur. If the ore is over-milled, this might lead to the loss of valuable and economic minerals (Liddell et al., 1986, Ekmekci et al., 2003).

Different chemicals are added to the system, to help recover the valuable minerals by means of flotation and reduce the floatability of silicates and chromite (Liddell et al., 1986, Lotter et al., 2008).

Plagioclase, orthopyroxene, and chromite are the dominant gangue mineral phases, while talc, chlorite, hornblende, and phlogopite are the minor gangue mineral phases in the UG-2 chromitite (McLaren and de Villiers, 1982, Liddell et al., 1986, Wesseldijk et al., 1999, Penberthy 2000, Nel et al., 2005, Becker et al., 2008). Talc, orthopyroxene, and chromite are not desirable in the concentrator, since they cause furnace operational problems, by reducing the efficiency in down stream processing. Chromite shorten the campaign life of the furnace (Jones, 1999, Wesseldijk et al., 1999, Ekmekci eta l., 2003, Martinovic et al., 2004, Nel et al., 2005, Lotter et al., 2008). Talc and orthopyroxene increase volume in the furnace without valuable ore grade.

Orthopyroxene is a major silicate mineral. It is anhydrous in nature and has the ability to alter into hydrous mineral such as talc and serpentine (Lotter et al., 2008). Talc forms around the rims and in cleavage planes of orthopyroxene. Talc floats naturally and it has the ability to enhance froth stability and increase the entrainment of silicates and chromite (Martinovic et al., 2004, Lotter et al., 2008).

In the primary rougher circuit, the concentrations of silicates and chromite increase in abundance along the circuit. Some silicates and chromite report to the concentrate by means of:

1. Entrainment and Natural flotation: a process whereby silicates and chromite floats naturally in the absence of chemical activation and report to the flotation concentrate. Talc (hydrophobic in nature), causes orthopyroxene, and chromite (hydrophilic in nature) to float. This problem is solved by addition of carboxy methyl cellulose (CMC) or a guar gum to the flotation system (Wesseldijk et al., 1999, Ekmekci eta l., 2003, Martinovic et al., 2004, Nel et al., 2005, Lotter et al., 2008).

2. Composite particle: a floating economic mineral of interest, is attached to the naturally floating undesirable mineral, such as talc or orthopyroxene and report to the flotation concentrate. This problem is solved by additional milling of composite mineral, liberating economic ore mineral from gangue mineral (Lotter et al., 2008).

3. Inadvertent ion activation – reagents suite such as copper sulphate when added as an activator, might transform inert pyroxene into a floatable mineral (Wesseldijk et al., 1999, Ekmekci eta l., 2003, Martinovic et al., 2004, Lotter et al., 2008).

Silicates and chromite reports to the final concentrate due to the decrease of concentration of depressors. The concentration of depressors is decreased from PRC 1 (high grade) to PRC 10 (low grade), to ensure that complete depression of unwanted material does not occur. If there is a high concentration of depressors in low grade cells, this might lead to the loss of valuable PGM and BMS, due to suppression of both liberated PGM and BMS (Penberthy, 1999, Merkle and McKenzie, 2002).

PRF has a 14.6 weight percent chromium concentration and 13.9 weight percent iron concentration (Figure 7.1). In PRC 1 concentrate, the concentration of chromium and iron is approximately 8 weight percent and 2 weight percent. The decrease in concentration is due to addition of depressors.

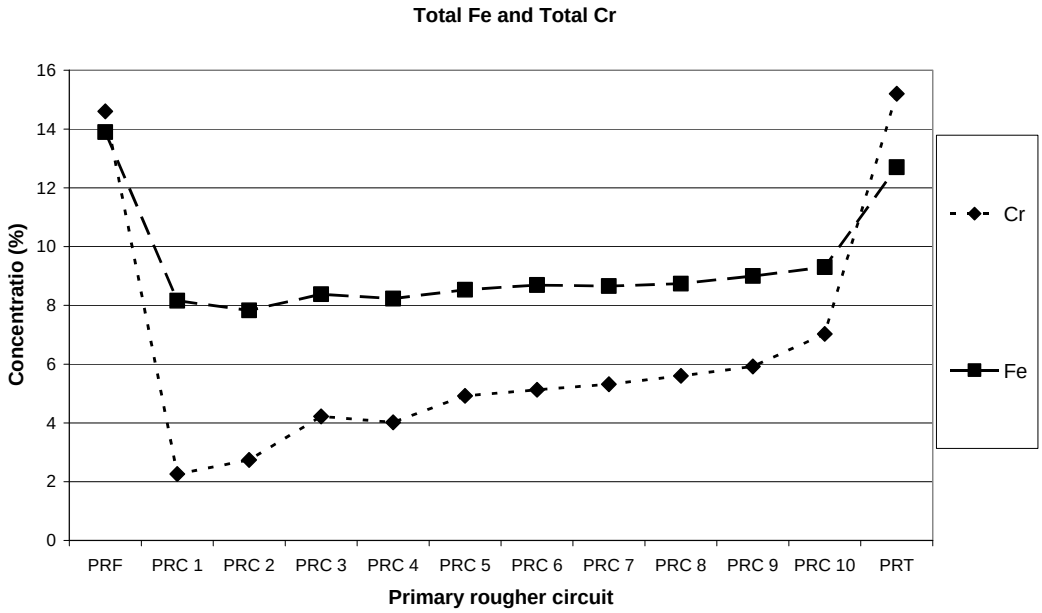

Figure 7.1: Analysis of total Fe and total Cr in primary rougher circuit.

The concentration of Cr and Fe increase in abundance along the circuit, this is due to the presence of chromite and iron rich pyroxene, that were introduced in the concentrate by the process of entrainment, inadvertent ion activation, and natural flotation (Wesseldijk et al., 1999, Ekmekci eta l., 2003, Martinovic et al., 2004, Nel et al., 2005, Lotter et al., 2008).

7.2. Flotation behavior of PGM.

In PRF, more than 50 volume percent of the PGM are liberated. This resulted from the process of crushing and milling, where by the PGM grains are freed from the silicates and chromite (Liddell et al., 1986, Penberthy and Merkle, 1999). Liberated PGM and PGM associated with liberated BMS are expected to float during the concentration stage and report to the final concentrate.

Platinum containing sulphide makes up approximately 80 volume percent of PGM in PRF, followed by laurite (approximately 14 volume percent). PGM alloy together with PGM containing arsenic and PGM containing tellurium (makes up approximately 5 volume percent). Platinum containing sulphides are expected to be recovered in large quantities, since they are the most abundant in the feed material.

It is always desirable to float PGM together with BMS, since BMS with larger ECD (of greater than 10 µm), will help smaller PGM, with ECD (of less than 3 µm) to float and report to the final concentrate. PGM associated with pentlandite and chalcopyrite reports to the fast floating concentrate, since pentlandite and chalcopyrite are fast floating BMS (depending on grain sizes and degree of liberation of BMS). PGM associated with pyrrhotite reports to the slow floating concentrate, since pyrrhotite is a slow floating BMS (Penberthy, et al., 2000, Xiao and Laplante, 2004).

The grade of PGE in PRC 1 concentrate is double the grade of PGE in PRC 2 concentrate; therefore we expect to recover more PGM from PRC 1. The shift in Pt:Pd concentration is approximately 0.5 in PRC 1 and approximately 0.68 in PRC 2 (Figure 7.2), therefore more palladium is taken out in PRC 1 than in PRC 2, as compared to platinum (Chetty et al., 2009).

The Pt:Pd ratio in the primary rougher circuit is approximately 2:1, except for PRC 1, where Pt:Pd ratio is approximately 1 (Figure 7.2). This might be due to poor recovery of platinum in PRC 1. The poor recovery of platinum might be due to small grains of mineral containing platinum, and also small mineral grains of platinum associated with coarser silicates and chromite.

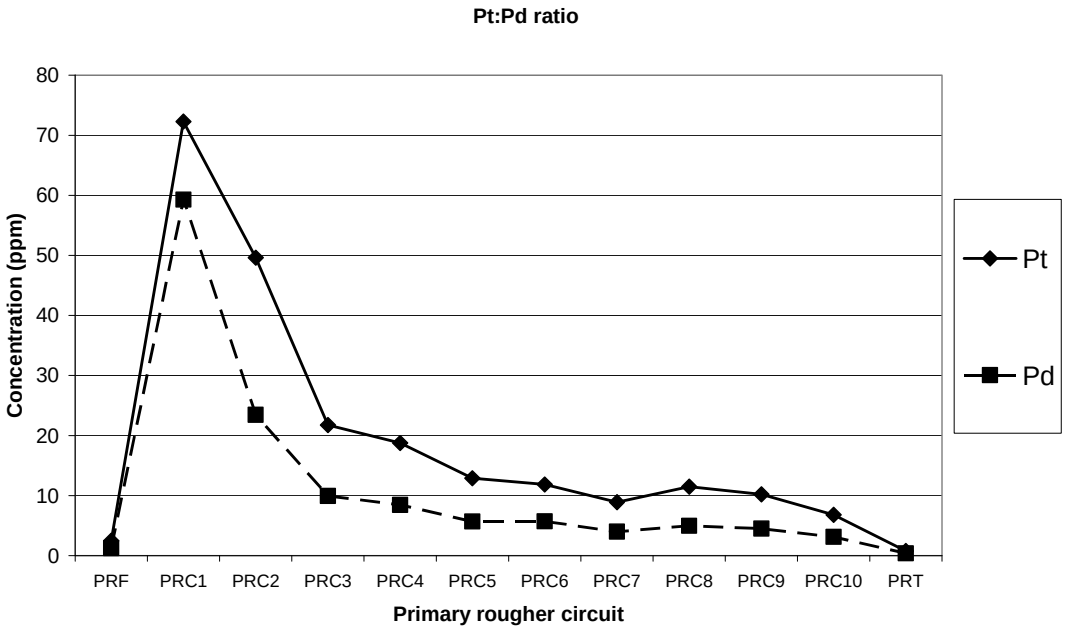

Figure 7.2: Summary diagram of Pt:Pd ratio along the primary rougher circuit. See also figure 6.2 in the previous chapter.

Liberated PGM and PGM associated with BMS make up more than 80 volume percent of PGM, which are recovered from PRC 1 concentrate. Less than 20 volume percent of PGM and BMS associated with silicates and chromite reports to the PRC 1 concentrate (see also figure 6.27 in the previous chapter).

PGM that are recovered from PRC 1 concentrate, in order of abundance are: platinum containing sulphides (approximately 78 volume percent), laurite (approximately 13 volume percent). PGM alloy, PGM containing arsenic, and PGM containing tellurium makes up approximately 9 volume percent of the recovery (see also figure 6.22 in the previous chapter). The dominating platinum containing sulphides in order of abundance in PRC 1 are PtPdNiS (42 volume percent), PtS (22 volume percent), and PtRhCuNiS (16 volume percent).

In PRC 1 concentrate, the recovery of fast floating, high grade, liberated PGM is due to their grain liberation index of greater than 0.8 and high floatability index of greater than 3 µm ECD. More than 70 volume percent of PGM in PRC 1 have liberation index of greater than 0.8. The recovery of PGM with high liberation index of 0.8, decreases from PRC 1 (approximately 70 volume percent) to PRC 10 (approximately 37 volume percent). The recovery of liberated PGM and PGM associated with liberated BMS decreases from approximately 85 volume percent in PRC 1 to approximately 38 volume percent in PRC 10. The recovery of PGM and BMS associated with silicates and chromite increases from PRC 2 (approximately 20 volume percent) to PRC 10 (approximately 80 volume percent).

PGM and BMS associated with silicates and chromite are considered as slow floaters, this is due to their small floatability index of less than 3 µm ECD and the liberation index of less than 0.2. In order to successfully recover these PGM, more resident time is required in the flotation cells (Liddell et al., 1986, Lotter et al., 2008). In all primary rougher cells, the most dominating platinum containing sulphides are PtPdNiS, PtS, and PtRhCuNiS (see also figure 6.22 in chapter 6).

In PRT, liberated PGM and PGM associated with liberated BMS make up less than 20 volume percent. PGM and BMS associated with silicates and chromite (either attached or locked) makes up more than 80 volume percent. PGM that reported in the PRT, are mostly liberated PGM with less than 3 µm ECD, PGM less than 3 µm ECD attached to silicates or chromite, and PGM more than 3 µm ECD attached to silicates or chromite (see also figure 6.28 in the previous chapter). These PGM were unable to float in the primary rougher circuit due to their grain sizes and mode of occurrence. PGM in the PRT (approximately 60 volume percent) has a liberation index of less than 0.2; this might be the cause of PGM non floatability in the primary rougher circuit.

Platinum containing sulphide (approximately 62 volume percent) is the dominating PGM in the PRT, followed by laurite (26 volume percent). PGM alloy, PGM containing arsenic and PGM containing tellurium makes up approximately 12 volume percent of detectable PGM in the PRT. PGM and BMS that report to the PRT are milled again and re-floated (MF2: mill-float, mill-float), in order to recover more PGM and BMS, and eliminate silicates and chromite.

Fast floating PGM in the primary rougher circuit are recovered together with "Coarser, liberated, and fast floating BMS", such as pentlandite (with the ideal formula $(Fe,Ni)_9S_8$) and chalcopyrite (with the ideal formula $CuFeS_2$). Pentlandite and chalcopyrite are major sources of nickel (Ni), copper (Cu), cobalt (Co), and sulphur (S).

Fine grained PGM with < 3 µm ECD, PGM associated with pyrrhotite (with the ideal formula $Fe_{1-x}S$), and non sulphide PGM are recovered from the slow floating cells.

The concentration of nickel, copper, cobalt, and sulfur decrease in abundance along the circuit (Figure 7.3 and 7.4). This is due to high concentration of coarser, liberated BMS that were successfully recovered from the fast floating cells. There is only low concentration of nickel, copper, cobalt, and sulfur in the last few cells. The presence of these elements in the last few cells might be due to the presence of pentlandite and chalcopyrite that are locked in silicates and chromite, and also the slow floating pyrrhotite (Penberthy et al., 2000, Wiese et al., 2007).

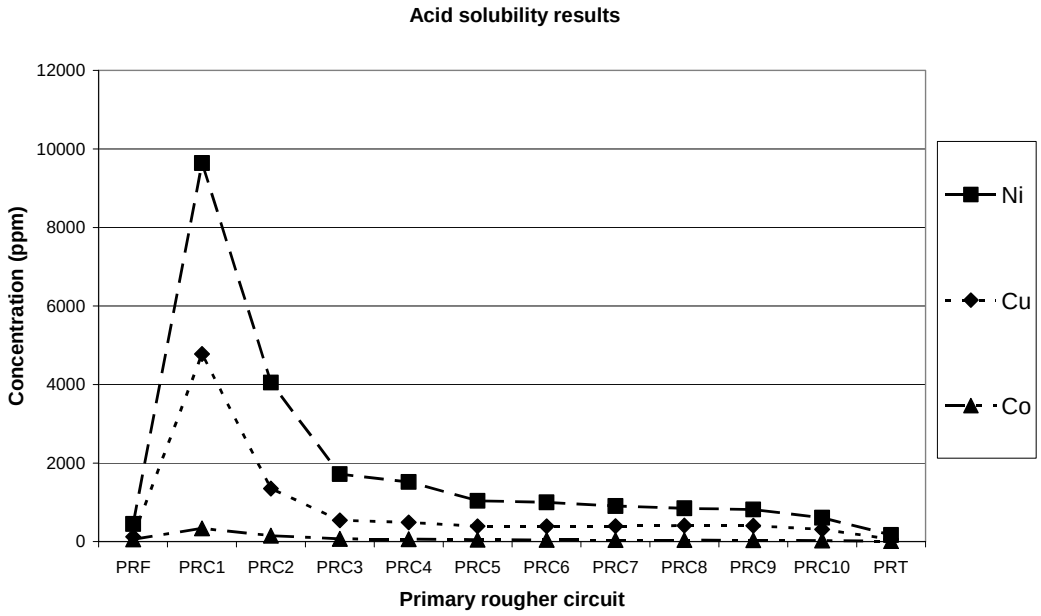

Figure 7.3: Summary diagram of base metals results of primary rougher circuit. See also figure 6.8 to figure 6.12 in the previous chapter.

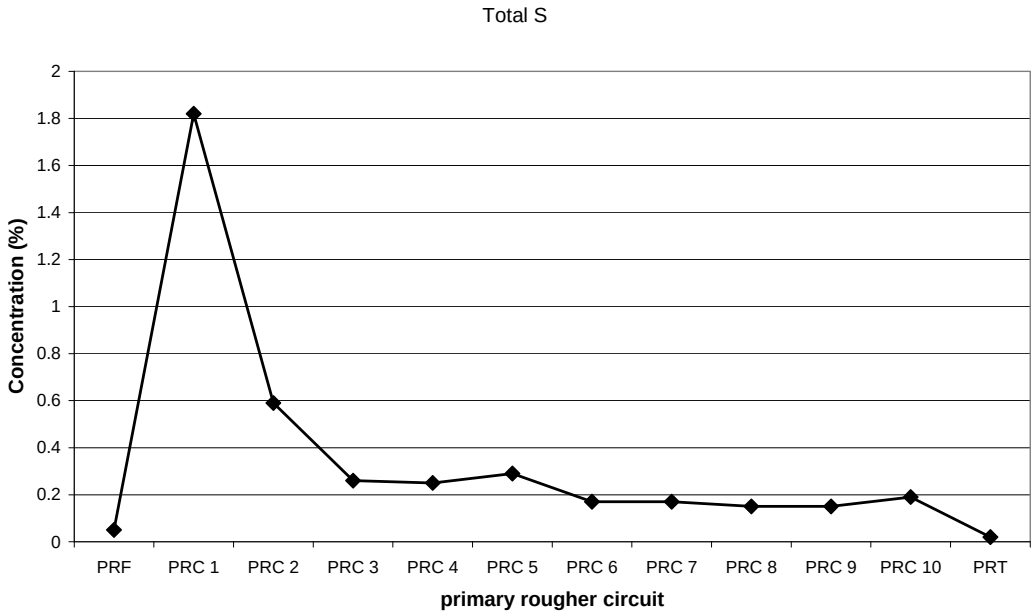

Figure 7.4: Summary diagram of total S from primary rougher concentrate.

There is a linear relationship and a positive correlation between nickel and sulphur; this is due to the fast floating and coarse grains of pentlandite that are recovered successfully in the primary rougher concentrates (Figure 7.5). Liberated, coarse, and fast floating pentlandite is recovered in PRC 1 and PRC 2 (first two data points from right to left in the graph). In the bottom left corner of the graph are the data points of PRC 3 to PRC 10. There is no linear relationship between nickel and sulphur in these cells. Pentlandite in these cells has small grain sizes and it is mostly associated with gangue minerals.

There is also a linear relationship between cobalt and sulphur (Figure 7.6). Cobalt and sulphur behave in the same manner as nickel and sulphur in the primary rougher concentrate, hence there is a perfect linear relationship between cobalt and nickel with spearman correlation coefficient of r = 1.00 (Figure 7.7). This is due to cobalt that is present in pentlandite (cobalt rich pentlandite), or nickel that are present in solid solution with cobalt in pentlandite (Merkle and Von Gruenewaldt, 1986, McLaren and De Villiers, 1982).

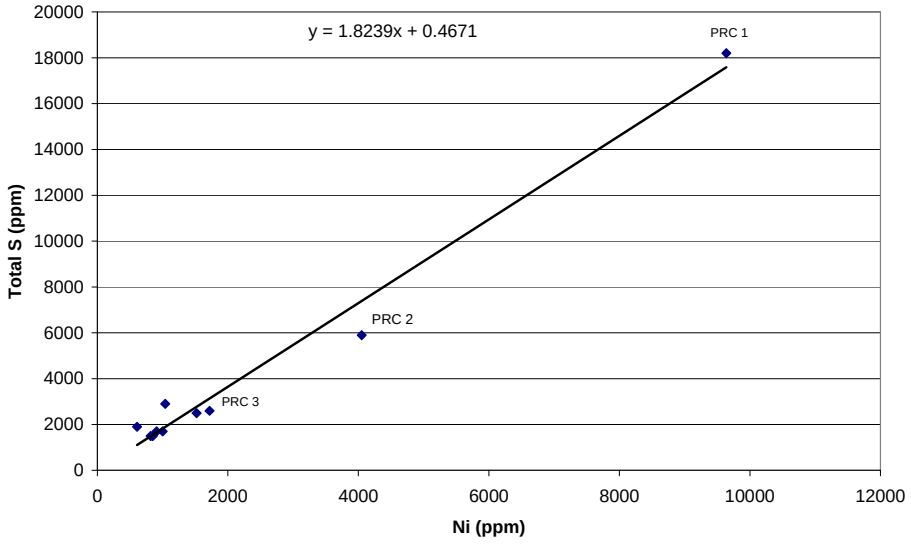

Figure 7.5: Relationship between acid soluble nickel and sulphur from PRC 1 to PRC 10. Spearman correlation coefficient r = 0.99. The solid line represents the linear regression.

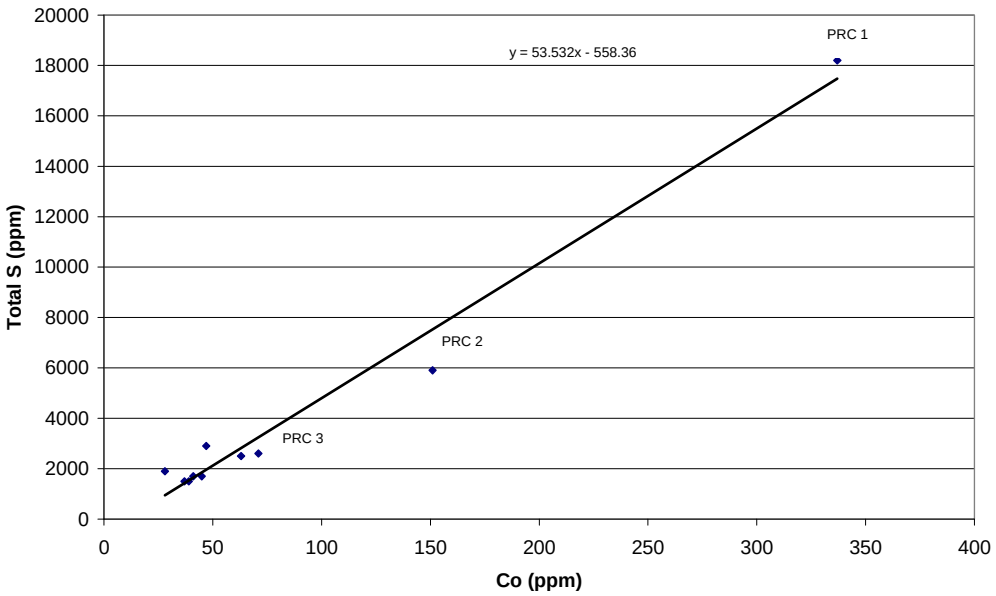

Figure 7.6: Relationship between acid soluble cobalt and sulphur from PRC 1 to PRC 10. Spearman correlation coefficient r = 0.99. The solid line represents the linear regression.

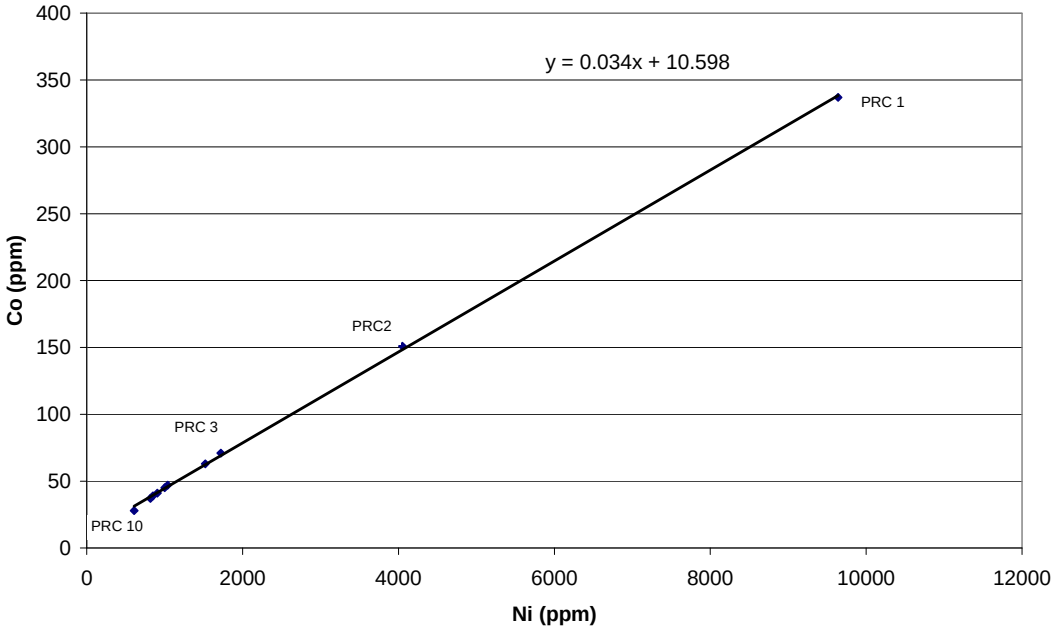

Figure 7.7: Relationship between nickel and cobalt from PRC 1 to PRC 10. Spearman correlation coefficient r = 1.00. The solid line represents the linear regression.

Chalcopyrite is the second fastest floating BMS in the UG-2 concentrate. Coarse and liberated chalcopyrite grains are mostly recovered in PRC 1 and PRC 2; hence there is a strong linear relationship between PRC 1 and PRC 2 (Figure 7.8). There is no linear relationship from PRC 3 to PRC 10, since chalcopyrite grains are associated with gangue minerals and have small grain sizes.

There is no linear relationship between nickel and copper in the primary rougher concentrate (Figure 7.9). The ratio of pentlandite and chalcopyrite in the PRC is not constant, but in all the concentrates more pentlandite is recovered as compared to the chalcopyrite. In PRC 1 concentrate, 24 percent of chalcopyrite grains are associated with gangue minerals and PGM, while from PRC 2 to PRC 10 (70 percent to 90 percent) of the chalcopyrite grains are associated with gangue minerals and PGM. The association of pentlandite with gangue minerals and PGM is 40 percent in PRC 1 concentrate, and 53 percent to 75 percent between PRC 2 and PRC 10.

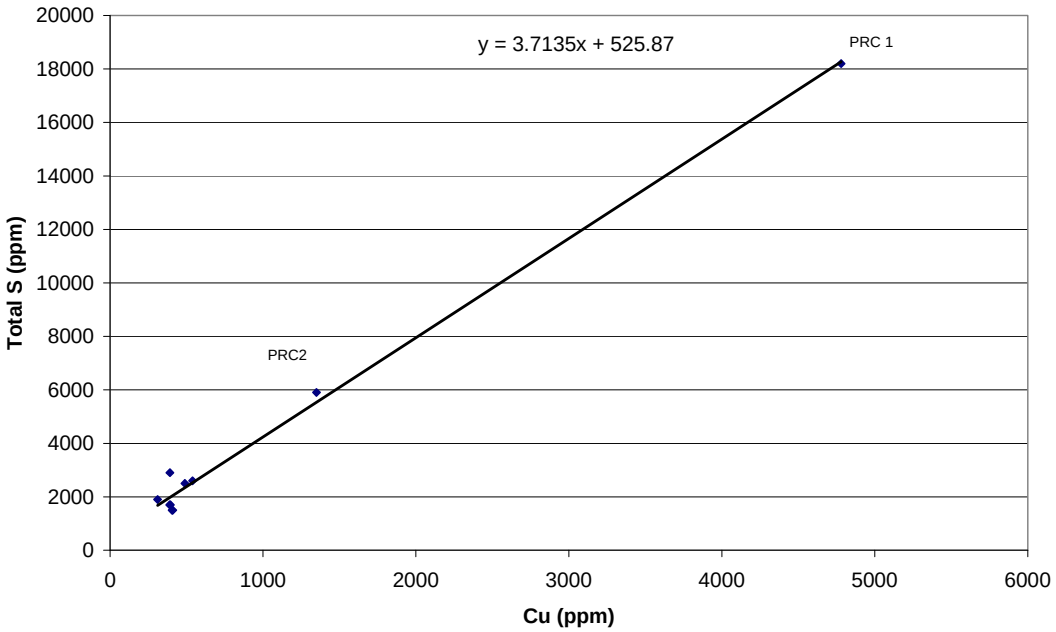

Figure 7.8: Relationship between acid soluble copper and sulphur from PRC 1 to PRC 10. Spearman correlation coefficient r = 0.99. The solid line represents the linear regression.

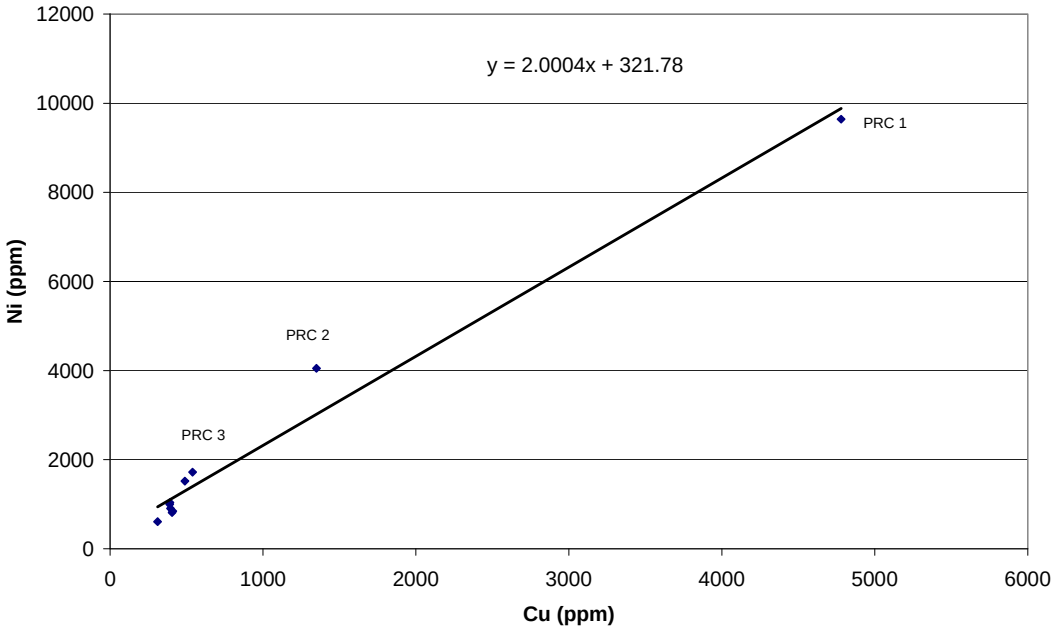

Figure 7.9: Relationship between copper and nickel from PRC 1 to PRC 10. Spearman correlation coefficient r = 0.99. The solid line represents the linear regression.

PGM are recovered together with BMS such as pentlandite and chalcopyrite, hence there is a positive linear relationship between palladium and sulphur from PRC 1 to PRC 3 (Figure 7.10). High concentration of sulphur is extracted from PRC 1 to PRC 3 (Figure 7.4). There is more scatter between palladium and sulphur from PRC 4 to PRC 10, since some of the PGM in these concentrates are associated with pyrrhotite and gangue minerals. There is also significant amount of PGE alloys that is being recovered in the slow floating concentrate (Merkle and McKenzie, 2002).

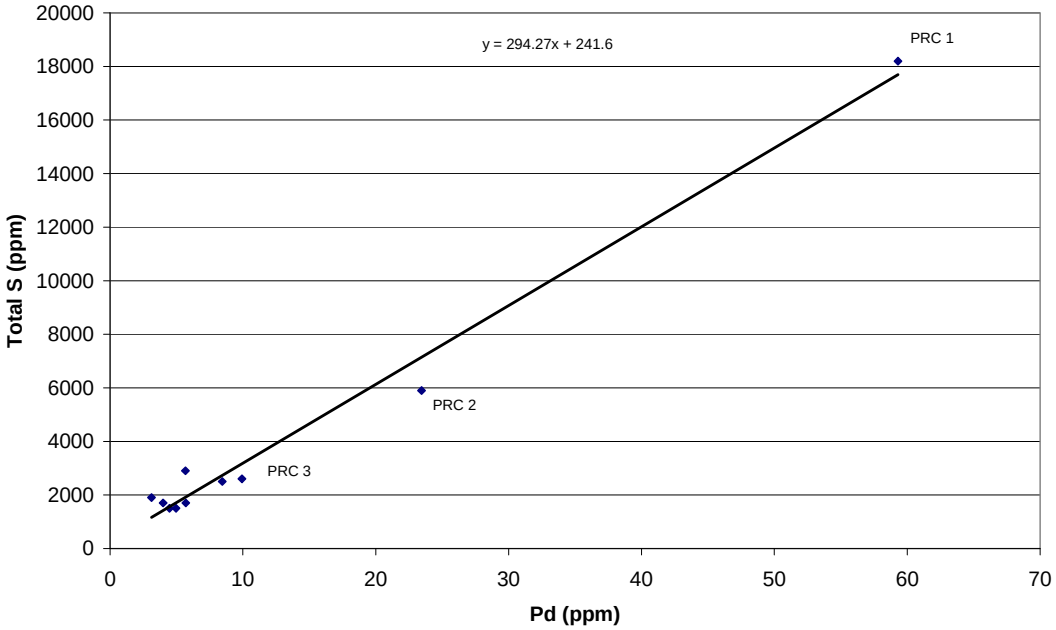

Figure 7.10: Relationship between palladium and sulphur from PRC 1 to PRC 10. Spearman correlation coefficient r = 0.99. The solid line represents the linear regression.

In PRC 1 concentrate, few PtPdNiS grains are associated with chalcopyrite. PtPdNiS grains that are associated with chalcopyrite and gangue minerals occurs mostly from PRC 2 to PRC 10 concentrates, hence there is no linear relationship between copper and palladium from PRC 1 to PRC 10 concentrates (Figure 7.11, regression line for illustration purpose only). In the UG-2 chromitite, braggite is rarely associated with chalcopyrite. There is no solid solution between palladium and copper in chalcopyrite, since chalcopyrite is barren of PGE (Penberthy and Merkle, 1999).

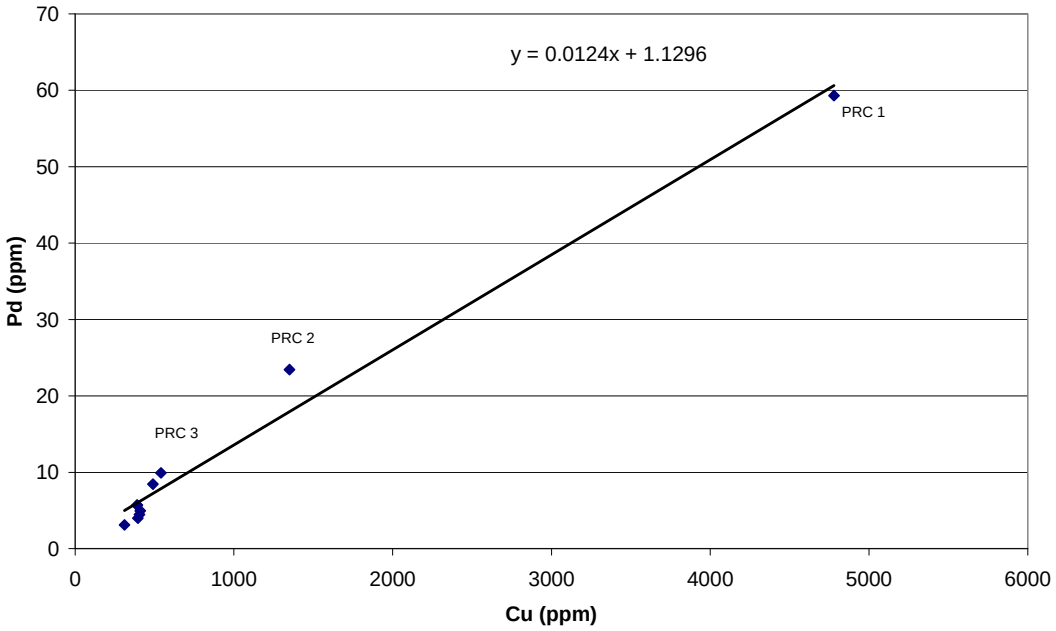

Figure 7.11: Relationship between copper and palladium from PRC 1 to PRC 10. Spearman correlation coefficient r = 0.99. The solid line represents the linear regression.

There is strong linear relationship between nickel and palladium (Figure 7.12); since braggite is mostly associated with pentlandite, and also nickel that is in solid solution with palladium in pentlandite (Kinloch, 1982, Xiao and Laplante, 2004). Larger grains of pentlandite will cause braggite to float and report to the final concentrate.

There is no perfect linear relationship between platinum and palladium from PRC 1 to PRC 10 concentrates (Figure 7.13 a, regression line for illustration purpose only). When PRC 1 concentrate is excluded, there is a perfect linear relationship between platinum and palladium (Figure 7.13 b). This is an indication that liberated, coarser PtPdNiS and PtS grains are recovered from fast floating PRC 1 concentrate, as compared to the other primary rougher concentrate (PRC 2 to PRC 10, see also Figure 6.22 in the previous chapter). In PRC 1 concentrate, more PtPdNiS (38 volume percent) is extracted as compared to PtS (22 volume percent), since braggite is a faster floating PGM than cooperite (Merkle and McKenzie, 2002).

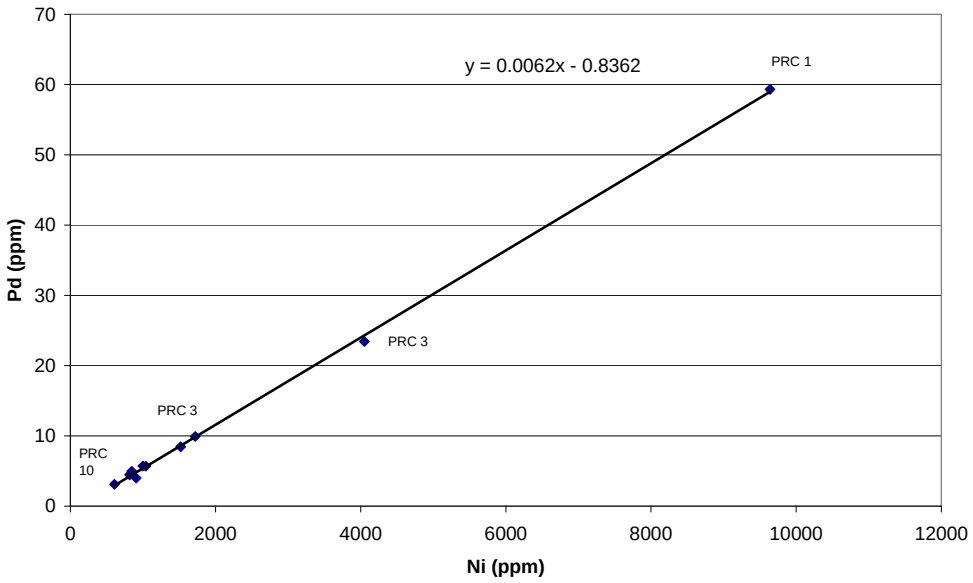

Figure 7.12: Relationship between nickel and palladium from PRC 1 to PRC 10. Spearman correlation coefficient r = 1.00. The solid line represents the linear regression.

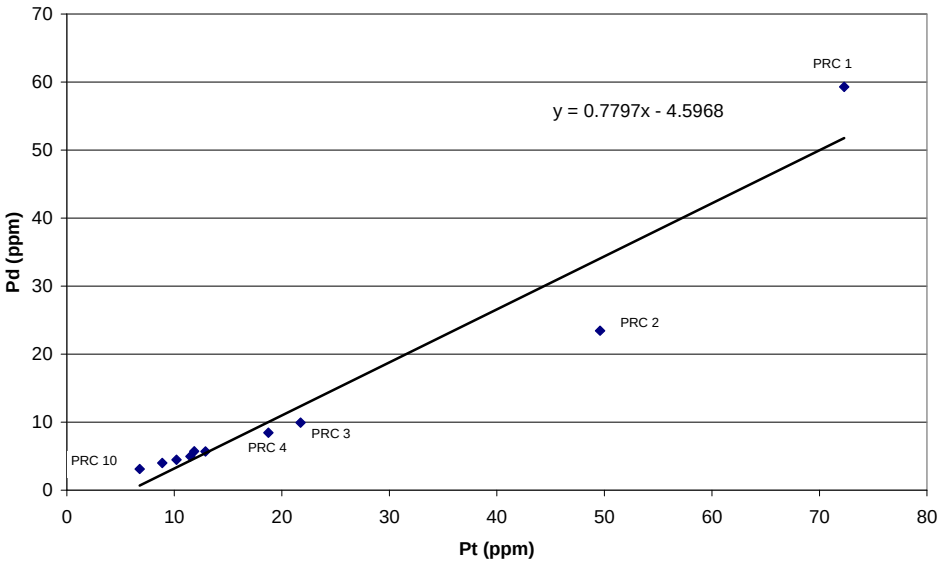

Figure 7.13 a: Relationship between platinum and palladium from PRC 1 to PRC 10. Spearman correlation coefficient r = 0.96. The solid line represents the linear regression.

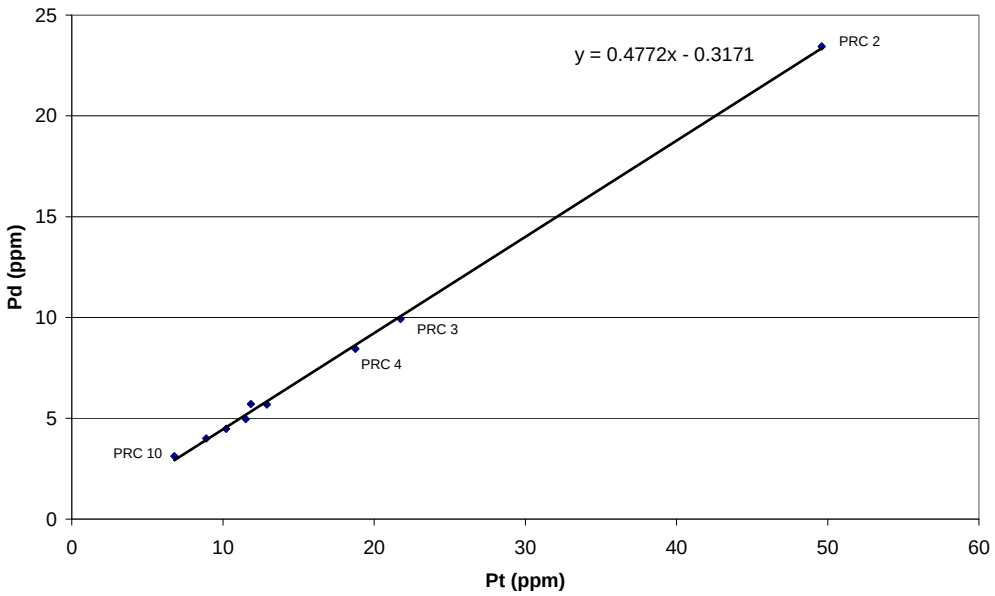

Figure 7.13 b: Relationship between platinum and palladium from PRC 2 to PRC 10. Spearman correlation coefficient r = 1.00. The solid line represents the linear regression.

Braggite (PtPdNiS) and malanite ($CuPt_2S_4$) in the UG-2 concentrate are mostly associated with pentlandite. Palladium is commonly concentrated in braggite and rhodium is commonly concentrated in malanite in the UG-2 chromitite. Palladium and rhodium usually undergoes solid solution in pentlandite (Kinloch, 1982, Penberthy and Merkle, 1999). Braggite floats faster than malanite. Braggite and malanite (depending on size and mode of occurrence) are fast floating minerals and their recovery occurs mostly in PRC 1 concentrate (Figure 7.14 a).

There is no perfect linear relationship between palladium and rhodium from PRC 1 to PRC 10, but when PRC 1 concentrate, is excluded there is a perfect linear relationship (Figure 7.14 b). Malanite and braggite grains that are recovered from PRC 1 concentrate, are coarser, liberated, and associated with liberated BMS, while braggite and malanite grains that are recovered from PRC 2 to PRC 10 concentrates, are associated with BMS and gangue minerals.

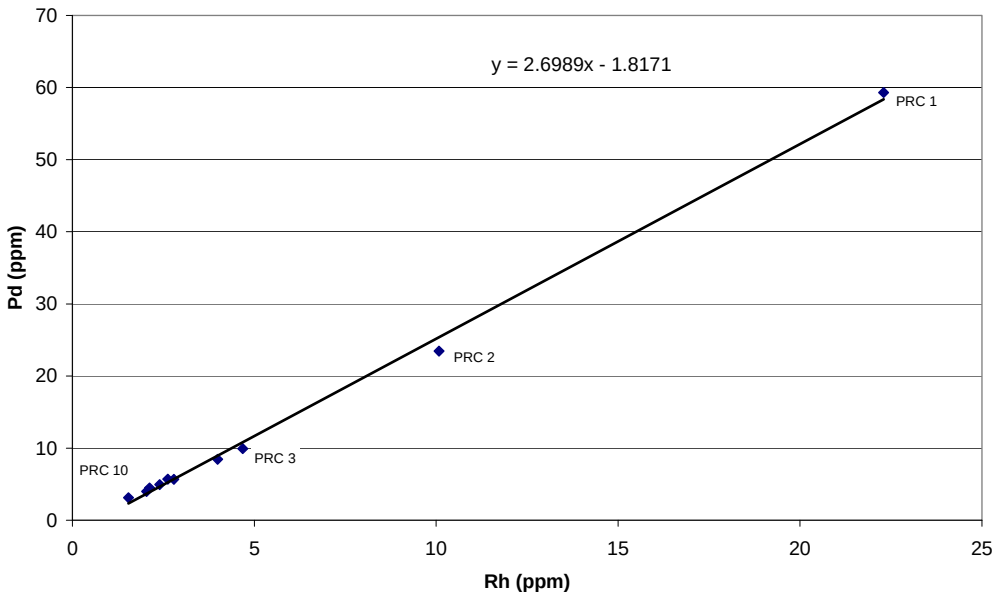

Figure 7.14 a: Relationship between rhodium and palladium from PRC 1 to PRC 10. Spearman correlation coefficient r = 0.99. The solid line represents the linear regression.

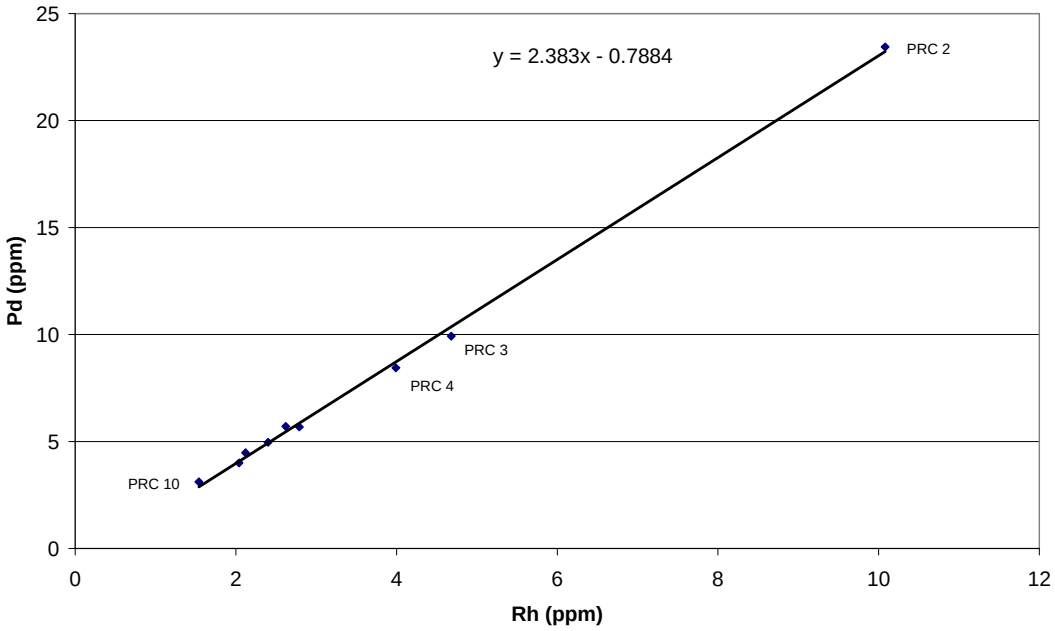

Figure 7.14 b: Relationship between rhodium and palladium from PRC 2 to PRC 10. Spearman correlation coefficient r = 0.99. The solid line represents the linear regression.

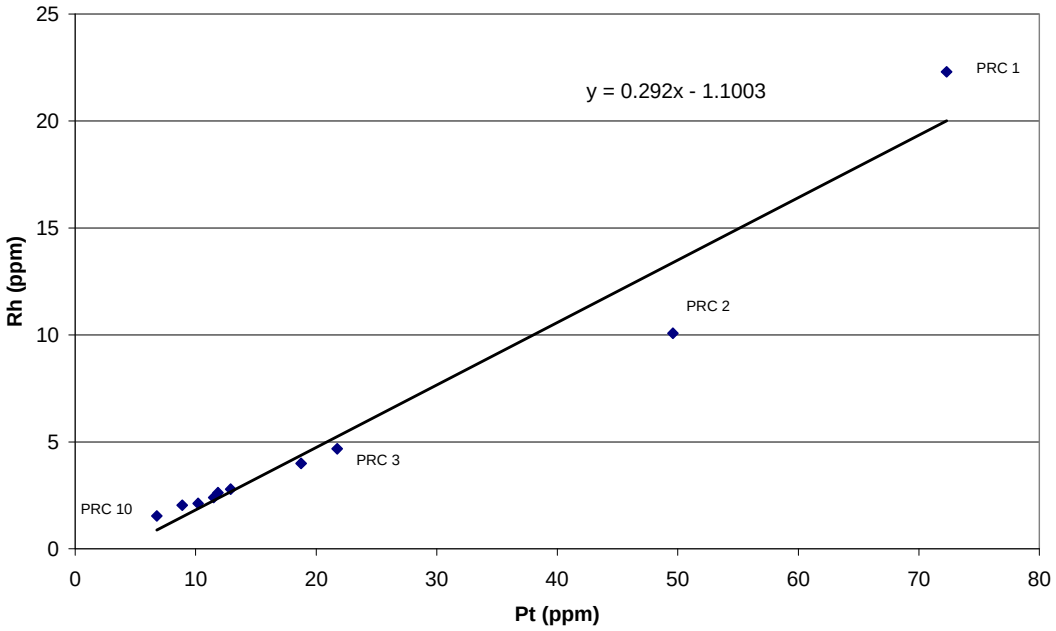

Figure 7.15 a: Relationship between platinum and rhodium from PRC 1 to PRC 10. Spearman correlation coefficient r = 1.00. The solid line represents the linear regression.

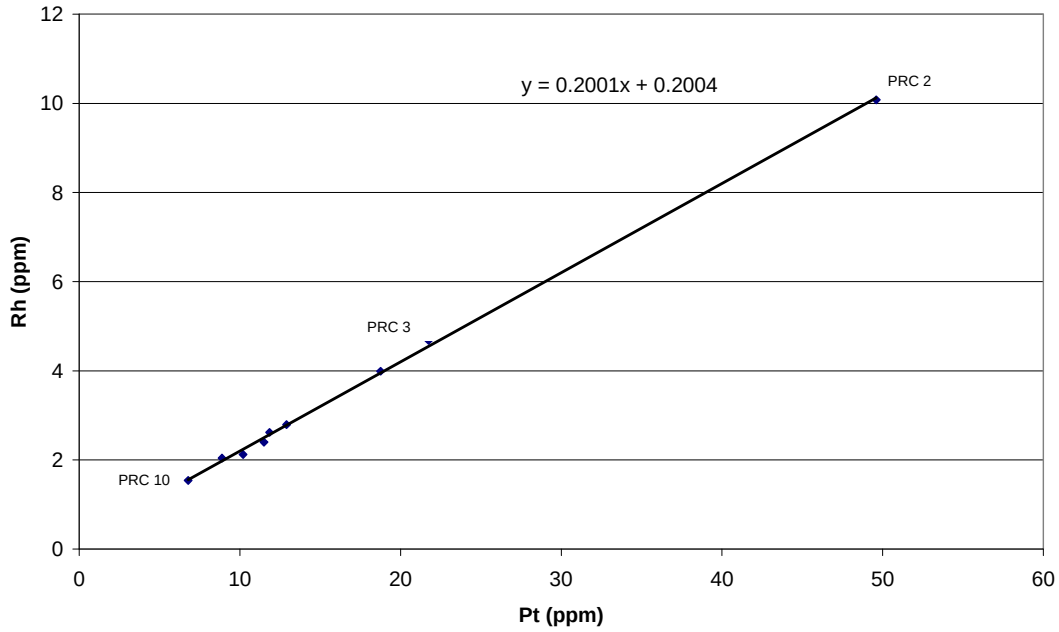

Figure 7.15 b: Relationship between platinum and rhodium from PRC 2 to PRC 10. Spearman correlation coefficient r = 1.00. The solid line represents the linear regression.

There is no linear relationship between platinum and rhodium from PRC 1 to PRC 10. In PRC 1 concentrate, most of the cooperite and malanite that are recovered are coarser, liberated, and associated with liberated BMS (Figure 7.15 a). Cooperite (PtS) floats faster than malanite ($CuPt_2S_4$). When PRC 1 concentrate, is excluded there is a perfect linear relation between platinum and rhodium (Figure 7.15 b). Cooperite and malanite that are recovered from PRC 2 to PRC 10 concentrates are associated with BMS and gangue minerals.

8. Conclusions

The variation between nickel and sulphur, cobalt and sulphur, copper and sulphur, nickel and cobalt in the primary rougher concentrate demonstrate that coarser, liberated, and fast floating pentlandite and chalcopyrite reports to the PRC 1 concentrate. The recovery of finer liberated BMS and finer BMS associated with gangue minerals increases from PRC 2 to PRC 10.

In the primary rougher concentrate more pentlandite is recovered as compared to chalcopyrite. High recovery of pentlandite contributes to the high recovery of palladium and rhodium, since both these elements substitutes for nickel in pentlandite. This doesn't apply to palladium in chalcopyrite, since palladium and copper do not form a solid solution in chalcopyrite.

In the primary rougher concentrates, more palladium is recovered from PRC 1 than in PRC 2. In PRC 1 concentrate the recovery of palladium is higher than of platinum. This is due to the liberated, coarser, and fast floating braggite that is recovered as compared to cooperite.

Liberated PGM and PGM associated with liberated, coarser and fast floating base metal sulphides decrease in abundance along the circuit, while PGM associated with silicates and chromite (either attached or locked) increase in abundance along the circuit. The combined

liberation index (CLI) of PGM decreases from greater than 0.8 in PRC 1 to less than 0.2 in PRC 10.

PRC 1 and PRC 2 are considered as fast floating concentrates, while PRC 3 to PRC 10 are considered as moderate to slow flow floating concentrates. The highest recovery of PGM is in PRC 1 and PRC 2.

Braggite, cooperite, and malanite are fast floating PGM, while pentlandite and chalcopyrite are fast floating BMS. PGM alloys are slow floating PGM, while pyrrhotite is a slow floating BMS.

In PRC 1 and PRC 2 concentrates, 75 volume percent to 85 volume percent of PGM with a CLI of greater than 0.8, are recovered successfully. The platinum containing sulphides recovered in PRC 1 and PRC 2 in the order of decreasing abundance are braggite (PtPdNiS), cooperite (PtS), malanite ($CuPt_2S_4$), and laurite (RuS_2). These PGM are liberated PGM and PGM associated with liberated, coarser and fast floating base metal sulphides (such as pentlandite and chalcopyrite). They also have large grain sizes.

PGM alloy recovered is mostly Pt-Fe alloy. PGM containing arsenic is mostly sperrylite. Liberated PGM and PGM associated with liberated BMS range from 70 volume percent in PRC 3 to 40 volume percent in PRC 10. PGM with CLI of greater than 0.8 range from 50 percent in PRC 3 to 30 percent in PRC 10. PGM from PRC 3 to PRC 10 have small grain sizes and are mostly associated with slower floating BMS and gangue minerals. The detectable platinum containing sulphides recovered from PRC 3 to PRC 10, in the order of decreasing abundance includes braggite (PtPdNiS), cooperite (PtS), malanite ($CuPt_2S_4$), and laurite (RuS_2).

The recovered platinum containing sulphides make up more than 90 volume percent of PGM in each cell in the primary rougher circuit. PGM alloy, PGM containing arsenic and PGM containing tellurium make up only less than 10 volume percent of recovered PGM in each cell in the primary rougher circuit.

9. References

Becker, M., Mainza., A.N, Powell., M.S, Bradshaw., D.J. and Knopjes, B. (2008). Quantifying the influence of classification with the 3 product cyclone on liberation and recovery of PGM in UG2 ore. Minerals Engineering, 21, 549 – 558.

Buick, I.S., Maas, R. and Gibson, R. (2001). Precise U-Pb titanite age constraints on the emplacement of the Bushveld complex, South Africa. Journal of Geological Society of London, 158, 3-6.

Buswell., A.M, Bradshaw., D.J, Harris, P.J. and Ekmekci, Z. (2002). The use of electrochemical measurement in the flotation of platinum group minerals (PGM) bearing ore. Minerals Engineering, 15, 395 – 404.

Cabri, L.J. (2002). The mining and beneficiation of South African PGE Ores – an overview. In: Cabri, L.J. (Editor), The Geology, Geochemistry, Mineralogy and Mineral Beneficiation of platinum group elements. Canadian institute of Mining, metallurgy and petroleum, pp. 793 – 809.

Cabri, L.J., Laflamme, J.H.G. and Stewart, J.M. (1978). On cooperate, braggite and vysotkite. American Mineralogist 63, 832 -839.

Cameron, E.N. (1978). The lower zone of the eastern Bushveld complex in the olifants river trough: Journal of Petrology, 19, 437 – 462.

Carr, H.W., Groves, D.I. and Cawthorn, R.G. (1994). The importance of synmagmatic deformation in the formation of Merensky reef potholes in the Bushveld complex: Economic Geology, 89, 263 – 276.

Cawthorn, R.G., Merkle, R.K.W. and Viljoen, M.J. (2002). Platinum group elements deposits in the Bushveld complex, South Africa. In: Cabri, L.J. (Editor.), The Geology,

Geochemistry, Mineralogy and Mineral Beneficiation of platinum group elements. Canadian Institute of Mining, Metallurgy and Petroleum, pp 793 – 809.

Chetty, D., Gryffenberg, L., Lekgetho, T.B. and Molebale, I.J. (2009). Automated SEM study of PGM distribution across a UG2 flotation concentrate bank: implications for understanding PGM floatability. The journal of South African Institute of Mining and Metallurgy, 109, 587-593.

Cousins, C.A. and Feringa, G. (1964). The chromitite deposit in the western belt of the Bushveld Complex, in Haughton, S.H., ed., The geology of some ore deposit in Southern Africa: Johannesburg, Geological Society of South Africa, 2, 183 – 202.

Davey, S.R. (1992). Lateral variations within the upper critical zone of the Bushveld Complex on the farm Rooikoppies 297 JQ, Marikana, South Africa. South African Journal of Geology, 95, 141 – 149.

Deeplaul, V. and Bryson, M. (2004). Mintek, a natural resource of minerals processing expertise for platinum ores. International Platinum Conference 'Platinum Adding Value', the South African Institute of Mining and Metallurgy.

Eales, H.V. and Reynolds, I.M. (1986). Cryptic variations within chromitites of the upper critical zone, north western Bushveld complex. Economic Geology, 81, 1056 – 1066.

Eales H.V., de Klerk W.J., Butcher A.R. and Kruger F.J. (1990). The cyclic unit beneath the UG1 chromitite (UG1FW Unit) at RPM Union Section Platinum Mine—Rosetta Stone of the Bushveld Upper Critical Zone. Mineral Magazine, 54, 23–43.

Ekmecki, Z., Bradshaw, D.J., Allison, S.A. and Harris, P.J. (2003). Effects of frother type and froth height on the flotation behavior of chromite in the UG2 ore. Minerals Engineering, 16, 941 – 949.

Engelbrecht J.P. (1990). The Marico Hyperbyssal Suite, and the marginal zone of the Bushveld Complex in the Marico District, Western Transvaal, South Africa. South African Journal of Geology, 93, 318–328.

Fandrich, R, Gu., Y, Burrows, D. and Moeller, K. (2007). Modern SEM-based mineral liberation analysis. International Journal of Mineral Processing, 84, 310 – 320.

Garruti, G. and Gazzotti, M. (1995). Iridium, Rhodium and platinum sulphides in chromitite from the ultramafic massifs of finero, Italy, and Ojen, Spain. Journal of the Mineralogical Association of Canada, 33, 509 – 520.

Goodall, W.R., Scales, P.J. and Butcher, A.R. (2005). The use of qemscan and diagnostic leaching in the characterization of visible gold in complex ores. Minerals Engineering, 18, 877-886.

Goodall, W.R. (2008). Characterization of mineralogy and gold deportment for complex tailings deposits using qemscan. Minerals Engineering, 21, 518-523.

Gottlieb, P., Wilkie, G., Sutherland, D., Ho-Tun, E., Suthers, S., Perera, K., Jenkins, B., Spencer, S., Butcher, A. and Rayner, J. (2000). Using quantitative electron microscopy for process mineralogy applications (testing and analysis). Journal of Metals, 52, 24-25.

Gros, M., Lorand, J.P. and Luguet, A. (2002). Analysis of platinum group elements and gold in geological material using NiS fire assay and Te coprecipitation; the NiS dissolution step revisited. Chemical Geology, 185, 179-190.

Gu,Y. (2003). Automated scanning electron microscope based mineral liberation analysis. An introduction to JKMRC/FEI mineral liberation analyzer. Journal of Minerals and Materials Characterization and Engineering, 2, 33 – 41.

Hamilton, P.J. (1977). Sr-isotope and trace element studies of the great dyke and Bushveld mafic phase and their relation to early proterozoic magma genesis in Southern Africa. Journal Petrology, 18, 24 – 52.

Hawthorne, F.C., Fleischer,M., Grew, E.S., Grice, J.D., Jambor, J.L., Puziewicz, J., Robeerts, A.C., Vanko, D.A. and Zilczer, J.A. (1986). New mineral names. American Mineralogist, 71, 1277 – 1282.

Jones, R.T. (1999). Platinum smelting in South Africa. South African Journal of Science, 95, 525 – 534.

Kinnaird, J.A., Kruger, P.A.M. and Cawthorn, R.G. (2002). Chromitite of the Bushveld complex – processes of formation and PGE enrichment. Economic geology research institute. Information circular No. 369. University of the Witwatersrand, Johannesburg.

Kinloch, E.D. (1982). Regional trends in the platinum group mineralogy of the critical zone of the bushveld complex, South Africa. Economic Geology, 77, 1328–1347.

Kleeberg, R., Bergmann, J. (1998). Quantitative Röntgenphasenanalyse mit den Rietveldprogrammen BGMN und AUTOQUANT in der täglichen Laborpraxis. Berichte der Deutschen Ton- und Tonmineralgruppe Greifswald, **6,** 237-250.

Kleeberg, R. and Bergmann, J. (2002). Quantitative Phase Analysis using the Rietveld Method and a Fundamental Parameter Approach. *In:* S.P. SenGupta and P. Chatterjee (Editors), Powder Diffraction. *Proc.* II International School on Powder Diffraction, IACS, Kolkata, India, Allied Publishers Limited, New Delhi, 63-76.

Klein, C. (2002). The 22nd edition of the manual of mineral science. John Wiley and sons, Inc. - 340pp.

Kruger, F.J. (1990). The Stratigraphy of the Bushveld Complex: a reappraisal and the relocation of the Main Zone boundaries. South African journal of geology, 93, 376–381.

Kruger, F.J. (1994). The Sr-isotopic stratigraphy of the Western Bushveld Complex. South African Journal of Geology, 97, 393–398.

Kruger, F.J. (2005). Filling the Bushveld Complex magma chamber: lateral expansion, roof and floor interaction, magmatic unconformities, and the formation of giant Chromitite, PGE and Ti-V- Magnetitite deposits. Mineralium Deposita, 40, 451–472.

Lastra, R. (2007). Seven practical application cases of liberation analysis. International Journal of Mineral processing, 84, 337-347.

Lee, C.A. (1996). A review of mineralization in the bushveld complex and some other layered intrusions. In R.G Cawthorn (Editor) Layered Intrusions, 103 – 105.

Liddell, K.S., McRae, L.B. and Dunne, R.C. (1986). Process routes for beneficiation of noble metals from Merensky and UG-2 ores. Mintek Review, 4, 33-44.

Lotter, N.O., Bradshaw, D.J., Becker, M., Parolis, L.A.S. and Kormos, L.J. (2008). A discussion of the occurrence and undesirable flotation behavior of orthopyroxene and talc in the processing of mafic deposit. Minerals Engineering, 21, 905-912.

Loubser, M. and Verryn, S. (2008). Combining XRF and XRD analyses and sample preparation to solve mineralogical problems. South African Journal of Geology, 111, 229-238.

Martinovic, J., Bradshaw, D.J. and Harris, P.J. (2004). Investigation of surface properties of gangue minerals in platinum bearing ores. International platinum conference 'platinum adding value'. South African Institute on Mining and Metallurgy, 105, 1 – 7.

McLaren, C.H. and de Villiers, J.P.R. (1982). The platinum group chemistry and mineralogy of the UG2 chromitite layer of the bushveld complex. Economic Geology, 77, 1348 – 1366.

Maier, W.D. (2005). Platinum group element (PGE) deposits and occurrences: Mineralization styles, genetic concepts, and exploration criteria. Journal of African Earth Science 41, 165 – 191.

Maier W.D. and Eales H.V. (1994). A facies model for the interval between the UG2 and Merensky Reef Western Bushveld Complex. Transvaal Institute of Mining and Metallurgy Section B Applied Earth Science, 103,B22–B30.

Merkle, R.K.W. and Mckenzie, A.D. (2002). The mining and beneficiation of South African PGE Ores – an overview. In: Cabri, L.J. (ED.), The Geology, Geochemistry, Mineralogy and Mineral Beneficiation of platinum group elements. Canadian Institute of Mining, Metallurgy and Petroleum, pp 793 – 809.

Merkle, R.K.W., Franklyn, C.B., Przybylowicz, W. and Verryn, S.M.C. (2002). Intercomparison of electron micro-analyses and particle induced X-ray emission analyses of Pt-Pd-Ni-S matrices. Nuclear Instruments and methods in Physics Research, B190, 821-825.

Merkle, R.K.W. and Verryn, S.M.C. (2003). Cooperate and braggite from the bushveld complex: implications for the miscibility gap and identification. Mineral Deposita, 38, 381 – 388.

Merkle, R.K.W. and Von Gruenewaldt, G. (1986). Compositional variation of Co-rich pentlandite: relation to the evolution of the upper zone of the western Bushveld Complex, South Africa. Canadian Mineralogist, 24, 529-546.

Mitchell A.A. (1990). The stratigraphy petrography and mineralogy of the Main Zone of the Northwestern Bushveld Complex. South African Journal of Geology, 93, 818–831.

Mitchell, A.A., Eales, H.V. and Kruger, F.J. (1998). Magma replenishment and the significance of poikilitic textures in the Lower Main Zone of the Western Bushveld Complex South Africa. Mineral Magazine, 64, 435–450.

Molyneux, T.G. (1974). A geological investigation of the Bushveld Complex in Sekhukhuneland and part of the Steelpoort Valley. Transvaal Geological Socoety of South Africa, 77, 329–338.

Nel, E., Valenta, M. and Naude, N. (2005). Influence of open circuit regrind milling on UG 2 ore composition and mineralogy at Impalas UG 2 concentrator. Minerals Engineering, 18, 785 – 790.

Penberthy, C.J. (2000). The effect of mineralogical variation in the UG2 chromitite on the recovery of platinum group elements. PhD. Thesis (unpublished), University of Pretoria, Pretoria, South Africa.

Penberthy, C.J. and Merkle, R.K.W. (1999). Lateral variation in the platinum group element content and mineralogy of the UG2 chromitite layer, Bushveld Complex. South African Journal of Geology, 102(3), 240 - 250.

Pentberthy, C.J., Oosthuyzen, E.J. and Merkle, R.K.W. (2000). The recovery of platinum group elements from the UG-2 chromitite, Bushveld complex – a mineralogical perspective. Mineralogy and Petrology, 68, 213-222.

Peyerl, W. (1982). The influence of the driekop dunite pipe on the platinum group mineralogy of the UG2 chromitite in its vicinity. Economic Geology, 77, 1432-1438.

Schouwstra, R.P., Kinloch, E.D. and Lee, C.A. (2000). A short geological review of the Bushveld complex. Platinum Metals Review, 44, 33 – 39.

Schwellnus, J.S.I., Engelbrecht, L.N.J., Coertze, F.J., Russell, H.D., Malherbe, S.J., Van Rooyen, D.P. and Cooke, R. (1962) The geology of the Olifants River area, Transvaal. Explanation of sheets 2429B (Chuniespoort) and 2430A (Wolkberg). Geological Survey of South Africa, 87pp.

Scoon, R.E. and Teigler, B. (1994). Platinum group element mineralization in the critical zone of the western Bushveld complex: I. sulphide poor-chromitites below the UG2. Economic Geology, 89, 1094 – 1121.

Sutherland, D.N., Gottlieb, P., Jackson, R., Wilkie, G. and Stewart, P. (1988). Measurement in section of particles of known composition. Minerals Engineering, 4, 317 – 326.

Sutherland, D.N. and Gottlieb, P. (1991). Application of automated quantitative mineralogy in mineral processing. Minerals Engineering, 4, 753 – 762.

Teigler B., Eales H.V. and Scoon R.N. (1992). The cumulate succession of the Critical Zone of the Rustenburg Layered Suite at Brits, Western Bushveld Complex. South African Journal of Geology, 95, 17–28.

Valenta, M.M. (2007). Balancing the reagent suite to optimize grade and recovery. Minerals Engineering, 20, 979 – 985.

Vermaak, C.F. (1985). The UG2 Layer – South Africa's Slumbering Chromitite giant. Chromium Review, 5, 9 – 22.

Verryn, S.M.C. and Merkle, R.K.W. (1994). Compositional variation of cooperate, braggite and vysotkite from the bushveld complex. Mineralogical Magazine, 58, 223 – 234.

Viljoen, M.J. (1994). A review of regional variations in facies and grade distribution of the Merensky reef, western Bushveld complex, with some mining implications: Proceedings, 15th CMMI congress, South African Institute of Mining and Metallurgy, 183 – 194.

Viljoen, M.J. and Hieber, R.W. (1986). The Rustenburg section of Rustenburg platinum mines limited, with reference to the Merensky reef in mineral deposit of south Africa, 2 (C.R. Anhaeusser and S. Maske, eds): Geological Society of South Africa, Johannesburg, 1107 – 1134.

Viljoen, M.J. and Schurman, L.W. (1998). Platinum group metals in: M.G.C. Wilson and C.R. Anhaeusser (Editors),*The mineral resources of South Africa.* Council for Geoscience, South Africa, 532-568.

Voordouw, R,J., Gutzmer, J. and Beukes, N.J. (2010). Zoning of platinum group minerals assemblages in the UG2 chromitite determined through in situ SEM-EDS- based image analysis. Mineral Deposita, 45, 147-159.

Von Gruenewaldt, G., Sharpe, M.R. and Hatton, C.J. (1985). The Bushveld Complex: Introduction and Review. Economic Geology, 80(4), 803 – 812.

Von Gruenewaldt, G. (1977). The mineral resources of the Bushveld complex. Minerals Science Engineering 9, 83 – 95.

Vos, C.F., David, T.Z. and Miller, J.D. (2007). Trithiocarbonates for PGM flotation. International platinum conference 'platinum surges ahead'. South African Institute of Mining and Metallurgy, 2007.

Wager, L.R. and Brown, G.M. (1968). Layered igneous rocks. Olivier and Boyd, Edinburgh, 588 pp.

Weller, K.R., Morrell, S. and Gottlieb, P. (1996). Use of grinding and liberation models to simulate tower mill circuit performance in a lead / zinc concentrator to increase flotation recovery. International Journal of Mineral Processing, 44-45, 683 – 702.

Wesseldijk, Q.I., Reuter, M.A., Bradshaw, D.J. and Harris, P.J. (1999). The flotation behavior of chromite with respect to the beneficiation of UG2 ore. Minerals Engineering, 12(3), 1177-1184.

Wiese, J.G., Becker, M., Bradshaw, D.J. and Harris, P.J. (2007). Interpreting the role of reagents in the flotation of platinum-bearing Merensky ores. The Journal of South African Institute of Mining and Metallurgy, 107, 29-36.

Willemse, J. (1969). The Geology of the Bushveld Complex the largest repository of magmatic ore deposits in the World. Economic Geology, 4,1–22.

Willemse, J. (1959). The ''floor'' of the Bushveld Igneous Complex. Proceedings of the Geological Society of South Africa LXII:xxilxxx.

Xiao, Z .and Laplante, A.R. (2004). Characterizing and recovering the platinum group minerals – a review. Minerals Engineering, 17, 961 – 979.

Young, R.A. (Editor) (1993). The Rietveld method, international union of crystallography, monographs on crystallography, 5, oxford science publication, 298pp.

Appendix A – Percentage solids

	Wet sample					
sample	Bucket + sample (Kg)	Bucket (kg)	Wet sample (kg)	Dried sample (kg)	solid	Percentage Solid
1 PRC 1	17.55	1.17	16.38	3.59	0.22	21.92
2 PRC 1	18.55	1.16	17.39	3.8	0.22	21.85
3 PRC 1	19.25	1.16	18.09	3.52	0.19	19.46
1 PRC 2	17.9	1.16	16.74	3.25	0.19	19.41
2 PRC 2	19.4	1.16	18.24	3.34	0.18	18.31
3 PRC 2	18.95	1.16	17.79	3.55	0.2	19.96
1 PRC 3	18.05	1.18	16.87	2.21	0.13	13.1
2 PRC 3	19.15	1.17	17.98	2.35	0.13	13.07
3 PRC 3	19.15	1.18	17.97	2.33	0.13	12.97
1 PRC 4	19.35	1.17	18.18	2.93	0.16	16.12
2 PRC 4	18.45	1.18	17.27	2.63	0.15	15.23
3 PRC 4	19.1	1.18	17.92	2.73	0.15	15.23
1 PRC 5	18	1.17	16.83	1.99	0.12	11.82
2 PRC 5	18.15	1.15	17	1.97	0.12	11.59
3 PRC 5	17.75	1.17	16.58	1.59	0.1	9.59
1 PRC 6	16.4	1.16	15.24	1.83	0.12	12.01
2 PRC 6	17.05	1.17	15.88	2.03	0.13	12.78
3 PRC 6	17.05	1.18	15.87	1.94	0.12	12.22
1 PRC 7	17.85	1.18	16.67	1.99	0.12	11.94
2 PRC 7	17.46	1.08	16.38	2	0.12	12.21
3 PRC 7	17.95	1.17	16.78	2.02	0.12	12.04
1 PRC 8	17.75	1.17	16.58	1.94	0.12	11.7
2 PRC 8	17.55	1.18	16.37	1.97	0.12	12.03
3 PRC 8	17.8	1.17	16.63	2	0.12	12.03
1 PRC 9	19.1	1.18	17.92	2	0.11	11.16
2 PRC 9	20.05	1.19	18.86	2.12	0.11	11.24
3 PRC 9	19.85	1.17	18.68	2.1	0.11	11.24
1 PRC 10	17.95	1.16	16.79	1.62	0.1	9.65
2 PRC 10	17.45	1.18	16.27	1.53	0.09	9.4
3 PRC 10	17.3	1.16	16.14	1.52	0.09	9.42
1 PRF	22.2	1.16	21.04	8.337	0.4	39.62
2 PRF	21.45	1.17	20.28	8.456	0.42	41.7
3 PRF	17.15	1.16	15.99	6.271	0.39	39.22
1 PRT	17.3	1.18	16.12	6.53	0.41	40.51
2 PRT	15.1	1.18	13.92	6.02	0.43	43.25
3 PRT	16.85	1.17	15.68	6.94	0.44	44.26

Appendix B.1 - Fire Assay results

	Au	Pd	Pt	Rh	Ru	Ir
	parts per million	parts per million	parts per million	parts per million	parts per million	parts per million
PRF	<0.1	1.14	2.28	0.48	0.89	0.23
PRF	<0.1	1.35	2.66	0.54	1.05	0.2
PRC1	0.79	58.3	71.8	22	37.4	6.69
PRC1	0.96	60.3	72.8	22.5	38.5	6.91
PRC2	0.4	22.2	48.5	9.65	15.7	1.92
PRC2	0.42	24.7	50.7	10.5	17.8	<0.1
PRC3	0.26	10.5	22.7	4.77	7.62	<0.1
PRC3	0.18	9.36	20.8	4.58	7.4	0.74
PRC4	0.15	7.92	18	3.98	6.08	0.25
PRC4	0.31	9.05	19.5	3.99	6.09	0.98
PRC5	0.15	5.7	13	2.85	4.36	<0.1
PRC5	0.14	5.66	12.8	2.73	4.44	<0.1
PRC6	0.13	5.72	11	2.45	3.96	0.29
PRC6	0.14	5.69	12.7	2.79	4.43	<0.1
PRC7	<0.1	4.13	9.39	2.15	3.38	0.27
PRC7	0.11	3.86	8.39	1.93	2.93	<0.1
PRC8	0.17	4.91	11.5	2.37	3.76	0.41
PRC8	0.16	5.08	11.5	2.43	3.78	<0.1
PRC9	0.18	4.71	10.6	2.12	3.49	<0.1
PRC9	0.13	4.24	9.79	2.12	3.32	<0.1
PRC10	0.11	3.48	7.89	1.65	2.64	<0.1
PRC10	<0.1	2.57	5.66	1.42	2.2	<0.1
PRT	<0.1	0.36	0.75	0.2	0.28	<0.1
PRT	<0.1	0.4	0.76	0.2	0.26	<0.1

Appendix B.2 – Chemical analysis results of Nickel, copper, and cobalt.

	Nickel (%)	Copper (%)	Cobalt (%)
PRF	448	126	56
PRC1	9640	4780	337
PRC2	4050	1350	151
PRC3	1720	540	71
PRC4	1520	490	63
PRC5	1040	392	47
PRC6	999	390	45
PRC7	907	395	41
PRC8	848	410	39
PRC9	816	405	37
PRC10	608	311	28
PRT	168	60	10

Appendix B.3 – Chemical analysis results of total iron and chromium.

	Chromium (%)	Iron (%)
PRF	14.6	13.9
PRC 1	2.26	8.16
PRC 2	2.74	7.83
PRC 3	4.22	8.38
PRC 4	4.02	8.23
PRC 5	4.92	8.53
PRC 6	5.13	8.69
PRC 7	5.32	8.66
PRC 8	5.6	8.74
PRC 9	5.92	9
PRC 10	7.03	9.3
PRT	15.2	12.7

Appendix C – XRD Results (wt %)

Table C.1

	PRF	**Errors (3sigma)**	**PRC1**	**Errors (3sigma)**	**PRC2**	**Errors (3sigma)**
Chlorite	3.35	0.99	8.37	1.68	3.4	4.8
Chromite	25.96	0.72	5.26	0.84	6.55	0.63
Enstatite	25.95	1.05	29	4.5	31	3
Hornblende	2.88	0.75	5.88	1.56	2.63	0.6
Phlogopite	3.98	0.87	8.11	1.62	4.08	0.57
Plagioclase	30.87	1.08	9.6	1.65	10.79	1.2
Talc	7	1.23	33.8	9.6	41.6	4.8
Total	**99.99**		**100.02**		**100.05**	
	PRC3	**Errors (3sigma)**	**PRC4**	**Errors (3sigma)**	**PRC5**	**Errors (3sigma)**
Chlorite	5.28	0.87	3.56	0.84	4.05	1.14
Chromite	8.91	0.84	7.92	0.78	8.01	1.32
Enstatite	28.89	2.94	30.31	2.73	23.6	3.9
Hornblende	3.15	0.63	3.09	0.54	0	0
Phlogopite	2.87	0.54	2.69	0.69	3.57	0.84
Plagioclase	9.63	0.96	12.64	1.32	8.4	1.47
Talc	41.3	5.4	39.8	5.4	52.3	8.1
Total	**100.03**		**100.01**		**99.93**	

Table C.2

	PRC6	Errors (3sigma)	PRC7	Errors (3sigma)	PRC8	Errors (3sigma)
Chlorite	3.57	0.93	6.9	0.9	3.04	0.99
Chromite	12.7	1.08	14.37	0.54	10.7	2.67
Enstatite	32.88	2.76	39.43	1.26	25.6	6.3
Hornblende	2.25	0.78	1.32	0.51	2.12	0.6
Phlogopite	5.09	0.78	5.35	0.66	4.28	1.17
Plagioclase	14.76	1.41	15.74	1.02	11.72	2.94
Talc	28.7	5.7	16.89	1.68	42.5	14.1
Total	**99.95**		**100**		**99.96**	
Chlorite	**PRC9**	**Errors (3sigma)**	**PRC10**	**Errors (3sigma)**	**PRT**	**Errors (3sigma)**
Chromite	8.31	1.59	6	1.26	1.94	1.08
Enstatite	15.37	0.84	16.33	0.93	23.52	0.69
Hornblende	35.82	1.74	33.94	1.89	25.18	1.17
Phlogopite	1.84	0.57	3.17	0.63	2.92	0.72
Plagioclase	3.72	0.72	3.8	0.87	4.5	0.84
Talc	15.35	1.08	18.76	1.41	35.39	1.17
Total	19.6	3.3	18	3.6	6.54	1.29
	100.01		**100**		**99.99**	

Appendix D.1 – Modal distribution of PGM (Vol %)

	PGM Sulphides	Laurite	PGM Alloy	PGM Arsenides	PGM Tellurides
PRF	79	14	2	1	3
PRC1	79	14	4	2	1
PRC2	76	16	5	2	1
PRC3	76	17	4	1	0
PRC4	52	40	2	6	0
PRC5	79	10	3	5	2
PRC6	75	19	2	3	1
PRC7	70	17	7	6	1
PRC8	65	29	1	2	3
PRC9	73	19	3	3	2
PRC10	68	28	2	0	0
PRT	62	26	9	1	2

Appendix D.2 – Modal distribution of dominating PGM sulphides and platinum alloy (Vol %).

	PtPdNiS	PtS	PtRhCuNiS	RuIrOsS	PtFe
PRF					
PRC1	145	236	136	108	11
PRC2	72	140	97	70	6
PRC3	55	111	61	48	10
PRC4	36	44	33	108	5
PRC5	43	101	55	53	18
PRC6	64	134	91	57	12
PRC7	38	93	61	44	12
PRC8	36	91	41	39	3
PRC9	33	46	30	21	2
PRC10	40	17	31	26	2
PRT	21	29	12	23	3

Appendix D.3 – Mode of occurrence along the primary rougher circuit.

	L	SL	SAG	AG	SG	G
PRF	906	196	372	133	55	36
PRC1	11694	2774	1334	429	179	142
PRC2	4744	1031	1197	231	0	86
PRC3	1661	137	516	240	14	5
PRC4	1688	175	875	448	54	38
PRC5	934	152	911	219	14	30
PRC6	798	296	367	149	5	18
PRC7	751	72	454	148	3	69
PRC8	853	82	479	179	0	105
PRC9	908	215	791	112	0	44
PRC10	1047	125	1538	274	7	89
PRT	73	17	195	54	44	113

L- liberated PGM, SL – PGM associated with liberated BMS, SAG – PGM associated with BMS locked in silicates or oxide gangue particles, AG – PGM attached to silicate or oxide gangue particle, SG – PGM associated BMS attached to silicate or oxide gangue particle, and G - PGM locked within silicate or oxide gangue particle.

Appendix D.4 – PGM grain liberation index, along the primary rougher circuit (%)

CLI	<0.2	0.2 - 0.4	0.4 - 0.6	0.6 - 0.8	0.8 - 1.0
PRF	22.3	10.3	11.8	2.3	53.3
PRC1	9.2	10.4	6.6	2.9	70.8
PRC2	6.6	11.5	14	2.3	65.6
PRC3	13.8	8.2	27.7	1.4	48.9
PRC4	14.8	3.6	21.1	2.5	58
PRC5	22.6	8	14.3	1.4	53.8
PRC6	24.8	13.6	7.2	5.2	49.2
PRC7	30.6	19.8	6.5	3.1	39.9
PRC8	23.3	10.8	11.5	6.4	48
PRC9	22.1	8.9	18.7	5.7	44.5
PRC10	18.6	12	33.7	0.6	35
PRT	58.8	19.9	6.1	3.1	12

Appendix D.5 – PGM size distribution, along the primary rougher circuit (%).

CLI	0 - 3	3 -6	6 - 9	>9
PRF	14	43	30	14
PRC1	6	30	24	40
PRC2	10	39	23	28
PRC3	16	38	27	19
PRC4	18	32	12	37
PRC5	16	33	31	20
PRC6	21	41	29	10
PRC7	26	45	19	10
PRC8	15	40	22	23
PRC9	13	25	29	33
PRC10	9	20	15	56
PRT	24	66	10	0

Appendix E – Micro probe results

Quantitative Analysis Declaration

Label:Ptiden

Date:Fri Feb 6 06:11:21 2009

Type:Normal

Take Off Angle:40.

Iteration Limit:0.000

Condition #1 15.0 kV 20.0 nA

Sp1 LIF

Fe Ka Shift:0 Valence:2

Time(sec):15 Bkg(sec):0.0

(+)Bkg:0 (-)Bkg:-500 Slope:1.000

Standard:hemvz Esti 3 Sig.D.L.(parts per million): 1717.67

Bias(V):1299 Gain(*):407 DeadTime(us):3

Baseline:953 Window:2252 Mode:Pha Diff

SineTheta:48084 I(C/s/nA):82.415 Date:21/Jan/ 9

Co Ka Shift:0 Valence:2

Time(sec):15 Bkg(sec):0.0

(+)Bkg:500 (-)Bkg:-350 Slope:0.000

Standard:skux Esti 3 Sig.D.L.(parts per million): 1489.65

Bias(V):1300 Gain(*):412 DeadTime(us):3

Baseline:1076 Window:2348 Mode:Pha Diff

SineTheta:44436 I(C/s/nA):19.668 Date:28/Jan/ 9

Ni Ka Shift:0 Valence:2

Time(sec):15 Bkg(sec):0.0

(+)Bkg:0 (-)Bkg:-500 Slope:1.000

Standard:nick Esti 3 Sig.D.L.(parts per million): 2382.11

Bias(V):1300 Gain(*):412 DeadTime(us):3

Baseline:1207 Window:2442 Mode:Pha Diff

SineTheta:41181 I(C/s/nA):76.231 Date:28/Jan/ 9

Cu Ka Shift:0 Valence:2

Time(sec):15 Bkg(sec):0.0

(+)Bkg:0 (-)Bkg:-500 Slope:1.000

Standard:ChalcoTmp Esti 3 Sig.D.L.(parts per million): 2651.40

Bias(V):1300 Gain(*):409 DeadTime(us):3

Baseline:1348 Window:2530 Mode:Pha Diff

SineTheta:38268 I(C/s/nA):24.710 Date:17/Mar/ 8

Os La Shift:0 Valence:3

Time(sec):15 Bkg(sec):0.0

(+)Bkg:0 (-)Bkg:-500 Slope:1.000

Standard:G2Os Esti 3 Sig.D.L.(parts per million): 14246.25

Bias(V):1296 Gain(*):403 DeadTime(us):3

Baseline:1561 Window:2666 Mode:Pha Diff

SineTheta:34551 I(C/s/nA):25.054 Date:26/Nov/ 8

Ir La Shift:0 Valence:4

Time(sec):15 Bkg(sec):0.0

(+)Bkg:0 (-)Bkg:-600 Slope:1.000

Standard:G2Ir Esti 3 Sig.D.L.(parts per million): 17645.07

Bias(V):1296 Gain(*):403 DeadTime(us):3

Baseline:1631 Window:2696 Mode:Pha Diff

SineTheta:33565 I(C/s/nA):19.445 Date:26/Nov/ 8

Sp2 LPET

Te La Shift:0 Valence:4

Time(sec):15 Bkg(sec):0.0

(+)Bkg:600 (-)Bkg:0 Slope:1.000

Standard:ag2te Esti 3 Sig.D.L.(parts per million): 1054.85

Bias(V):1806 Gain(*):760 DeadTime(us):3

Baseline:776 Window:3768 Mode:Pha Diff

SineTheta:37590 I(C/s/nA):298.765 Date:09/Jul/ 7

Sb La Shift:0 Valence:3

Time(sec):15 Bkg(sec):0.0

(+)Bkg:0 (-)Bkg:-600 Slope:1.000

Standard:stibx Esti 3 Sig.D.L.(parts per million): 986.18

Bias(V):1806 Gain(*):760 DeadTime(us):3

Baseline:708 Window:3672 Mode:Pha Diff

SineTheta:39305 I(C/s/nA):577.997 Date:09/Jul/ 7

Sn La Shift:0 Valence:2

Time(sec):15 Bkg(sec):0.0

(+)Bkg:600 (-)Bkg:0 Slope:1.000

Standard:sn Esti 3 Sig.D.L.(parts per million): 1249.76

Bias(V):1826 Gain(*):815 DeadTime(us):3

Baseline:630 Window:3600 Mode:Pha Diff

SineTheta:41138 I(C/s/nA):853.347 Date:16/Oct/ 8

Pd La Shift:0 Valence:2

Time(sec):15 Bkg(sec):0.0

(+)Bkg:600 (-)Bkg:0 Slope:1.000

Standard:G4PdS Esti 3 Sig.D.L.(parts per million): 1397.20

Bias(V):1822 Gain(*):802 DeadTime(us):3

Baseline:560 Window:3072 Mode:Pha Diff

SineTheta:49934 I(C/s/nA):396.998 Date:26/Nov/ 8

Rh La Shift:0 Valence:3

Time(sec):15 Bkg(sec):0.0

(+)Bkg:0 (-)Bkg:-500 Slope:1.000

Standard:G3FeRhS Esti 3 Sig.D.L.(parts per million): 991.33

Bias(V):1822 Gain(*):802 DeadTime(us):3

Baseline:560 Window:2930 Mode:Pha Diff

SineTheta:52559 I(C/s/nA):1.464 Date:26/Nov/ 8

Sp3 LPET

Pt Ma Shift:0 Valence:4

Time(sec):15 Bkg(sec):0.0

(+)Bkg:500 (-)Bkg:0 Slope:1.000

Standard:G3PtFe Esti 3 Sig.D.L.(parts per million): 3770.46

Bias(V):1869 Gain(*):982 DeadTime(us):3

Baseline:560 Window:2274 Mode:Pha Diff

SineTheta:69121 I(C/s/nA):94.002 Date:26/Nov/ 8

Hg Ma Shift:0 Valence:2

Time(sec):15 Bkg(sec):0.0

(+)Bkg:600 (-)Bkg:0 Slope:1.000

Standard:hgs Esti 3 Sig.D.L.(parts per million): 2430.47

Bias(V):1881 Gain(*):1072 DeadTime(us):3

Baseline:560 Window:2420 Mode:Pha Diff

SineTheta:64520 I(C/s/nA):179.851 Date:23/Oct/ 8

S Ka Shift:0 Valence:4

Time(sec):15 Bkg(sec):0.0

(+)Bkg:600 (-)Bkg:0 Slope:1.000

Standard:pyrvz Esti 3 Sig.D.L.(parts per million): 500.64

Bias(V):1865 Gain(*):1030 DeadTime(us):3

Baseline:560 Window:2540 Mode:Pha Diff

SineTheta:61392 I(C/s/nA):582.992 Date:23/Jan/ 9

Pb Ma Shift:0 Valence:2

Time(sec):15 Bkg(sec):0.0

(+)Bkg:600 (-)Bkg:0 Slope:1.000

Standard:galevz Esti 3 Sig.D.L.(parts per million): 3951.57

Bias(V):1851 Gain(*):911 DeadTime(us):3

Baseline:560 Window:2580 Mode:Pha Diff

SineTheta:60368 I(C/s/nA):231.311 Date:09/Jul/ 7

Bi Ma Shift:0 Valence:3

Time(sec):15 Bkg(sec):0.0

(+)Bkg:600 (-)Bkg:0 Slope:1.000

Standard:bitevz Esti 3 Sig.D.L.(parts per million): 1692.64

Bias(V):1848 Gain(*):887 DeadTime(us):3

Baseline:560 Window:2659 Mode:Pha Diff

SineTheta:58448 I(C/s/nA):154.495 Date:09/Jul/ 7

Ru La Shift:-33 Valence:4

Time(sec):15 Bkg(sec):0.0

(+)Bkg:600 (-)Bkg:0 Slope:1.000

Standard:Ru Esti 3 Sig.D.L.(parts per million): 1362.04

Bias(V):1850 Gain(*):895 DeadTime(us):3

Baseline:574 Window:3530 Mode:Pha Integral

SineTheta:55410 I(C/s/nA):546.067 Date:16/Feb/ 1

Sp4 TAP

As La Shift:0 Valence:3

Time(sec):20 Bkg(sec):10.0

(+)Bkg:600 (-)Bkg:0 Slope:1.000

Standard:gaas Esti 3 Sig.D.L.(parts per million): 906.71

Bias(V):1300 Gain(*):2674 DeadTime(us):3

Baseline:560 Window:4960 Mode:Pha Diff

SineTheta:37647 I(C/s/nA):234.489 Date:06/Nov/ 8